BLaER1 Macrophage Model for the Investigation of RNA Stimulation and Viral Infections

Dissertation

Zur Erlangung des Grades

Doktor der Naturwissenschaften

Am Fachbereich Biologie

Der Johannes Gutenberg-Universität Mainz

Sarah Ruth Pawusch

geb. am 22.06.1996 in Pirmasens

Mainz, 27.02.2026

Dekan: Prof. Dr. Eckhard Thines

1. Berichterstatter:

2. Berichterstatter:

Tag der mündlichen Prüfung:

„Man darf nie an die ganze Straße auf einmal denken, verstehst du? Man muss nur an den nächsten Schritt denken, an den nächsten Atemzug, an den nächsten Besenstrich. Und immer wieder nur an den nächsten. Dann macht es Freude; das ist wichtig, dann macht man seine Sache gut. Und so soll es sein.“

“You must never think of the whole street at once, understand? You must only concentrate on the next step, the next breath, the next stroke of the broom, and the next, and the next. Nothing else. That way you enjoy your work, which is important, because then you make a good job of it. And that's how it ought to be.”

- Michael Ende in *Momo*

Table of contents

Preface

The work presented in this thesis was primarily conducted by me, while parts of this study were supported by research collaborations. I was involved in the conceptualization of the project and responsible for planning and executing the experiments. For this work I received support for the following experiments and techniques:

- Flow cytometry of BLaER1 cells during transdifferentiation was performed with Dr. Ulrike Blohm (Institute of Immunology, FLI, Greifswald)
- FACS of transfected BLaER1 cells was performed with Laura Timm (Institute of Immunology, FLI, Greifswald)
- EBOV and BOMV infection experiments were performed by PD Dr. Thomas Hoenen (Institute of Molecular Virology and Cell Biology, FLI, Greifswald)

This work was supported by the Deutsche Forschungsgemeinschaft (DFG, German Research Foundation) - project number 439669440 TRR319.

Parts of the text and figures included in this dissertation were used to prepare the following scientific manuscript:

Nunes, I. V., Breitenbach, L., Pawusch, S., Eigenbrod, T., Ananth, S., Schad, P., Fackler, O. T., Butter, F., Dalpke, A. H., & Chen, L. S. (2024). Bacterial RNA sensing by TLR8 requires RNase 6 processing and is inhibited by RNA 2'O-methylation. EMBO reports, 25(11), 4674–4692. https://doi.org/10.1038/s44319-024-00281-9

Summary

The innate immune system is the first line of defense against pathogens and environmental threats, as it is responsible for their recognition and elimination. Macrophages, in concert with other immune cells, fulfill a crucial function in the orchestration of this response. In the context of infection by pathogens, the endolysosomal Toll-like receptor 8 (TLR8), which is present in macrophages, recognizes foreign RNA, thereby unlocking a signaling cascade that results in the secretion of cytokines, thus triggering an appropriate immune response and pathogen clearance. However, TLR8 activation is inhibited by the presence of 2'-O-methylation (2'-O-me), a known marker of eukaryotic RNA. The exact molecular mechanisms upstream of TLR8 activation, in particular regarding the inhibitory capacity of 2'-O-me, remained to be elucidated. Therefore, we aimed to investigate the mechanisms that underlie cell stimulation by foreign RNA, with a focus on the identification of 2'-O-me-dependent RNA-binding proteins (RBPs) that could determine the recognition of exogenous RNA upstream of TLR8. To this end, we employed the BLaER1 cell model, a B cell line that allows for the transdifferentiation to macrophage-like cells, in combination with state-of-the-art mass spectrometry techniques.

The initial phase of our work consisted of the characterization of the BlaER1 proteome during transdifferentiation. The subsequent optimization of the protocol allowed us an efficient generation of macrophages. Next, we employed *in vitro* RNA-pull-downs and mass spectrometry-based proteomics for protein quantification to identify RBPs that exhibited significant differences in binding affinity in the presence of 2'-O-me. With this approach, we were able to identify TRMT61A as a potential RBP candidate with an enhanced binding to unmodified RNA. This lead us to formulate the hypothesis that TRMT61A supports the necessary processing of foreign RNA upstream of TLR8. While the generation of a BLaER1 cell line with TRMT61A KO has yet to be accomplished, the investigation of Ribonuclease (RNase) 6 as a further candidate upstream of TLR8 has led to the determination of its subcellular localization within the endolysosome. The following work by our collaborators confirmed the role of RNase6 with a 2-O-me-dependent digestion of bacterial RNAs, which is necessary for TLR8 activation (Nunes *et al.*, 2024).

Subsequently, we aimed to assess the potential of using BLaER1 macrophages as a model system to study viral infections and elucidate the pathogenicity of orthoebolaviruses, which exhibit a natural tropism for macrophages. To this end, BSL-4-compatible workflows were implemented, enabling the investigation of viral and host proteomes during infections of the BLaER1 model system. Indeed, BlaER1 demonstrated susceptibility and permissiveness to EBOV. A comprehensive analysis of time-resolved proteome data revealed an elevated rate of viral protein replication during EBOV infection, in comparison to infections with the related, though non-pathogenic, BOMV. The analysis of host proteome and secretome samples led to the identification of proteins that could be involved in EBOV pathogenicity and the modulation of the immune

response during the infection. This includes both known factors, such as ubiquitin-protein transferases, interferon (IFN)-induced proteins, and the growth factor TGFβ1, as well as novel factors such as the oxidase IL4I1, the immune regulator GOLM1, and the anti-inflammatory PLTP.

In sum, in this work we demonstrated the suitability of BLaER1 macrophages as a valuable model system for investigating the sensing of exogenous RNA within the innate immune response. We further identified an effector responsible for the 2'-O-me-dependent recognition of bacterial RNA upstream TLR8 activation. In addition, we demonstrated the BLaER1 macrophages model as a useful tool for investigating EBOV pathogenicity, thereby validating the wide applicability of this system and enhancing our understanding of the innate immune response towards the virus.

Zusammenfassung

Das angeborene Immunsystem ist als erste Verteidigungslinie für die Erkennung und Eliminierung von Pathogenen und Gefahren aus der Umwelt verantwortlich. Makrophagen erfüllen dabei, gemeinsam mit weiteren Immunzellen, wichtige Funktionen in der Organisation dieser Immunantwort. Während der Infektion durch Pathogen ist der endolysosomale Toll-like-Rezeptor 8 (TLR8) in Makrophagen für die Erkennung fremder RNA zuständig. Die Aktivierung von TLR8 löst eine Signalkaskade aus, welche die Ausschüttung von Zytokinen und dadurch eine entsprechende Immunantwort und die Beseitigung des Pathogens verursacht. Allerdings wird die Aktivierung von TLR8 durch die Anwesenheit einer 2'-O-Methylierung (2'-O-me), die ein bekannter Marker von eukaryotischer RNA ist, inhibiert. Der exakte molekulare Mechanismus stromaufwärts der TLR8-Aktivierung, besonders in Hinblick auf die inhibitorische Wirkung von 2'-O-me, war lange nicht bekannt. Daher wollen wir den Mechanismus hinter der Zellstimulierung durch fremde RNA mit Fokus auf die Identifikation von 2'-O-me-abhängigen RNA-Bindeproteinen (RBPs) aufklären, da diese die Erkennung fremder RNA stromaufwärts von TLR8 bestimmen. Dafür verwendeten wir das BLaER1 Zellmodell, eine B-Zelllinie die zu Makrophage-ähnlichen Zellen transdifferenziert werden kann, in Kombination mit modernsten Techniken in der Massenspektrometrie.

Das erste Ziel unserer Arbeit war die Charakterisierung des BLaER1 Proteoms während der Transdifferenzierung. Eine darauffolgende Optimierung des Differenzierungs-Protokolls ermöglichte uns die effiziente Erzeugung von Makrophagen. Daraufhin führten wir *in vitro* RNA-Pull-Downs und Massenspektrometrie-basierte Proteomik Analysen durch, um RBPs zu identifizieren, die unterschiedliche Bindeaffinität bei 2'-O-me aufzeigten. Mit dieser Herangehensweise identifizierten wir TRMT61A als potenziellen RBP-Kandidaten mit einer erhöhten Affinität für unmodifizierte RNA. Dies führte uns zu der Hypothese, dass TRMT61A die

notwendigen Prozessierungsschritte fremder RNA stromaufwärts von TLR8 unterstützt. Während die Erzeugung einer BLaER1 Zelllinie mit TRMT61A Knockout noch aussteht, wurde mit RNase6 ein weiterer Kandidat stromaufwärts von TLR8 untersucht. Dabei wurde die endolysosomale Lokalisierung von RNase6 innerhalb der Zelle bestimmt. Die darauffolgende Arbeit unserer Kollaborationspartner bestätigte die Rolle der RNase6 durch den Nachweis von 2‘-O-me-abhängigem Verdau bakterieller RNA, der für die Aktivierung von TLR8 notwendig ist.

Weiterhin planten wir das Potential von BLaER1 Makrophagen als Modellsystem für virale Infektionen aufzuklären und untersuchten die Pathogenität von Orthoebolaviren, die einen natürlichen Tropismus für Makrophagen aufweisen. Dafür implementierten wir BSL-4-kompatible Arbeitsabläufe, welche die Untersuchung von viralen Proteomen und Wirtsproteomen während der Infektion des BLaER1 Modells ermöglichten. Somit konnten wir die Empfänglichkeit und Permissivität von BLaER1 für EBOV nachweisen. Eine umfassende Analyse von zeitaufgelösten Proteomdaten zeigte einen Anstieg von viraler Proteinreplikation während der EBOV-Infektion, der allerdings nicht beim nicht pathogenen und verwandten BOMV festgestellt wurde. Die Analyse von Wirtsproteom- und Sekretomproben führte zur Identifizierung von Proteinen, die an der Pathogenität von EBOV beteiligt sein könnten und die Immunantwort modulieren könnten. Dies beinhaltete sowohl bekannte Proteine, wie Ubiquitin-Proteintransferasen, Interferon-induzierte Proteine und den Wachstumsfaktor TGFβ1, als auch neuartige Proteine, wie die Oxidase IL4I1, den Immunregulator GOLM1 und das anti-inflammatorische PLTP.

Insgesamt zeigten wir in dieser Arbeit die Eignung von BLaER1 Makrophagen als wertvolles Modellsystem für die Untersuchung der Erkennung von fremder RNA durch das angeborene Immunsystem. Weiterhin identifizierten wir einen Effektor, der für die 2‘-O-me-abhängige Erkennung von bakterieller RNA stromaufwärts von TLR8 zuständig ist. Zusätzlich zeigten wir die Anwendung des BLaER1 Makrophagenmodells für die Untersuchung von EBOV-Pathogenität, validierten dadurch die weitreichende Anwendbarkeit von BLaER1 und erweiterten unser Verständnis der angeborenen Immunantwort auf das Virus.

Abbreviations

°C	Degrees Celsius
µl	Microliter
2'-O-Me	2'-O-methylation
A	Adenine
ABC	Ammonium bicarbonate
BDBV	Bundibugyo virus
BLaER1	B cell Leukemia C/EBPαER clone 1
BOMV	Bombali virus
BP	Biological process
BSL-4	Biosafety level 4
C	Cytosine
C/EBPα-ER	CCAAT enhancer binding protein alpha-Estrogen Receptor
Cas9	CRISPR-associated protein 9
CC	Cellular component
CD	Cluster of differentiation
CLR	C-type lectin receptor
CpG	Cytosine-guanine dinucleotide
CRISPR	Clustered regularly interspaced short palindromic repeats
CSF1R	Colony stimulating factor receptor 1
DAMP	Damage-associated molecular pattern
DMSO	Dimethyl sulfoxide
DNA	Desoxyribonucleic acid
DPBS	Dulbecco's phosphate-buffered saline
DSB	Double-strand break
dsRNA	Double-stranded RNA
DTT	Dithiothreitol
DYNLL	Dynein light chain
EBOV	Ebola virus
EDTA	Ethylenediamine tetraacetic acid
EL	Endolysosome
EPRS	Gene for bifunctional aminoacyl-tRNA synthetase
EVD	Ebola virus disease
FACS	Fluorescence-activated cell sorting
FBS	Fetal bovine serum
FLI	Friedrich-Loeffler-Institute
FSC-W	Forward scatter width

G	Guanosine
gDNA	Genomic DNA
GFP	Green fluorescent protein
GO	Gene ontology
GP	Glycoprotein
$GP_{1,2}$	Glycoprotein subunit 1 and 2
GPI	Glucose-6-phosphate isomerase
gRNA	Guide RNA
HCD	Higher-energy collisional dissociation
HERC5	HECT and RLD Domain Containing E3 Ubiquitin Protein Ligase 5
HIV	Human immunodeficiency virus
hpi	Hours post infection
HPLC	High-performance liquid chromatography
IAA	Iodoacetamide
iBAQ	Intensity based absolute quantification
IFIT	Interferon Induced proteins with tetratricopeptide repeats
IFN	Interferon
IL	Interleukin
IL1RN	Interleukin-1 receptor antagonist
IL4I1	Interleukin 4 induced 1
IRAK	Interleukin-1 receptor associated kinase
IRES	Internal ribosome entry site
kbp	Kilo base pairs
KCl	Potassium chloride
kDa	Kilodalton
KO	Knockout
l	Liter
L	Viral polymerase L
LC-MS/MS	Liquid chromatography-tandem mass spectrometry
LFQ	Label free quantification
LPS	Lipopolysaccharide
M1	Pro-inflammatory macrophage
M2	Anti-inflammatory macrophage
Mac-1	Macrophage-1 antigen
MARV	Marburg virus
M-CSF	Macrophage colony-stimulating factor
MF	Molecular function
MgCl2	Magnesium chloride hexahydrate
MHC	Major histocompatibility complex

min	Minutes
mm	Millimeter
MMP9	Matrix metalloproteinase-9
MOI	Multiplicity of infection
mRNA	Messenger RNA
MS	Mass spectrometry
MX	Myxovirus resistance protein
MyD88	Myeloid differentiation primary response protein 88
NF-κB	Nuclear factor kappa-light-chain-enhancer of activated B cells
ng	Nanogram
NK cell	Natural killer cell
nl	Nanoliter
NLRP3	NOD-like receptor pyrin domain containing 3
Nm	2’-O-methylation of any base
NP	Nucleoprotein
NPC1	Niemann-Pick C1 receptor
OAS	2’-5’-oligoadenylate synthase
ORF	Open reading frame
PAMP	Pathogen-associated molecular pattern
PASEF	Parallel accumulation-serial fragmentation
PC	Principal component
PCA	Principal component analysis
PCR	Polymerase chain reaction
PLTP	Phospholipid transfer protein
PNS	Post-nuclear supernatant
PTX3	Pentaxin-related protein 3
RaPID	RNA-protein interaction detection
RBP	RNA-binding protein
RESTV	Reston virus
RIG-I	Retinoic acid-inducible gene I
RLR	Retinoic acid inducible gene I-like receptors
RNA	Ribonucleic acid
RNase	Ribonuclease
RNP	Ribonucleoprotein
rpm	Rounds per minute
RPMI	Rosewell Park Memorial Institute medium
RPMIs	Supplemented RPMI
rRNA	Ribosomal RNA
SD	Standard deviation

SDS	Sodium lauryl sulphate
sGP	Soluble glycoprotein
SP3	Single-pot solid-phase-enhanced sample preparation
SSC-A	Sideward scatter area
ssRNA	Single-stranded RNA
STAT3	Signal transducer and activator of transcription 3
SUDV	Sudan virus
T	Thymine
TAFV	Taï Forest virus
TDM	Transdifferentiation medium
TGFβ	Transforming growth factor β
TIRAP	Toll-interleukin 1 receptor domain-containing adaptor protein
TLR	Toll-like receptor
TNF	Tumor necrosis factor
TRIM	Tripartite motif-containing protein
TRMT61A	TRNA methyltransferase 61A
tRNA	Transfer RNA
trVLP	Transcription- and replication-competent virus-like particles
U	Uracil
UHPLC	Ultra high-performance liquid chromatography
VLP	Virus-like particle
VP24	Viral protein 24
VP30	Viral protein 30
VP35	Viral protein 35
VP40	Viral protein 40
XLink	Crosslink

Introduction

Immunity

The risk of infection by pathogens has been a constant of life since long before the existence of the first humans and could, in the case of the last common ancestor of *Bamfordviridae*, date back more than a billion years (Barreat and Katzourakis, 2023). Ancient bacterial pathogens, such as *Corynebacterium diphteriae,* have been found in human bone samples from the Mesolithic period, indicating infections more than 11,250 years ago (Sikora *et al.*, 2025). Against these pathogens, the fundamental purpose of the immune response is to detect and eliminate threats in order to maintain the health and homeostasis of an organism (Nahrendorf, Ginhoux and Swirski, 2025).

Various defense mechanisms have evolved in organisms to survive the large variety of pathogens and environmental threats. Specific antiviral systems are conserved even between eukaryotes and prokaryotes, supporting the hypothesis of ancestral immunity within the different domains of life (Bernheim, Cury and Poirier, 2024). Defense mechanisms generally aim to identify danger to the host organism and to distinguish features from the self and non-self; they can be separated into the innate and adaptive immunity in mammals (Chaplin, 2010). Innate pathogens sensing is essential as a first line of defense, and to generate various signals that activate an adaptive response and form an immune memory (Medzhitov, 2009; Wang *et al.*, 2024). The following chapter will introduce the current knowledge on the innate immune response, detection mechanisms, and pathogenic threats relevant to this work.

Innate immune response

A first system of immunity has been found in basal animals, such as sponges, and is referred to as the innate immune system (Avelino and Montenegro, 2025). In mammals, it is evolved further and includes physical and chemical barriers in epidermal tissues, which block the entry of pathogens at the surface level with a low pH, reduced water content, and the competing cutaneous microflora (Elias, 2007). The innate immune response is defined by germline-encoded systems expressed in many cell types to detect molecular patterns in a broad spectrum of pathogens for a rapid response (Chaplin, 2010). These include multiple classes of PRRs, such as Toll-like receptors (TLRs), which can recognize conserved pathogen-associated molecular patterns (PAMPs) and Damage-associated molecular patterns (DAMPs) and will be discussed in more detail later (Janeway, 1989a; Chen *et al.*, 2025). The complement system is an ancient component of the innate immune response, which is responsible for detection of PAMPs and DAMPs and consists of proteins that are located either on cell surfaces or circulating in blood serum (Ricklin *et al.*, 2010; Li and Woodruff, 2025). This effector system is activated by the presence of pathogens through

various pathways and transforms components from a pro-enzyme form to active proteins, which rapidly recruit immune cells and lyse pathogens (Tschopp, Podack and Müller-Eberhard, 1982; Freeley, Kemper and Le Friec, 2016). Various cell types, which do not belong to the group of specialized immune cells, are also involved in pattern recognition. This cell-autonomous immunity is defined as an intrinsic defensive system using intracellular pathways in non-immune cells, such as epithelial cells or fibroblasts (Han *et al.*, 2025). The CRISPR-Cas system against phages in bacteria, Toll-Interleukin-Receptor domains conserved over all domains of life, and antimicrobial peptides in *Caenorhabditis elegans* are examples of this form of immunity (Barrangou *et al.*, 2007; Pujol *et al.*, 2008; Doron *et al.*, 2018).

Pattern recognition primarily occurs in specific mononuclear phagocytes of myeloid origin within the innate immune system, such as monocytes, dendritic cells, and granulocytes (Wang *et al.*, 2024). These cells internalize pathogens through mechanisms such as phagocytosis for processing them and presenting antigens in major histocompatibility complex (MHC) molecules, while also expressing receptors that activate adaptive immune cells (Lendeckel, Venz and Wolke, 2022). Recognition of pathogens by specific cytosolic PRR also activates the intracellular inflammasome, which consists of various multiprotein complexes that mediate an inflammatory response (Martinon, Burns and Tschopp, 2002; Yao *et al.*, 2024). This acute inflammation is characterized by vasodilation and the recruitment of immune cells to facilitate the inactivation and clearance of pathogens, as well as the repair of damaged tissue (Sherwood and Toliver-Kinsky, 2004). Mononuclear phagocytes are responsible for the release of cytokines, such as interleukins, tumor necrosis factors, and chemokines, which balance inflammation with further pro- and anti-inflammatory mediators (Arnold *et al.*, 2014; Das *et al.*, 2014; Wang *et al.*, 2024). Natural killer (NK) cells are the fourth type of innate immune cells, which, according to the missing self-hypothesis, are derived from lymphoid stem cells and recognize virus-infected or tumor cells with reduced surface expression of MHC I molecules (Kärre *et al.*, 1986; Chen, Zhu and Jounaidi, 2024). Detected cells are then rendered harmless to the organism through cell-mediated cytotoxicity and cytokine release, leading to rapid cell death and even the formation of memory NK cells, therefore thinning the line between the innate and adaptive immune responses (Mujal, Delconte and Sun, 2021).

After resolving the threat and inflammation, the immune system aims to return to immune homeostasis and restore the initial state of surveillance, while, in specific cases, immune memory is developed (Austermann, Roth and Barczyk-Kahlert, 2022). Overall, the innate immune response is a highly complex interplay of various systems that respond rapidly to non-specific threats by controlling pathogens, recruiting further immune cells, and initiating an inflammatory response.

Monocytes, macrophages, and the BLaER1 model

Blood-circulating monocytes that differentiate into tissue macrophages are essential phagocytes of the innate immune response and are responsible for interfering with pathogens and regulating an inflammatory response (Gordon and Taylor, 2005; Austermann, Roth and Barczyk-Kahlert, 2022). Tissue-resident macrophages can be traced back to embryonic progenitors which are planted into various tissues during embryonic development (Cline and Moore, 1972; Hoeffel and Ginhoux, 2015). During steady state, tissue-resident macrophages have the capacity to renew themselves and support tissue homeostasis through the production of anti-inflammatory signals (Hashimoto *et al.*, 2013). A second type of macrophage is generated from circulating monocytes, which originate from the bone marrow, where rapidly dividing progenitor cells generate monocytes for the release into peripheral blood (Volkman and Gowans, 1965; van Furth and Cohn, 1968). In homeostasis, they can repopulate specific types of tissue-resident macrophages by modifying their chromatin profile to a phenotype that is indistinguishable to macrophages with an embryonic origin (Hashimoto *et al.*, 2013; Mildner, Kim and Yona, 2024). Furthermore, circulating monocytes monitor the vascular system by crawling along endothelial cells and can, during an infection, rapidly emigrate to invade the inflamed tissue (Ebert and Florey, 1939; van Furth and Cohn, 1968; Auffray *et al.*, 2007). This phenomenon is facilitated by specific intracellular or secretory cytokines that are released to signal tissue injury, inflammation, and cell death during a pathogenic state, by which monocytes are recruited through chemotaxis (Truman *et al.*, 2008). In this environment, depending on present transcription factors, monocytes undergo differentiation resulting in monocyte-derived dendritic cells or macrophages with adapted gene expression for phagocytosis and an inflammatory response (Dong *et al.*, 2013; Villar *et al.*, 2023). These macrophages can be arranged on a functional spectrum from pro-inflammatory M1 to anti-inflammatory M2 cells, depending on the context of stimulation (Mills *et al.*, 2000; Austermann, Roth and Barczyk-Kahlert, 2022).

Within the tissue, macrophages are mainly responsible for phagocytosis, inflammation control with cytokines, and antigen presentation for an adaptive immune response (Asano *et al.*, 2011; Murray and Wynn, 2011; Guan *et al.*, 2025). In detail, pathogens are recognized via PAMPs for phagocytosis and subsequent degradation through hydrolases and reactive oxygen species, which allows the metabolic recycling of bacterial components (Mechnikov, 1988; Herb and Schramm, 2021; Lesbats *et al.*, 2025). However, the predominant function of bacteria processed in endolysosomes is the generation of antigens, which are presented on MHC II to lymphocytes of the adaptive immune response (Brancewicz *et al.*, 2025). During these bacterial infections, macrophages secrete pro- and anti-inflammatory cytokines, chemokines, and complement factors which can recruit additional immune cells and modulate the local immune response (Arango Duque and Descoteaux, 2014). The diverse roles of macrophages are a testimony for their significance within the innate immune response, thereby making them the primary focus of this work.

To study the complex behavior of macrophages within the innate immune response, different cellular models are available. This includes primary cells from various species and tissues, as well as immortalized cell lines, which have the advantage of their indefinite lifespan and more straightforward cultivation requirements (Ding *et al.*, 2025). For the purpose of this work, the B cell Leukemia C/EBPαER Clone 1 (BLaER1) cell line was selected as the most suitable model for human macrophages. The B cell line was generated in 2013 from the B cell precursor leukemia cell line RCH-ACV and can be transdifferentiated to a macrophage-like phenotype due to a lentiviral transduction with the C/EBPα transcription factor (Rapino *et al.*, 2013, 2017). It was previously established that C/EBP can induce the conversion of B cells to macrophages by inhibiting lymphoid processes, accompanied by increasing expression of myeloid genes, which results in a complete transdifferentiation (Xie *et al.*, 2004; Bussmann *et al.*, 2009). The generation of a cell line exhibiting an inducible macrophage-like phenotype was achieved through the fusion of the transcription factor with a domain of the estrogen receptor, resulting in a C/EBPα-ER-IRES-GFP construct, which facilitated nuclear translocation upon estrogen-stimulation (Rapino *et al.*, 2013; Gaidt *et al.*, 2018). Consequently, treatment of proliferative BLaER1 B cells with estradiol, macrophage colony-stimulating factor (M-CSF), and interleukin (IL)-3, led to transdifferentiation to post-mitotic macrophages within seven days (Gaidt *et al.*, 2018). Thereafter, cells show a stable phenotype characterized by adherent growth and phagocytotic capacity, accompanied by the expression of macrophage surface markers and a transcriptome that closely resembles primary macrophages (Rapino *et al.*, 2013; Schüssler *et al.*, 2023).

This approach allows infection studies with bacterial pathogens that naturally target macrophages, such as *Legionella pneumophilia* or *Leishmania major*, as well as viral infections by the human immunodeficiency virus HIV (Klatt *et al.*, 2023; Schüssler *et al.*, 2023; Volkmar *et al.*, 2024). From a functional standpoint, the BLaER1 macrophage model facilitates the examination of complex immunological signaling pathways, including inflammasome activation in response to TLR4 stimulation (Gaidt *et al.*, 2016). Also TLR7 and TLR8 signaling was shown in BLaER1 macrophages, as previously demonstrated by cytokine secretion following stimulation with receptor-specific ligands (Wegner *et al.*, 2021). Furthermore, the proliferative B cell state of BLaER1 allows the performance of Clustered regularly interspaced short palindromic repeats-CRISPR-associated protein 9 (CRISPR-Cas9) single gene or screening library knockouts (Arnan *et al.*, 2022a). In summary, BLaER1 macrophages are a suitable model for studies of the innate immune response due to their phenotype, transcriptome, and immunological signaling pathways that are analogous to those of primary cells. Additionally, their genetic editability gives them clear advantages over other cell models.

Toll-like receptors

The innate immune system in vertebrates uses PRR for the detection of non-self PAMPs (Janeway, 1989b). Also, according to the danger theory, the detection of threats can be expanded to include the distinction of dangerous self- and non-self antigen signals (Matzinger, 1994, 2002). This mechanism enables immune cells to identify both endogenous DAMPs, such as molecules released from damaged cells, and exogenous PAMPs, which refer to conserved structures of microorganisms, such as LPS (Poltorak *et al.*, 1998; Janeway and Medzhitov, 2002; Chen *et al.*, 2025). The detection of PAMPs and DAMPs relies on PRRs, which comprise multiple families of receptors capable of binding specific ligands for the activation of intracellular signaling pathways to initiate an appropriate immune response (Li and Wu, 2021). These families include, for instance, retinoic acid inducible gene I-like receptors (RLRs), which sense viral RNA in the nucleus and cytoplasm of infected cells (Liu *et al.*, 2018). Another example are C-type lectin receptors (CLRs), a diverse family of receptors characterized by a carbohydrate-binding domain, which detect PAMPs as well as DAMPs to sense cell death and elicit an appropriate immune response (Scur *et al.*, 2023).

However, the first discovered PRRs belong to the family of TLRs. TLRs are transmembrane proteins with an ectodomain in the shape of a horseshoe, which is comprised of leucine-rich repeats and is responsible for binding ligands (Gao and Li, 2017). In 1995, it was postulated that the *Toll* gene in *Drosophila melanogaster* plays a role in antibacterial responses (Rosetto *et al.*, 1995). Subsequently, a human *Toll* homologue was found to have the capacity to activate the nuclear factor kappa-light-chain-enhancer of activated B cells (NF-κB) pathway, which triggers the production of inflammatory cytokines (Medzhitov, Preston-Hurlburt and Janeway, 1997). Of the ten human TLRs that have been identified, the majority is expressed in phagocytes of the immune system, while some TLRs were detected in all tissues examined, showing the ubiquitous presence of the TLR family (Zarember and Godowski, 2002). In a subcellular context, TLRs localize to the cell surface, as well as to specific intracellular compartments, including endosomes and lysosomes (Latz *et al.*, 2004; Lee and Barton, 2014). While the TLR1, TLR2, TLR4, and TLR5, which are localized on the cell surface, mainly detect pathogenic lipids and proteins, the endosomal TLR3, TLR7, TLR8, TLR9 and TLR13 are activated by foreign nucleic acids (Kawai *et al.*, 2024).

An early study showed that TLR4 on the cell surface detects LPS in mammals using a TLR4-deficient mouse model that did not respond to LPS stimulation, which made the model highly susceptible to infection with Gram-negative bacteria (Coutinho and Meo, 1978; Poltorak *et al.*, 1998). The detection of protein-PAMPs was demonstrated for TLR5, which is activated by binding to the conserved bacterial flagellin to protect organisms against infection (Hayashi *et al.*, 2001). TLR3 is an example of an endosomal PRR that detects nucleic acids, which is activated by double-stranded RNA (dsRNA) that can be generated during viral infection or stem from damaged tissue which had been phagocytosed (Alexopoulou *et al.*, 2001; Karikó *et al.*, 2004). Furthermore, TLR7 and TLR8

are both activated by single-stranded RNA (ssRNA); while TLR8 is primarily expressed in primarily in monocytes, TLR7 is found in dendritic cells and B cells, which suggests complementary functions (Hornung *et al.*, 2002; Heil *et al.*, 2004a). For the majority of TLRs, ligand binding leads to receptor dimerization, which subsequently activates the intracellular Toll/IL-1 receptor homology signaling domain and the downstream signaling cascade that mainly involves the myeloid differentiation primary response protein 88 (MyD88) (Akira and Takeda, 2004; Gao and Li, 2017). This process ultimately activates signaling pathways, such as NF-κB, which induce the expression of type I interferon (IFN) or pro-inflammatory cytokines and consequently lead to the generation of an adaptive immune response (Cai *et al.*, 2013; Duan *et al.*, 2022).

Bacterial RNA detection in macrophages

Upon crossing the initial physical and chemical barriers, bacterial pathogens can be recognized directly by the PRR of the innate immune response (Figure 1). In the case of macrophages, the binding of ligands to TLRs induces a signaling cascade causing significantly higher phagocytotic activity towards bacteria (Doyle *et al.*, 2004). Phagocytosis is defined as internalization of particles larger than 0.5 µm in a phagosome, which involves the activation of surface receptors, reshaping of the actin cytoskeleton, and the uptake of bacteria (Aderem and Underhill, 1999; Li and Underhill, 2025). In addition to phagocytosis, clathrin-dependent endocytosis and macropinocytosis are alternative mechanisms of the endocytic pathway for the uptake of bacterial particles (Doherty and McMahon, 2009; Li *et al.*, 2019). Subsequently, the resulting endosomes mature by fusion with endocytic vesicles including lysosomes, which generates endolysosomes, wherein bacteria are degraded in an acidic milieu through protease, lipase, and nuclease activity (Flannagan, Jaumouillé and Grinstein, 2012; Luzio *et al.*, 2014). This degrades bacterial structure and therefore facilitates the release of nucleic acids into the endolysosomal lumen, which enables the detection of bacterial RNA while reducing the exposure to self-RNAs, that could otherwise lead to autoimmune reactions (Barton and Kagan, 2009). The detection of bacterial RNA itself is significant evidence for the presence of viable bacteria, consequently it is regarded as viability-associated PAMP that elicits a specific innate and adaptive immune response, which is not triggered by the presence of dead bacteria (Sander *et al.*, 2011).

Endolysosomes contain various TLRs for sensing nucleic acids, including TLR3 for dsRNA, TLR7 and TLR8 for ssRNA, and TLR9 for unmethylated CpG motifs in DNA (Dalpke and Helm, 2012; Lin *et al.*, 2025). Macrophages predominantly express TLR8, which exhibits a substantial increase in expression following bacterial stimulation (Hornung *et al.*, 2002; Zarember and Godowski, 2002). TLR8 facilitates the efficient detection of endolysosomal bacterial RNA and, in the context of *Streptococcus pyogenes* and *Streptococcus aureus* infection, it is the predominant stimulus that leads to macrophage cytokine production (Bergstrøm *et al.*, 2015; Eigenbrod *et al.*, 2015).

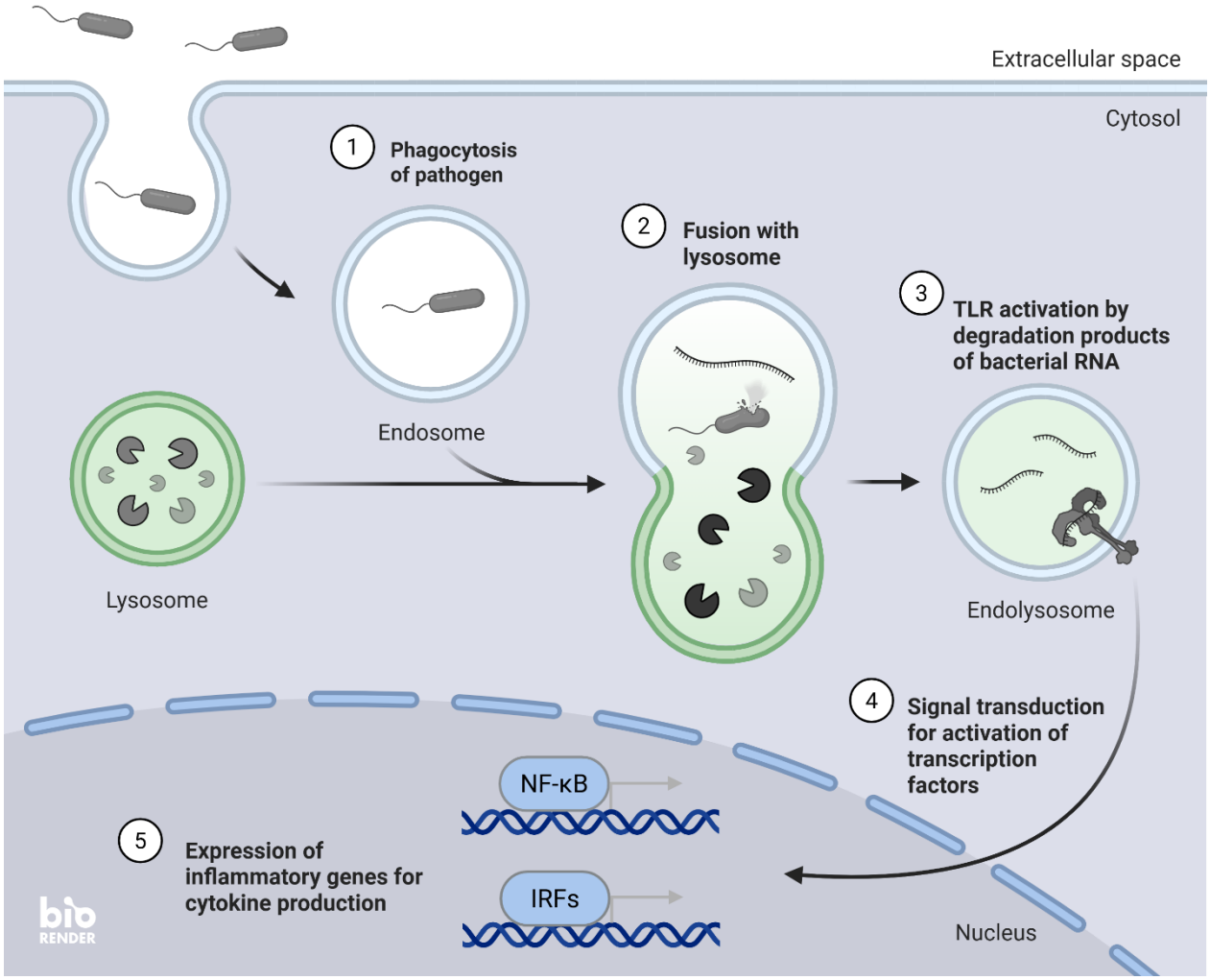

Figure 1: Innate immune response to pathogenic RNA. The phagocytosed pathogen is degraded in an endolysosomal compartment for the release of RNA, which is recognized by TLRs. This causes the activation of transcription factors to produce inflammatory cytokines. Figure was created with BioRender.com.

Notably, TLR8 activation requires synergistic binding of two distinct ssRNA degradation products within specific binding pockets, namely uridine mononucleosides and short oligonucleotides (Tanji *et al.*, 2015). Subsequent studies have revealed that bacterial RNA is digested into stimulatory fragments by the endoribonucleases RNase2 and RNaseT2 within the endolysosome, thereby allowing receptor binding (Greulich *et al.*, 2019; Ostendorf *et al.*, 2020). However, the stimulatory capacity of specific oligoribonucleotides was still maintained in PBMCs lacking both RNase2 and RNaseT2, suggesting the involvement of additional endolysosomal RNases (Ostendorf *et al.*, 2020). An intriguing candidate for this is RNase6, which exhibits high expression in human monocytes comparable to the levels of RNase2 and RNaseT2 (Rosenberg and Dyer, 1996; Tong *et al.*, 2023). Furthermore, RNase6 shows activity as antimicrobial peptide, enhancing the efficiency of bacterial inactivation in macrophages (Becknell *et al.*, 2015; Ruiz-Rosado *et al.*, 2023). These

findings indicate a function of RNase6 in the antimicrobial defense, which may occur upstream of TLR8 activation in macrophages.

Following RNase-mediated RNA degradation, short ssRNA fragments bind to the allosteric site of the inactive TLR8 dimer, which increases the affinity of the first binding pocket for uridine (Tanji *et al.*, 2015). Uridine binding induces the activated form of the TLR8 dimer, in which the Toll-IL-1 receptor homology domains are brought together (Tanji *et al.*, 2013, 2015). The cytosolic region of TLR8 binds the adapter protein MyD88, which recruits several members of the Interleukin-1 receptor associated kinase (IRAK) family to form a signaling complex known as myddosome (O'Neill, 2003; Balka and De Nardo, 2019). Furthermore, Toll-interleukin 1 receptor domain-containing adaptor protein (TIRAP) is recruited to the Myddosome and activates downstream kinases for a signal transduction towards the nucleus (Nilsen *et al.*, 2022). This includes the MAPK, NF-κB, and interferon pathways for the activation of transcription factors leading to the expression of pro-inflammatory cytokines and type I IFNs (Bian *et al.*, 2023; Matziol *et al.*, 2025). In addition, TLR8 stimulation activates the formation of an NOD-like receptor pyrin domain containing 3 (NLRP3) inflammasome complex, which in turn leads to further production of pro-inflammatory cytokines, thereby supporting an appropriate immune response (Dietsch *et al.*, 2016; Bian *et al.*, 2023).

Impact of RNA modification on immune stimulation

The study of RNA modifications began in the 1950s with the discovery of previously unidentified nucleosides, including a phosphorylated RNA nucleoside and 5-methylcytosine, marking the beginning of a novel field in RNA research (Cohn and Volkin, 1951; Davis and Allen, 1957; Amos and Korn, 1958). Within the field of epitranscriptomics, a list of more than 170 RNA naturally occurring and artificially synthesized modifications is currently available in databases for biochemical, structural and functional information, documenting modifications found in all domains of life (McCown *et al.*, 2020; Sordyl *et al.*, 2026). RNA modifications are diverse chemical alterations on the RNA nucleotide ribose moiety or base, which are installed by writer proteins, recognized by reader proteins for their specific function, and removed by eraser proteins (Meyer and Jaffrey, 2017; Ontiveros, Stoute and Liu, 2019). RNA modifications themselves have been shown to affect base pairing and secondary RNA structure, as evidenced by the stabilization of base stacking by pseudouridine (Davis, 1995; Helm, 2006). The number and type of RNA modifications is highly dynamic, as it was found that stressed cells inhibit rRNA modifications and thereby slow ribosome formation as a protective mechanism (Szaflarski *et al.*, 2021). The epitranscriptome can also influence gene expression on various levels, such as co-transcriptional base methylations that affect mRNA processing, or heavily modified tRNAs allowing translation (Delaunay, Helm and Frye, 2024).

RNA Modifications have been identified in all three domains of life, with a high prevalence of modified nucleotides in tRNA and rRNA (Arzumanian *et al.*, 2022). However, the quantity of nucleic acid modification differs between various organisms. This includes the methylation of CpG dinucleotides typical for mammalian DNA; however, most prokaryotic genomes lack this modification, and therefore are recognized as non-self DNA by TLR9 (Hemmi *et al.*, 2000). The majority of RNA modifications show different quantities between eukaryotes and prokaryotes. For instance, human rRNA was found to have notably higher percentages of modified nucleotides compared to *E. coli* rRNA (Bachellerie and Cavaillé, 1998; Motorin and Helm, 2011). Accordingly, subsequent studies identified mechanisms that allowed the differentiation of self and non-self RNA, as shown for the detection of microbial RNA without endogenous modifications by TLRs of the innate immune response (Freund *et al.*, 2019). The initial evidence for this phenomenon was observed in human monocyte-derived dendritic cells, which were exposed to oligoribonucleotides containing single nucleotides with 2'-O-methylation (2'-O-me, also known as Nm), 5-methylcytodine, or pseudouridine, in contrast to an unmodified control (Karikó *et al.*, 2005). This resulted in robust tumor necrosis factor (TNF) secretion from unmodified RNA, while modified counterparts suppressed the stimulation of TLR, thereby supporting the hypothesis that non-self RNA recognition is facilitated not only through subcellular localization but also by nucleoside modification (Karikó *et al.*, 2005; Sioud, 2006).

The RNA modification of interest for this work is 2'-O-me, a methylation at the 2'-hydroxyl group of the ribose moiety found in RNA independent of the base (Schibler and Perry, 1977; Zhou, Pecot and Holley, 2024). Consequently, 2'-O-me does not disrupt canonical base pairing and has been shown to stabilize RNA duplexes, modulate the secondary structure of RNA, and influence the RNA affinity for protein binding (Zhou, Pecot and Holley, 2024). These properties enable 2'-O-me to exhibit central functions within various RNA species. In rRNA, 2'-O-me accounts for over 50 % of all modified nucleotides and is essential for the assembly of ribosomal subunits, for the stabilization of the 3'-endo confirmation in nucleotides within the ribonucleoprotein, and for the generation of heterogeneous rRNA for adapted ribosome activity in diverse settings (Natchiar *et al.*, 2018). Additionally, in tRNA, 2'-O-me stabilizes RNA structure and facilitates the interaction between codon and anticodon during translation, while 2'-O-me in the mRNA 5' cap functions as quality control mechanism and to prevent mRNA degradation (Höfler and Carlomagno, 2020). Regarding immune recognition, studies revealed that 2'-O-me in the cap structure of viral mRNA interfered with the antiviral response by modulating type I interferon signaling, thereby enabling evasion of the innate immune response (Daffis *et al.*, 2010; Züst *et al.*, 2011). A comparable effect was identified in bacteria, where a single 2'-O-me on tRNAs in a natural sequence context was found to cause suppressed TLR7 immunostimulation in innate immune cells (Gehrig *et al.*, 2012a; Jöckel *et al.*, 2012). In monocytic cells, the inhibitory effect of 2'-O-me relied on TLR8 in specific sequence context of synthesized oligoribonucleotides or in bacterial tRNA (Rimbach *et al.*, 2015; Schmitt *et al.*, 2017).

Collectively, nucleotide modifications are an important factor for the detection of non-self RNA within the innate immune response. While 2'-O-me affects the recognition of bacterial RNA through TLR, the specific molecular mechanisms underlying the inhibition of TLR signaling in response to 2'-O-me remain to be identified.

Orthoebolavirus outbreaks

BLaER1 cells are an ideal model for examining pathogens that demonstrate a natural tropism towards myeloid cells and allow the examination of the human innate immune response. This includes the *Orthoebolavirus zairense,* also known as Ebola virus (EBOV), which belongs to the family of *Filoviridae* that includes the genera of *Orthomarburgvirus* and *Orthoebolavirus,* among others (Biedenkopf *et al.*, 2023). As previously demonstrated, orthoebolaviruses have the capacity to infect and replicate within human primary monocytes and macrophages, thereby confirming their permissiveness (Ströher *et al.*, 2001). The Marburg virus (MARV) caused the first documented outbreak of filoviral disease in 1967 in Germany and Serbia at three different institutions through direct contact with monkey samples, resulting in 32 cases and seven fatalities (Slenczka, 2017). The infections were characterized by fever, headache, and gastrointestinal symptoms, but also hemorrhagic signs, such as hematemesis and bloody diarrhea in more severe cases, which led to an overall case fatality rate of over 70 % out of the 722 reported cases until 2024 (Pisapia *et al.*, 2025).

Other Filoviruses, such as orthoebolaviruses, can lead to Ebola virus disease (EVD) characterized by severe hemorrhagic fever and have caused numerous epidemic outbreaks predominantly on the African continent since 1976, but also in the United Kingdom, the United States of America, and Italy (Mahanty and Bray, 2004; Mohd *et al.*, 2024). These outbreaks are primarily attributed to the human pathogenic species EBOV, which was originally found in Zaire, now known as the Democratic Republic of the Congo, and to *Orthoebolavirus sudanese*, also referred to as Sudan virus (SUDV), that was first detected in Sudan (*Bulletin of the World Health Organization*, 1978b; *Bulletin of the World Health Organization*, 1978a; Cheng *et al.*, 2025a). The most probable natural reservoirs of the zoonotic EBOV are bats, which are asymptomatic during infection, but can cause spillover events that result in human index cases (Leroy *et al.*, 2005; Schuh, Amman and Towner, 2017). The transmission between humans occurs through exposure to bodily fluids from or direct physical contact with symptomatic or deceased patients (Osterholm *et al.*, 2015; Lawrence *et al.*, 2017). A total of over 30,000 cases of EVD have been reported until 2016, resulting in more than 12,000 fatalities, which includes the most significant outbreak classified as an EBOV epidemic in West Africa from 2013 to 2016 with over 28,000 cases (Shultz *et al.*, 2016). Subsequent outbreaks were documented until December 2025, when the 16th outbreak in the Democratic Republic of the Congo was declared over after 64 cases over the course of seven weeks (*Disease Outbreak News; Ebola virus disease in the Democratic Republic of the Congo*, 2025).

In summary, Filovirus and particularly EBOV outbreaks pose a significant threat to public health, as they have been responsible for widespread disease, often resulting in fatal outcomes over the past decades. However, one recombinant vaccine containing the EBOV GP is currently recommended as it shows a high level of protection against EVD and reduces the risk of fatality by half (Henao-Restrepo *et al.*, 2015; Coulborn *et al.*, 2024). While these findings show promising progress in the mitigation of EVD, a comprehensive understanding of the underlying molecular mechanisms within the virus and the host defense remains essential for the continued development of effective preventive and therapeutic interventions.

EBOV structure and life cycle

EBOV particles were initially identified during the first outbreak of EVD in Zaire and were found to present with a filamentous morphology characteristic for Filoviruses (Figure 2, Bowen *et al.*, 1977; Pattyn *et al.*, 1977). The virus is enveloped in matrix proteins which contain a nucleocapsid made of the genome and viral proteins in a helical shape, such that the viral particle has a length of around one micrometer (Bharat *et al.*, 2012). The negative-stranded RNA genome itself is organized with a non-coding leader and trailer sequence, between which the open reading frames for nucleoprotein (NP), viral protein 35 (VP35), viral protein 40 (VP40), glycoprotein (GP), viral protein 30 (VP30), viral protein 24 (VP24), and for RNA-dependent RNA polymerase (L) are encoded (Sanchez *et al.*, 1993). NP and the ssRNA genome form a condensed helical structure, that is bound by the accessory polymerase cofactor VP35, transcriptional activator VP30, and polymerase L (Bodmer, Hoenen and Wendt, 2024). This generates the ribonucleoprotein complex, which is further condensed by VP24 to form the nucleocapsid (Bodmer, Hoenen and Wendt, 2024). It is surrounded by the VP40 matrix layer and the viral membrane, which contains $GP_{1,2}$ trimers (Sanchez *et al.*, 1998; Martin *et al.*, 2016). The soluble GP (sGP) dimer is generated from the same open reading frame (ORF) by transcriptional editing through polymerase stuttering at a poly-U repeat in 70 % of transcriptions, which is secreted from the infected host cell (Sanchez *et al.*, 1996; Martin *et al.*, 2016).

The interplay among the viral genome, proteins, and host cells during the infection process can be illustrated clearly through the EBOV life cycle (Bodmer, Hoenen and Wendt, 2024). The entry of EBOV into a host cell is initiated by attachment to surface proteins, such as lectins, via the $GP_{1,2}$, leading to the uptake through macropinocytosis for bringing the virus towards the endolysosomal pathway (Saeed *et al.*, 2010; Dahlmann *et al.*, 2015). The endosome is acidified by the host cell, which supports $GP_{1,2}$ cleavage by cathepsins and allows binding to the host receptor Niemann-Pick C1 receptor (NPC1) for fusion of the viral and host membrane (Chandran *et al.*, 2005; Wang *et al.*, 2016; Das *et al.*, 2020). This process releases the nucleocapsid into the cytoplasm, facilitating the VP24 dissociation, and inducing the relaxation of the densely packed ribonucleoprotein (RNP) complex (Watt *et al.*, 2014). That enables the primary transcription of

viral RNA by L supported by the provided NP, VP35, and VP30, and followed by translation through host ribosomes to generate viral proteins within two hours of infection (Hoenen *et al.*, 2013; Bodmer, Hoenen and Wendt, 2024). To enhance the efficiency of transcription, the oligomerization of NP promotes the formation of inclusion bodies, which are membrane-less organelles that arise from liquid-liquid phase separation that contain the necessary viral and host proteins (Dolnik, Gerresheim and Biedenkopf, 2021; Bodmer, Vallbracht, *et al.*, 2023). Furthermore, within the inclusion body or viral factory, the viral genome is replicated and secondary transcription of viral ORFs takes place, from which mRNAs are exported to the cytoplasm for translation (Hoenen *et al.*, 2012; Bodmer, Hoenen and Wendt, 2024). The recruitment of L to NP and VP35 decreases the molecular exchange rate in inclusion bodies, thereby allowing the binding of NP to the newly transcribed viral genomes (Fang *et al.*, 2023; Bodmer, Hoenen and Wendt, 2024). This process enables the formation of the nucleocapsid, which is condensed by VP24 and transported individually from the inclusion body towards the plasma membrane using actin-dependent motor proteins (Watt *et al.*, 2014; Schudt *et al.*, 2015). Additionally, the translated VP40 matrix protein is moved along actin fibers towards the inner leaflet of the plasma membrane and assembles at the future budding site (Adu-Gyamfi *et al.*, 2012). For the complete assembly of new viruses, a GP precursor is translated at the endoplasmic reticulum and processed via furin cleavage (Volchkov *et al.*, 1998). Subsequently, $GP_{1,2}$ is transported towards the plasma membrane, most likely through the secretory pathway (Nanbo *et al.*, 2013; Bodmer, Hoenen and Wendt, 2024). At this location, VP40 interacts with the membrane and, supported by $GP_{1,2}$, NP, and VP24, enables the budding of the nucleocapsid to form a new virion (Licata *et al.*, 2004; Adu-Gyamfi *et al.*, 2013).

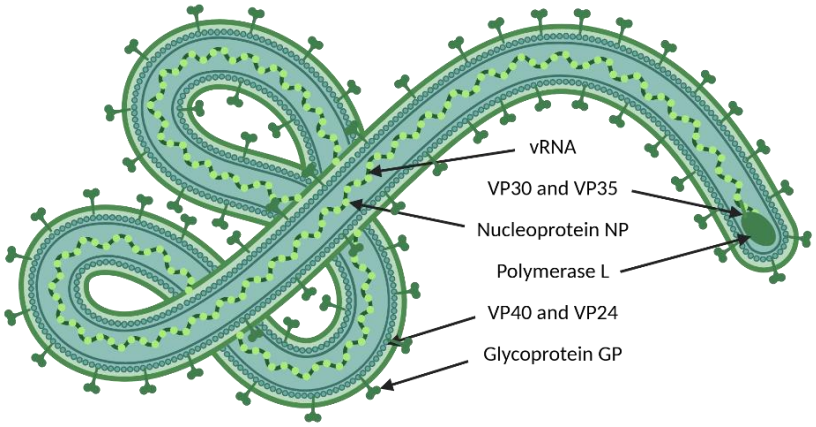

Figure 2: Orthoebolavirus structure. The filamentous virus is structured around the viral RNA (vRNA) with the nucleoprotein (NP), which forms the ribonucleoprotein complex with the viral proteins (VP) VP35, VP30, and polymerase L. This is condensed by VP24 into the nucleocapsid and surrounded by VP40 and the viral membrane with $GP_{1,2}$. Figure was created with BioRender.com.

Immune response to Ebola virus infection

When the described replication of EBOV occurs within a host, the immune system initiates an antiviral response to prevent substantial damage to the organism and to resolve the infection. However, the virus employs various immune evasion mechanisms and exhibits natural tropism for innate immune cells, thereby impeding the resolution of EBOV infection (Bodmer *et al.*, 2025). Subsequent to transmission, the virus is initially detected by tissue macrophages and dendritic cells, which become infected and spread the virus through the lymphatic and vascular systems (Geisbert *et al.*, 2003; Martines *et al.*, 2015). During the infection, PRR of the innate immune response are essential to detect viral structures, which in turn triggers inflammatory and antiviral pathways. This includes the TLR4, which detects EBOV GP and causes the NF-κB-mediated expression of pro-inflammatory cytokines (Okumura *et al.*, 2010). However, this can result in the recruitment of additional EBOV target cells, thereby accelerating the infection and inducing further pathology trough the amplification of the immune response (Hensley *et al.*, 2002; Bray and Geisbert, 2005). This cytokine storm, caused by an overactive innate immune system, frequently results in fatal outcomes (Wauquier *et al.*, 2010; Reynard *et al.*, 2019).

Recognition of viral structures also relies on the cytosolic retinoic acid-inducible gene I (RIG-I) receptor, which detects the viral RNA genome and thereby induces the production of type-I IFN to promote an antiviral state (Pichlmair *et al.*, 2006; Habjan *et al.*, 2008). This process is antagonized by the filoviral VP35, which has the capacity to bind viral RNA, thereby impeding recognition by host PRRs (Cárdenas *et al.*, 2006; Bodmer *et al.*, 2025). In addition, interferon signaling is disrupted by viral proteins such as VP24, which prevents the translocation of the interferon-activated STAT1 transcription factor into the nucleus to inhibit the expression of antiviral genes (Reid *et al.*, 2006; Bodmer *et al.*, 2025). Even in cases where interferon-induced genes are expressed, antagonistic mechanisms interfere with their functionality. An example of this phenomenon is the antiviral protein HECT and RLD Domain Containing E3 Ubiquitin Protein Ligase 5 (HERC5), which has been demonstrated to decrease the number of viral mRNAs, but is antagonized by GP in a still unknown mechanism (Paparisto *et al.*, 2021). Furthermore, the immune system is actively evaded by EBOV, as the secreted sGP are part of an antigenic subversion strategy through sequestering antibodies aimed against $GP_{1,2}$ (Mohan *et al.*, 2012). Finally, GP induces cytotoxicity in endothelial cells, resulting in the disruption of vascular integrity and subsequent hemorrhage, thereby facilitating viral spread (Yang *et al.*, 2000; Zampieri, Sullivan and Nabel, 2007). In summary, the pathogenicity of EBOV can be explained by the tropism of EBOV towards innate immune cells, the various ways to exploit immune mechanisms, and the effective antagonization of the antiviral response.

Non-pathogenic Bombali virus

The genus of orthoebolaviruses contains six species, namely the Bombali virus (BOMV), Bundibugyo virus (BDBV), Reston virus (RESTV), Sudan virus (SUDV), Taï Forest virus (TAFV), and Ebola virus (EBOV) (Biedenkopf *et al.*, 2023). These viruses demonstrate a high degree of evolutionary genome variance, resulting in 73 host-specific amino acid substitution sites within the viral proteins (Cheng *et al.*, 2025b). This accounts for the substantial differences in host tropism and pathogenicity, which ranges from case fatality rates from 70 % for EBOV to BDBV with 33 %, while TAFV was found to cause a single known symptomatic case in humans leading to a full recovery (Formenty *et al.*, 1999; Yamaoka and Ebihara, 2021). This phenomenon could be explained by VP24 and VP35 from highly pathogenic orthoebolavirus species, which exhibit a greater ability to impede the interferon response of the host compared to non-pathogenic viruses (Schwarz *et al.*, 2017; Cao *et al.*, 2023; Ramanathan *et al.*, 2023). Furthermore, the non-pathogenic RESTV GP does not activate TLR4-mediated signaling in comparison to EBOV, a process necessary for NF-κB mediated pro-inflammatory response that supports viral replication (Olejnik *et al.*, 2017).

Recently, novel filoviruses have been discovered that are closely related to EBOV, but either show no human pathogenicity as for RESTV or do not cause any known human infections as BOMV (Groseth and Hoenen, 2024). In 2016, the orthoebolavirus BOMV was discovered in samples from two insectivorous bat species in West Africa, representing a distinct species with an amino acid identity of approximately 70 % compared to other orthoebolaviruses (Goldstein *et al.*, 2018). However, serological studies have identified six people with BOMV GP-specific antibodies in the Democratic Republic of the Congo and Guinea, suggesting a prior exposure to the virus (Goldstein *et al.*, 2020; Hounmenou *et al.*, 2024). Using a recombinant virus, the BOMV GP was demonstrated to facilitate viral entry into human cells dependent on NPC1, thereby supporting the general potential of BOMV to infect humans (Goldstein *et al.*, 2018). The generation of recombinant BOMV was a significant achievement, as there are currently no infectious virus isolates available for study (Bodmer, Breithaupt, *et al.*, 2023). BOMV exhibited a decreased replication efficiency compared to EBOV *in vitro* using monkey and human cell lines (Bodmer, Breithaupt, *et al.*, 2023). Furthermore, a humanized mouse model revealed a fatality rate of 20 % for BOMV, while EBOV infection caused lethality in all mice, thereby validating the significantly lower pathogenicity of the novel virus (Bodmer, Breithaupt, *et al.*, 2023). Furthermore, an inhibitory effect of EBOV VP24 on the expression of interferon-activated genes is well known, while BOMV VP24 did not exhibit this immune suppression which could explain the lower pathogenicity of BOMV (He *et al.*, 2022). In summary, the non- or low-pathogenic orthoebolavirus species BOMV did not cause any documented infections in humans and is therefore an interesting model to explore the pathogenicity of the closely related EBOV.

Research aims

The BLaER1 macrophage model is a useful tool for examining the innate immune response during bacterial or viral infection. This cell line has previously been analyzed in regards to its cellular transcriptome and phenotypical properties (Rapino *et al.*, 2013). Therefore, we aim to characterize the cellular proteome during the transdifferentiation process with a time-resolved dataset using mass spectrometry-based quantitative proteomics. Following the confirmation of a macrophage-like proteome, BLaER1 will be used for the investigation of cellular responses towards RNA stimulation mediated by TLR8. As previously demonstrated, the modification of bacterial RNA with 2'-O-methylation (2'-O-me) inhibits the activation of innate immune pathways upstream of TLR8 through a process that remains to be characterized (Rimbach *et al.*, 2015). Therefore, we will identify RNA-binding proteins (RBP) that demonstrate varying binding affinities to 2'-O-me and unmodified RNA in BLaER1 protein extracts. Subsequently, the generation of BLaER1 CRISPR-Cas9 knockout cells of RBP candidates will be performed to confirm the inhibitory effect. Furthermore, it has been hypothesized that RNA processing by RNase6 is required upstream of TLR8. Therefore, our goal is to confirm the colocalization of RNase6 with endolysosomal proteins known to be involved in TLR8 stimulation using an organelle fractionation approach.

To expand the use of BLaER1 beyond RNA-stimulation experiments to real-life scenarios, the macrophage model will be used for the examination of viral infections. It has been demonstrated that orthoebolaviruses exhibit a natural tropism for macrophages (Martines *et al.*, 2015). However, EBOV exhibits a high pathogenicity, while the closely related BOMV is not known to cause human infections (Bodmer, Breithaupt, *et al.*, 2023). Therefore, a goal of this work is the establishment of biosafety level (BSL) 4-compatible workflows to compare BLaER1 infections with EBOV with those of the closely related BOMV. In doing so, we aim to identify differentially expressed host proteins that may be responsible for the unequal pathogenicity of the viral strains. Furthermore, time-resolved experiments will be conducted with EBOV, elucidating the viral and host proteome, while we will establish a method for the analysis of the secretome during infection. Overall, we will identify novel host proteins involved in EBOV pathogenicity that could serve as targets for the development of antiviral therapeutics.

Results

BLaER1 characterization

Surface markers convert during transdifferentiation

The usage of BLaER1 macrophages required the implementation of a transdifferentiation protocol as previously described, as well as the following cell characterization to ensure the validity of the model (Gaidt *et al.*, 2018). Accordingly, native BLaER1 cells were transdifferentiated from B cells to macrophage-like cells using β-Estradiol, M-CSF and IL-3 for seven days. The conversion of suspended B cells to adherent cells, accompanied by alterations in morphology and the formation of cell protrusions, provided visual evidence for transdifferentiation. Furthermore, flow cytometry was performed daily to study the expression of B cell and macrophage surface markers during that process.

Using forward- and sideward-scatter, singular cells were selected for analysis of a GFP signal (Figure 3A). According to viability staining, dead cells lost the expression of GFP (Supplementary Figure 1). A continuous decrease in the expression of the B cell marker in the main population of cells from day 0 to day 6 was revealed through staining with a fluorescent CD19 antibody (Figure 3B). Simultaneously, the signal from a CD14 macrophage marker increased, moving the cell population toward the lower right quadrant. This suggested a BLaER1 macrophage phenotype. Transdifferentiation-efficiency, defined as the percentage of CD14-positive and CD19-negative macrophage cells, exceeded 94 % after 6 days of BLaER1 treatment with cytokines and β-Estradiol. Interestingly, during the final days of transdifferentiation, a distinct population of cells accumulated in their B cell state in the upper left quadrant (Figure 3C). This suggests that few BLaER1 B cells resisted β-Estradiol-mediated transdifferentiation.

To examine the proportion of CD19-positive and CD14-negative B cells, as well as CD19-negative and CD14-positive macrophages directly, the percentage of each cell population was compared over time (Figure 3D). This revealed the rapid surface marker conversion around day 2 and showed only minor shares of non-monocytic cells from days 4 to 7. However, following day 5, the percentage of CD19+ CD14- B cells increased slightly, while double negative and double positive cells decreased or stagnated at low levels. Due to these observations, the BLaER1 transdifferentiation was concluded to be successful for the generation of monocytic cells within 4 days. Furthermore, flow cytometry analysis supported the successful transdifferentiation of BLaER1 within larger cultivation plates to achieve a higher cell yield for later protein extractions.

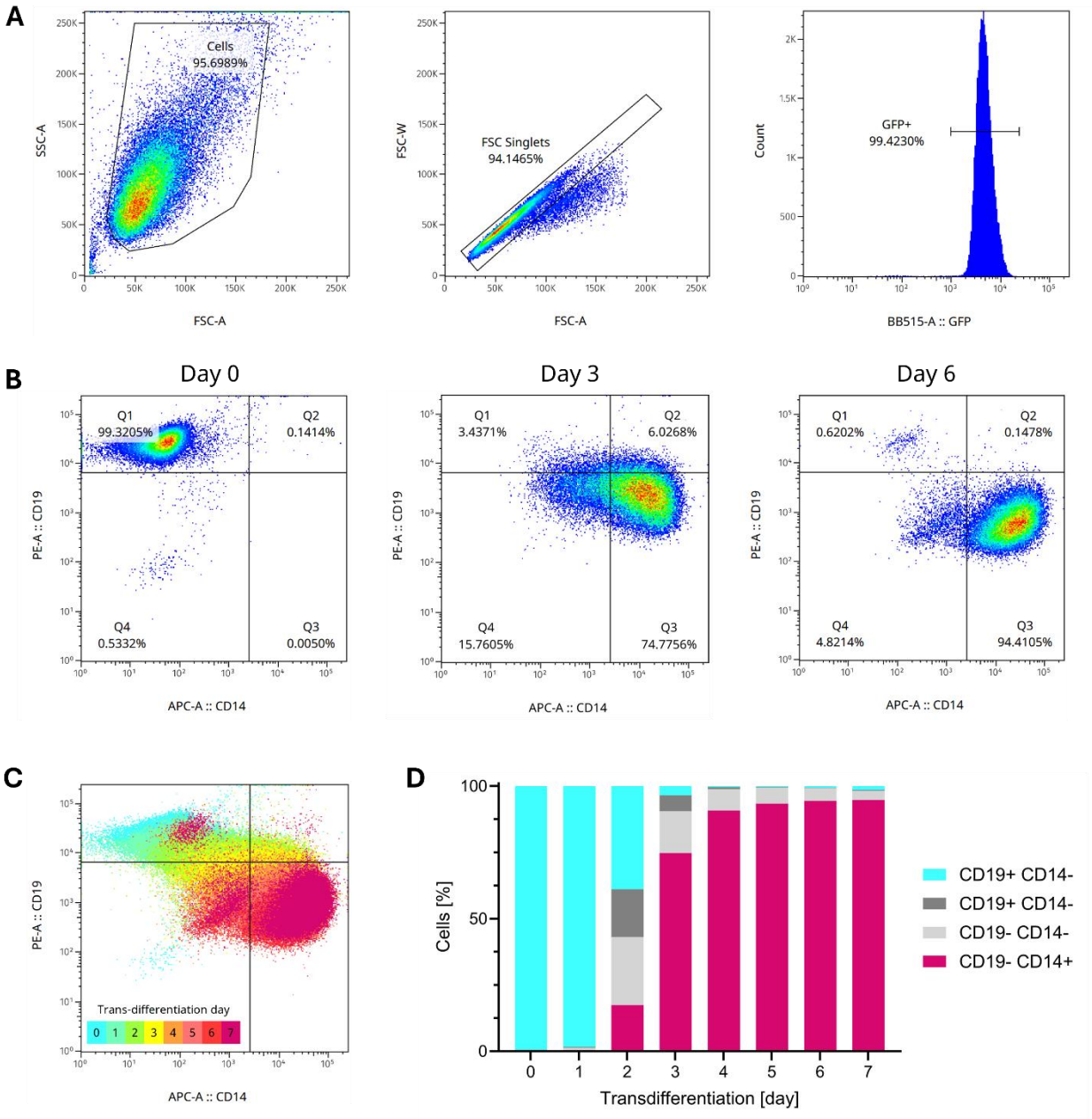

Figure 3: BLaER1 transdifferentiation analysis by flow cytometry. BLaER1 cells were transdifferentiated over seven days to detect cell type-specific surface markers. (A) Representative gating strategy for analysis of BLaER1 to select singular cells with GFP expression using the sideward scatter area (SSC-A), forward scatter width (FSC-W) and -area (FSC-A). (B, C) Detection of the B cell marker CD19 with PE and macrophage marker CD14 with APC fluorescence in GFP-positive cells over the seven-day transdifferentiation period for an exemplary timepoint (B) and for all timepoints (C). (D) Time course of proportionate B cell and macrophage marker expression during transdifferentiation.

Proteomes show transdifferentiation within 4 days

To the best of my knowledge, the literature so far focuses on transcriptome and functional investigations (Rapino *et al.*, 2013; Arnan *et al.*, 2022a), while the in-depth analysis of BLaER1 proteomes was still pending. Therefore, during transdifferentiation, the cellular proteome was examined to further characterize the BLaER1 cell line. For this purpose, BLaER1 cells were transdifferentiated and cell samples were collected over 7 days using an sodium lauryl sulphate (SDS)-based lysis protocol, as described for collecting viral infection samples. The samples were processed using single-pot solid-phase-enhanced sample preparation (SP3) for label-free LC-MS/MS measurements and MaxQuant data analysis. Quality controls in RStudio revealed consistent signal intensities across all samples and a low ratio of imputed to measured values as expected. After conducting a principal component analysis (PCA), the clear clustering of the quadruplicate samples along PC1, which accounted for nearly half of the total data variance, suggested distinct BLaER1 proteomes for each timepoint. (Figure 4A). Similar to the previous flow cytometry results, the PCA of BLaER1 proteomes revealed the greatest cellular changes around day 2 of transdifferentiation. Interestingly, the continuous cell development along principal component (PC) 1 was interrupted by samples from day 7. All replicates from this day clustered together to show a trend along PC2 compared to other samples, which implies changes in the global proteome after 7 days.

To analyze the BLaER1 proteomes in more detail, the expression of B cell and macrophage marker proteins was examined based on genes that were previously used as transdifferentiation markers (Rapino *et al.*, 2013). The average LFQ values for B cell markers decreased continuously over time, falling below the limit of detection around day 4, after which they were imputed (Figure 4B**,** Supplementary Figure 2A). Macrophage markers behaved in the opposite way. They could not yet be detected on day 0, but afterwards, most marker proteins increased in expression after day 2 of transdifferentiation (Figure 4C, Supplementary Figure 2B). Although the amount of matrix metalloproteinase-9 (MMP9) declined unexpectedly after the initial measurement on day 2, the average LFQ value of the macrophage markers still increased over time, indicating an effective transdifferentiation. Furthermore, TLR7 and TLR8 were only detected in BLaER1 proteomes after day 4 of transdifferentiation (Supplementary Figure 2C).

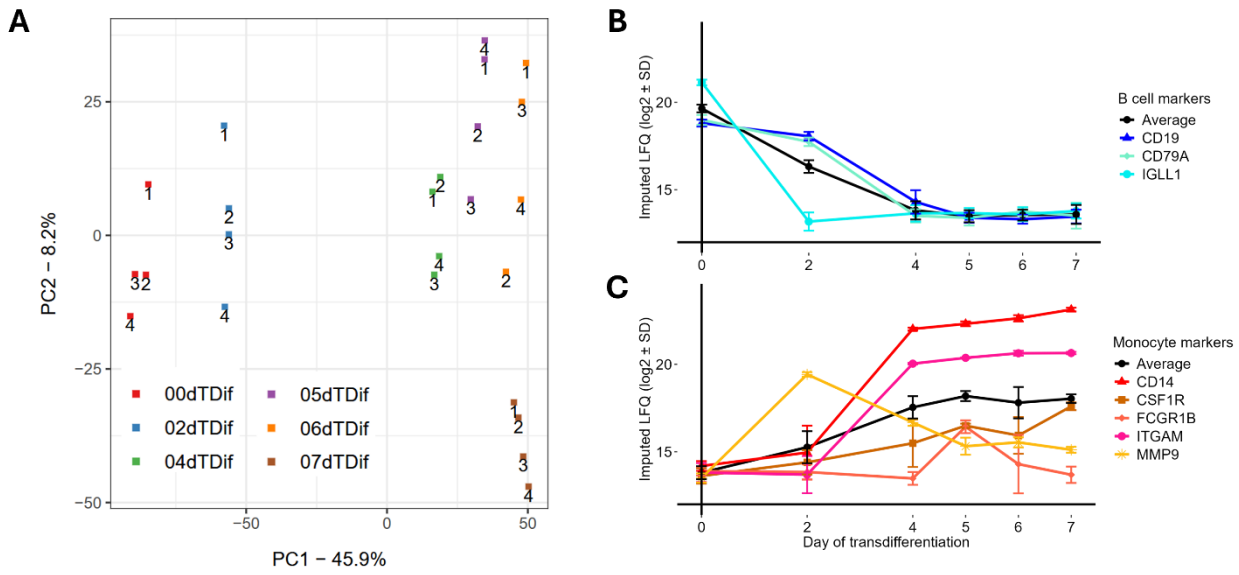

Figure 4: The BLaER1 proteome during transdifferentiation. BLaER1 cells were transdifferentiated to analyze quadruplicate cellular proteomes over time. (A) Principal component (PC) analysis of proteome samples from day 0 (00dTDif) to day 7 (07d TDif). (B, C) Imputed $\log_2$ label-free quantification (LFQ) values of B cell (B) and macrophage markers (C) with average values ± SD.

Influence of 2'-O-me on Immune Stimulation

RNase6 is localized in the endolysosome

During infection, bacterial RNA is digested by nucleases such as RNase2 and RNaseT2, which enables the recognition of oligoribonucleotides by TLRs of the innate immune response (Greulich *et al.*, 2019). However, the involvement of additional endolysosomal RNases was demonstrated by the remaining stimulatory capacity of specific RNAs in cells lacking RNase2 and RNaseT2 (Ostendorf *et al.*, 2020). To identify potentially involved RNases or further RBPs, monocytic BLaER1 organelles were separated by density to find protein candidates in the endolysosomal compartment via LC-MS/MS (Figure 5A). Therefore, the BLaER1 cells were transdifferentiated into a macrophage-like state and lysed by shear stress using a Dounce homogenizer. The resulting post-nuclear supernatant (PNS) was fractionated via ultracentrifugation in a discontinuous sucrose gradient to separate organelles by density. This process resulted in two distinct organelle bands between sucrose cushions, while some cellular material remained on top of the gradient (Figure 5B). Fractions were collected from lowest to highest density and were pooled from two gradients.

Sample processing was performed via in-gel protein digestion for analysis by LC-MS/MS to identify, quantify, and annotate proteins to subcellular compartments for each fraction. Gene ontology analysis using ShinyGO (Ge, Jung and Yao, 2020) allowed the quantification of proteins from specific organelles relative to the PNS. To assess the distribution of organelles in the gradient, the average iBAQ value from all proteins included in the cellular components term for the

mitochondrial proton-transporting ATP synthase complex (GO:0005753) and endolysosome (GO:0036019) was calculated. Endolysosomal proteins were enriched in fraction 3 to 140 %, while mitochondria were enriched to 740 % in fraction 5 compared to the PNS (Figure 5C). To draw conclusions on the distribution of proteins involved in TLR-mediated RNA stimulation, enrichment of specific TLRs and RNases was assessed as well. This revealed an enrichment of TLR7 and TLR8, especially in fraction 3, which also contained the highest amounts of RNase6 and RNaseT2 (Figure 5D). Meanwhile, RNase2 was not detected in any fraction.

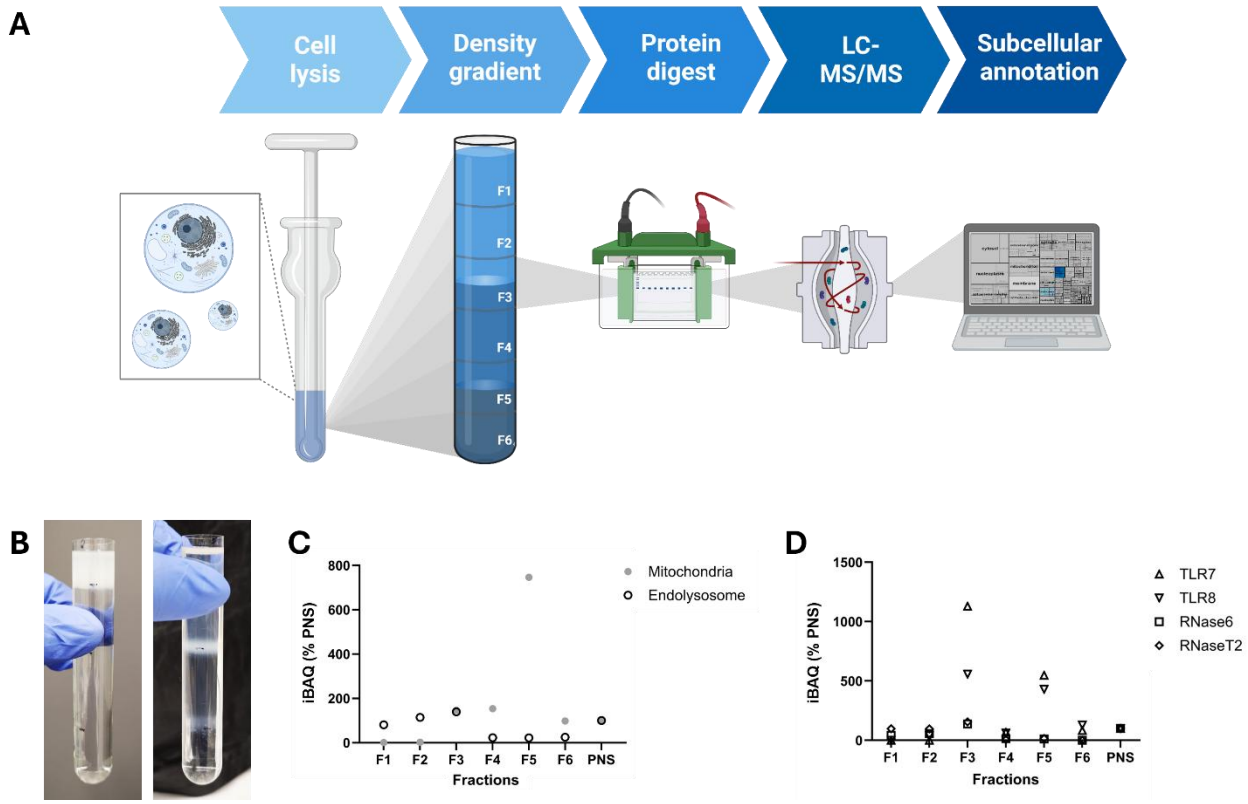

Figure 5: Fractionation of subcellular organelles. (A) Workflow for the separation of BLaER1 organelles by density for proteome analysis to determine the subcellular localization of proteins. (B) Representative images of sucrose density gradients with post-nuclear supernatant (PNS) before (left) and after (right) ultracentrifugation. (C, D) The fractions F1 – F6 from two pooled gradients were analyzed by LC-MS/MS to identify proteins and determine the intensity-based absolute quantification (iBAQ) values. Following normalization to the post-nuclear supernatant (PNS), the amount of marker proteins in mitochondria or endolysosomes (C), and the amount of proteins of interest (D) are shown for Fraction 1 – 6 (F1 – F6). Figure (A) was created with BioRender.com.

Binding of TRMT61A depends on 2'-O-me

To validate RNase binding and identify additional RBPs involved in RNA processing prior to TLR-binding, RNA pull-down experiments were performed. Following a density gradient, the dialyzed endolysosome-enriched protein extract from fraction 3 was used as the protein sample to focus

on RNPs that should be physiologically present at the subcellular site of interest. Since the activation of TLRs is known to be suppressed by the presence of 2'-O-methylation (2'-O-me) in foreign RNA (Gehrig *et al.*, 2012b; Jöckel *et al.*, 2012), biotinylated RNA baits containing this modification (Figure 6A) were used to identify 2'-O-me-specific binders relevant to this stimulatory pathway. As control condition, pull-down experiments with the same RNA sequences lacking the 2'-O-me modifications were conducted. After determining the ideal RNA bait concentration for the magnetic streptavidin beads (Supplementary Figure 3), the identification and quantification of RBPs was achieved through pull-downs by LC-MS/MS analysis. For the endolysosome-enriched protein extract, no significantly enriched specific RNA-binders for unmodified RNA40 or 2'-O-methylated RNA40mod were revealed, even though more proteins bound to the unmodified bait overall (Figure 6B). Therefore, pull-downs were performed using the complete PNS protein extract from transdifferentiated BLaER1 cells. This revealed an over 2-fold significant enrichment of the tRNA methyltransferase 61A (TRMT61A) and Gene for bifunctional aminoacyl-tRNA synthetase (*EPRS*) on unmodified RNA compared to the modified counterpart (Figure 6C). Furthermore, TRMT6, which assembles in a heterotetramer with TMRT61A to form a tRNA methyltransferase complex (Ozanick *et al.*, 2005) was identified just beyond the cutoff for proteins that are statistically significantly enriched on the RNA40 side. On the other hand, Dynein light chain (DYNLL1/ DYNLL12) protein was found to be enriched in samples from pull-downs with RNA40mod in comparison to the unmodified RNA40.

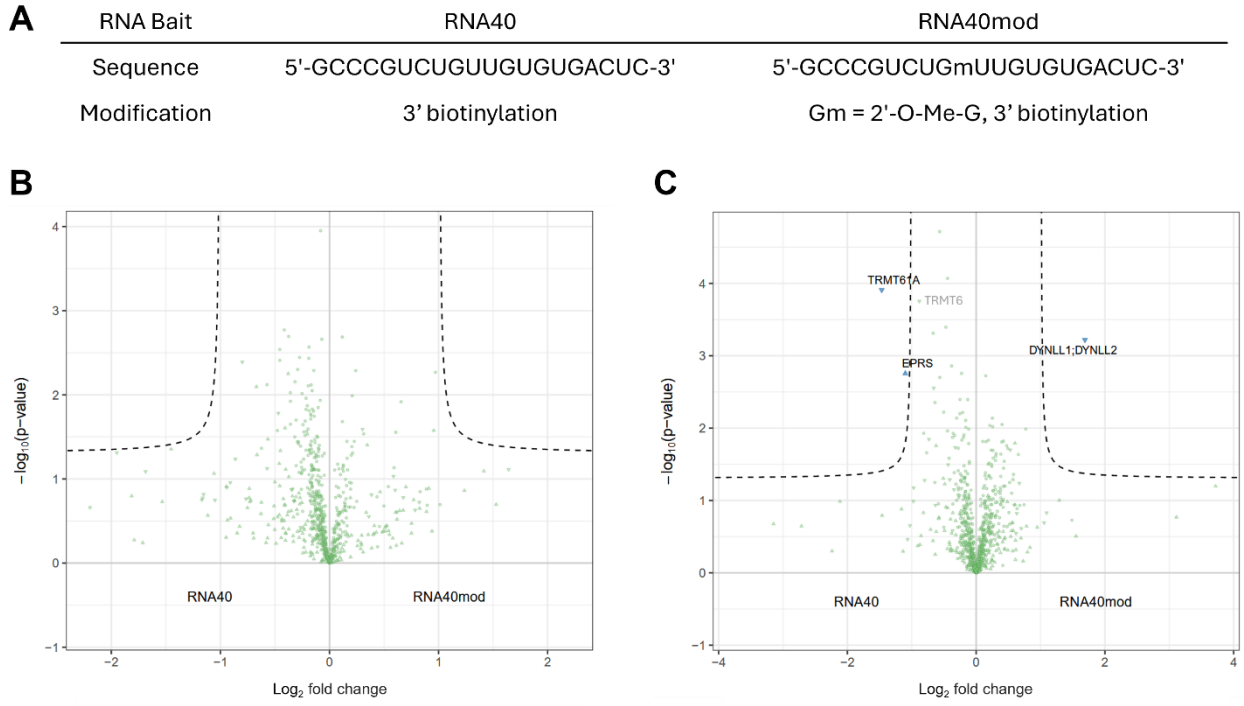

Figure 6: Mass spectrometry analysis of RNA pull-downs with 2'-O-methylation (2'-O-me). (A) BLaER1 quadruplicate protein samples were prepared for pull-downs with RNA40 or RNA40mod, which contained one 2'-O-me guanosine. (B, C) Pull-downs and LC-MS/MS analysis were used to

identify significantly enriched proteins in volcano plots with endolysosome-enriched protein extract from a density gradient (B) and the full PNS (C) as protein sample. Statistical analysis was performed with a Welch's t test for an enrichment threshold of fold change over 2 and p-value below 0.05.

To confirm RBP candidates with 2'-O-me dependent binding affinity, RNA baits with a different base sequence around the modified and unmodified nucleotide were used in further pull-down experiments. Additionally, the oligonucleotides contained a 4-Thio-modification to enable stable UV crosslinking with bound proteins (a kind gift by Dr. Timo Weinrich, Goethe University, Frankfurt). Following a binding test (Supplementary Figure 4), RNA_XLmod with 2'-O-me and RNA_XL without further modification were used for pull-down and crosslinking experiments (Figure 7A). After pull-down and UV-crosslinking, the proteins were eluted and processed by in-gel digestion. Gel staining with Coomassie provided an overview on the protein content in each eluted sample. Although the same amount of protein was used for each experiment, the staining was strongest in crosslinked samples, suggesting an overall higher protein concentration compared to pull-downs (Figure 7B).

To identify and quantify the proteins in detail, label-free LC-MS/MS measurements were performed. Interestingly, the comparison of unmodified and modified RNA revealed a higher number of significantly enriched proteins from pull-downs, but more total proteins from crosslinking experiments. The detailed analysis of pull-down (Figure 7C) and crosslinking experiment (Figure 7D) showed no enrichment of proteins that were also found in the previous pull-downs for the modified or unmodified RNA. While CALM2/CALM1 and HMGN4 were enriched in both experiments for the modified RNA_XLmod, they are involved in calcium signaling and nucleosome binding, respectively, which does not suggest a connection to RNA-related processes (Nanduri, Furusawa and Bustin, 2020; Munk *et al.*, 2022). Conversely, the tRNA-methyltransferase TRMT61A, a known RNA binding protein, exhibited significant enrichment to RNA40 and might have been captured in a complex with TRMT6. Consequently, it was selected as the most promising candidate for potential involvement of 2'-O-me-dependent TLR8 signaling and was chosen for further analysis.

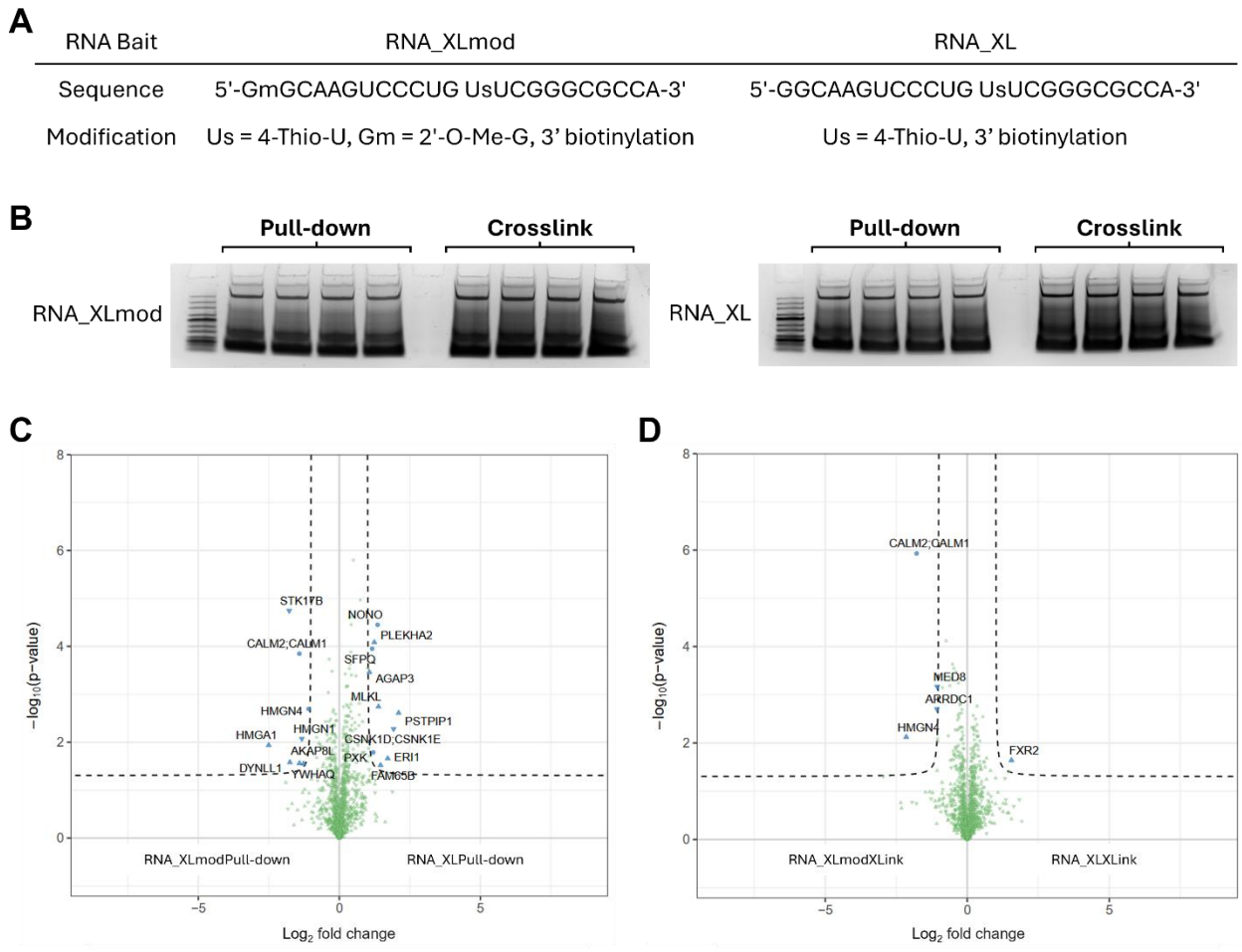

Figure 7: Mass spectrometry analysis of RNA pull-down and crosslinking experiments. (A) BLaER1 post-nuclear supernatant (PNS) protein extract from BLaER1 was used for pull-downs with 2'-O-methylated RNA_XLmod and unmodified RNA_XL. Both contained a 4-Thio-U modification, which was used for a UV-crosslinking step before LC-MS/MS analysis. (B) Protein visualization in a Coomassie-stained Bis-Tris gel for pull-down and crosslinking experiments with PNS. (C, D) Volcano plots showing enriched proteins from the BLaER1 WT protein extract for RNA pull-down (C) and crosslinking experiments (D). Statistical analysis was performed with a Welch's t test for an enrichment threshold of fold change over 2 and p-value below 0.05.

To verify the higher binding affinity of TRMT61A to unmodified RNA with a different approach for sample analysis, the eluted proteins were analyzed using a quantitative Western blot to detect the protein of interest directly. After confirming the appropriate protein concentration for detection by the TRMT61A antibody (Supplementary Figure 5), an RNA40 pull-down assay was performed. The eluted proteins were separated by molecular weight via gel electrophoresis, then transferred to a membrane and stained with polyclonal TRMT61A antibody and fluorescent secondary antibody. Fluorescence intensity was detected, revealing bands at the expected size of 31 kilodalton (kDa) as shown in a representative blot (Figure 8A, Supplementary Figure 6). The intensity of each protein band was quantified using Image Studio and compared between

experiments with unmodified RNA40 and RNA40mod (Figure 8B). These results confirmed that the TRMT61A binding affinity to 2'-O-me RNA was significantly lower than to an unmodified control. This suggests that it could be involved in 2'-O-me-dependent of TLR8 activation.

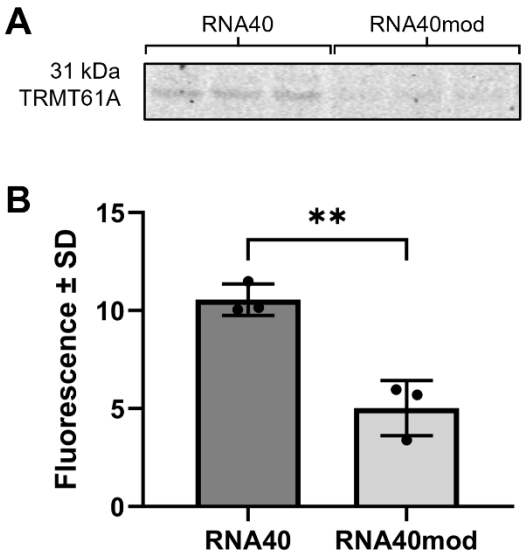

Figure 8: Western blot of TRMT61A after RNA40 pull-down. Pull-downs with BLaER1 PNS protein extract were performed with RNA40 and RNA40mod for analysis with a Western blot using a primary TRMT61A-specific and secondary IRDye antibody. (A) A representative blot from two experiments is shown. (B) The fluorescence signal was quantified, and a statistical comparison was performed using a two-tailed unpaired t-test (** p-value of 0.0041).

Generation of BLaER1 TRMT61A KO cells

To evaluate the potential role of TRMT61A during stimulation of endosomal TLR, BLaER1 TRMT61A KO cells for stimulation experiments with modified and unmodified RNA were to be generated. For this purpose, the plasmid pCas9-TRMT61A-gRNA was designed by Lan-Sun Chen (research group Alexander Dalpke, University Hospital of Heidelberg). It contained a *TRMT61A* guide RNA (gRNA) for the encoded Cas9 nuclease and an mCherry selection marker (Supplementary Figure 7). After preparing the plasmid from *E. coli*, BLaER1 cells were transfected in their proliferative B cell state. As an initial approach, lipofection was performed, which was followed by FACS to determine the transfection efficiency and generate single cell clones. An initial selection of singular GFP-expressing cells was performed according to the gating strategy shown below (Figure 9A). However, analysis of the plasmid marker revealed an mCherry expression in only 0.1 % of all cells, indicating a low transfection efficiency (Figure 9B). Therefore, the protocol was adapted by establishing a nucleofection protocol for BLaER1, using a primary cell kit for with the 4D Nucleofector (Lonza). Nucleofection was performed with 5.0E+05 cells and 1 µg of plasmid DNA using a program for human B cells. This resulted in an increased transfection efficiency with

marker expression in 1.1 % of all cells (Figure 9C). According to the manufacturer, efficiencies up to 30 % can be expected, therefore, the protocol was adapted by increasing the number of cells to 1.0E+06 with 2 µg of DNA. The 8.0 % of cells expressing mCherry confirmed this approach and were sorted as single cells for clonal expansion and genotyping (Figure 9D).

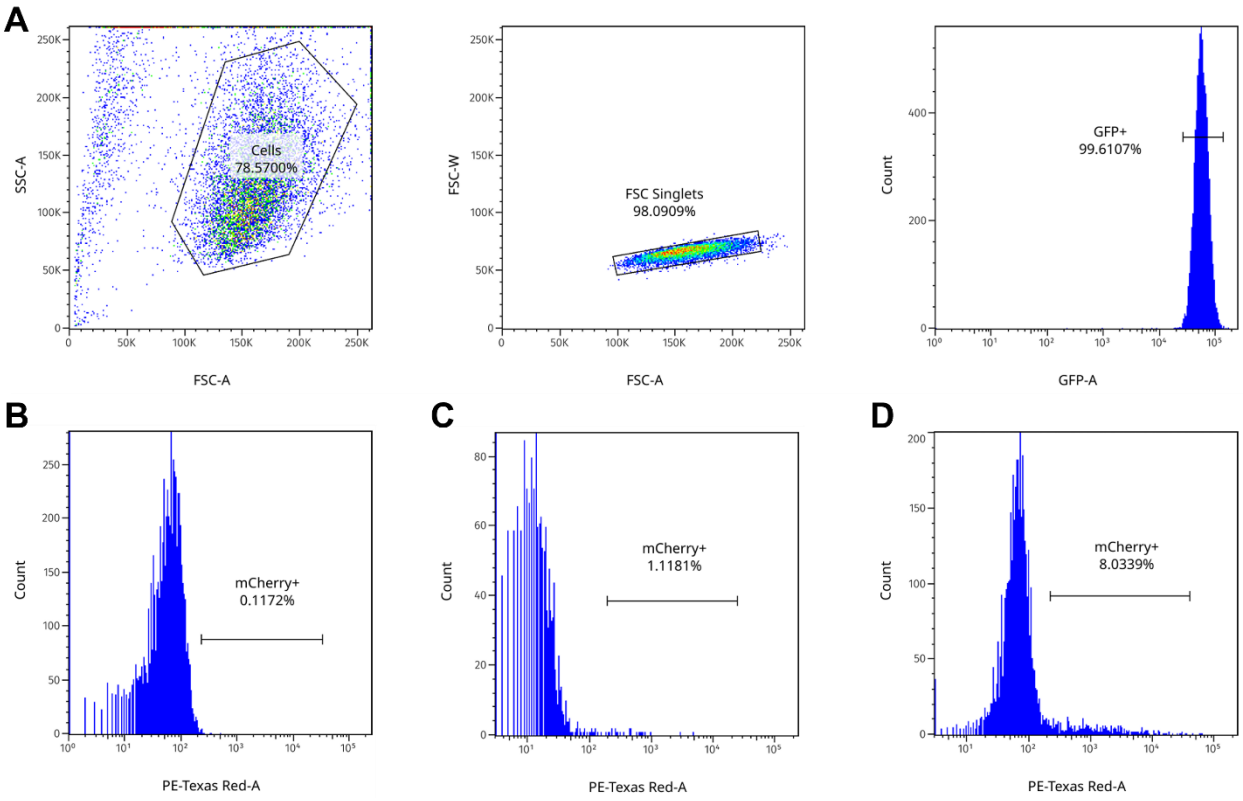

Figure 9: Fluorescence-activated cell sorting (FACS) of BLaER1 cells for selection of transfected cells. After transfection with pCas9-TRMT61A-gRNA, the cells were analyzed and sorted as single-cell knockout candidates using FACS. (A) A representative gating strategy is shown, which was used to select singular cells with GFP expression using the sideward scatter area (SSC-A), forward scatter width (FSC-W) and -area (FSC-A). (B – D) Cells expressing the plasmid marker mCherry were sorted after lipofection (B) or nucleofection using 5.0E+05 cells with 1 µg of DNA (C) or 1.0E+06 cells with 2 µg of DNA (D).

After the growth of clonal TRMT61A KO candidates, cells were collected for genomic DNA (gDNA) extraction and genotyping via Sanger sequencing. For this, primers were designed to amplify the genomic *TRMT61A* region surrounding the gRNA binding site. After PCR conditions were optimized, the amplified products were sent for Sanger sequencing. The analysis of mCherry-positive clones generated by lipofection showed no mutation of PCR products in comparison to the WT *TRMT61A* genomic sequence (Figure 10A). However, some clonal cell lines selected after nucleofection displayed significant changes in the sequencing chromatogram around and after the gRNA Cas9 binding site (Figure 10B). Clone N1 showed an insertion of 4 basepairs shortly after the

predicted double-strand break (DSB) site at base 941. According to the chromatograms, the mutations in clones N3, N11, and N21 began occurring even upstream of the DSB. As this could be explained by genomic mutations on one or both alleles of *TRMT61A*, the cell lines were examined further to confirm mutations, which could lead to a complete KO of TRMT61A.

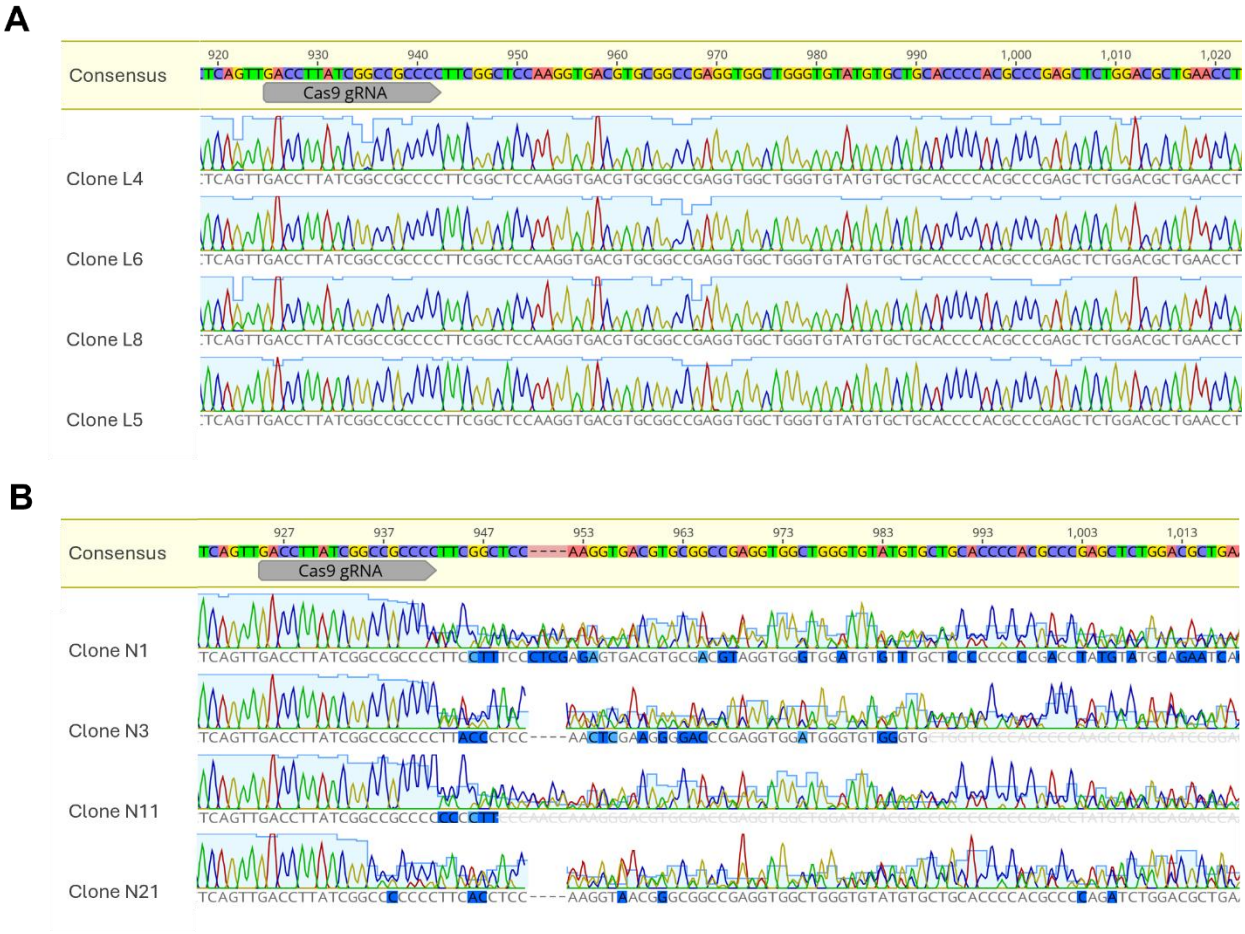

Figure 10: Sequencing results from the BLaER1 TRMT61A KO candidates. Genomic DNA was prepared from clonal KO candidates for PCR amplification of the genomic TRMT61A locus and direct Sanger sequencing. (A, B) The results were mapped to the genomic consensus sequence for cells that were transfected via lipofection (A, clones L4 – L8) or nucleofection (B, clones N1 – N21). The exemplary images shown were generated using Geneious software (Biomatters).

To examine TRMT61A expression in potential KO cell lines, full cell extracts were used for TRMT61A detection via Western blots. After sample preparation, cellular proteins were separated via gel electrophoresis and transferred to a membrane. Following an incubation with primary antibodies for TRMT61A and beta Actin, protein bands were detected using fluorescent secondary antibodies. The beta Actin bands at 42 kDa in each lane served as loading control, while bands at 31 kDa in WT and KO candidates revealed a clear TRMT61A expression in all cell lines (Figure 11).

Since no significant difference between WT and KO candidates was found, no further stimulation experiments were performed.

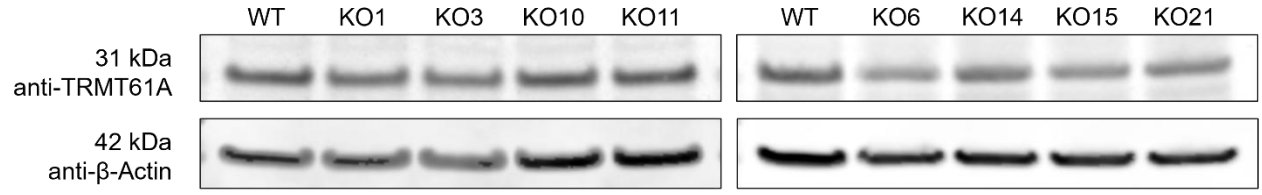

Figure 11: Western blots of BLaER1 TRMT61A KO candidates. After nucleofection, protein was extracted from BLaER1 clones with a genomic TRMT61A mutation (KO1 – KO21). Protein levels were detected via Western blot analysis using a primary TRMT61A-specific and secondary IRDye antibody; beta Actin was used as a control.

Orthoebolavirus infections

EBOV infects BLaER1 within 48 hours

BLaER1 cells are a macrophage model that can be used to study the infection and replication of viruses that target innate immune cells. Since there are currently no time-resolved proteome datasets of Ebola virus (EBOV) infected cells, the filovirus was selected as the pathogen of interest. With this, our goal is to identify proteins with an essential role during orthoebolavirus infection, life cycle, and host immune defense with a potential therapeutic potential. Therefore, BLaER1 cells were transdifferentiated for 7 days to test the susceptibility and permissiveness of BLaER1 macrophages to EBOV by infection with a recombinant reporter virus rgEBOV-iGFP at low and high multiplicity of infection (MOI) of 0.05 and 0.5. After 8, 24 and 48 hours, the GFP signal was visualized via fluorescence microscopy. This revealed an ubiquitous low-level expression of GFP in all cells throughout the experiment (Figure 12). While the signal did not change within 8 and 24 hours, few cells with a low MOI and most cells with a high MOI showed strong GFP expression after 48 hours. This suggested that the cells were infected and that the reporter virus encoding GFP replicated within 48 hours.

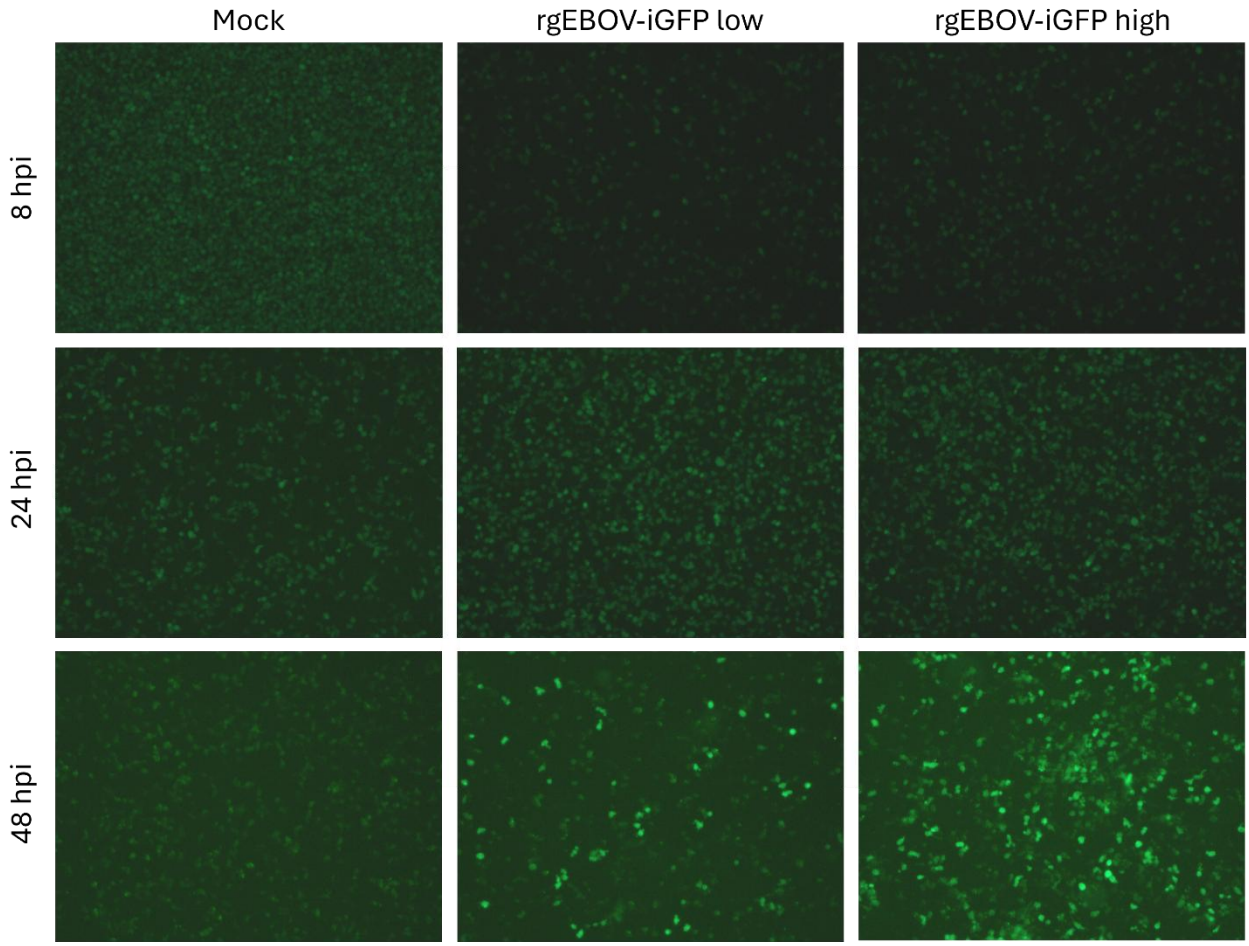

Figure 12: BLaER1 infection with reporter Ebola virus (rgEBOV-iGFP). BLaER1 cells were infected with recombinant EBOV expressing GFP at low (0.05) and high (0.5) multiplicity of infection. Imaging was performed at 8, 24, and 48 hours post infection (hpi).

Proteomes reveal slower replication of BOMV in BLaER1

Since the recombinant EBOV could infect and replicate in BLaER1 cells, the closely related EBOV and BOMV species were studied with our macrophage model to explore the significant difference in viral pathogenicity toward humans. Therefore, an infection experiment was conducted to generate a time-resolved proteome dataset of viral replication and host response. For this, BLaER1 cells were transdifferentiated for 7 days, after which the macrophages were infected in quadruplicates at a high and low MOI of EBOV and BOMV. Samples were inactivated at 8, 16, 24 and 48 hours post infection (hpi) for in-gel digestion, LC-MS/MS measurements and proteome data analysis.

The complete EBOV and BOMV proteomes were detected and ranked the identified host and viral protein groups by average abundance in all samples to reveal the total distribution of viral proteins (Figure 13A). As expected, EBOV proteins were more abundant overall than BOMV proteins.

Interestingly, the secretory EBOV-sGP displayed a much higher expression than $GP_{1,2}$, while BOMV-sGP had a lower abundance in comparison to $GP_{1,2}$. Further analysis of infected sample proteomes revealed an increase in viral protein LFQ values over time, which was dose-dependent for the low and high MOIs (Figure 13B). Additionally, the average amount of EBOV proteins was higher at all later timepoints compared to BOMV, while the low MOI of EBOV showed a similar development as the high BOMV MOI.

To study the previously seen difference in glycoprotein expression between the two viruses, the average signals from the infected samples were compared over time. This revealed that the amount of sGP was about three times higher than $GP_{1,2}$ for EBOV at the last timepoint (Figure 13C). Interestingly, the glycoproteins of BOMV did not show such a strong difference, but only a weaker increase in expression of both proteins over time.

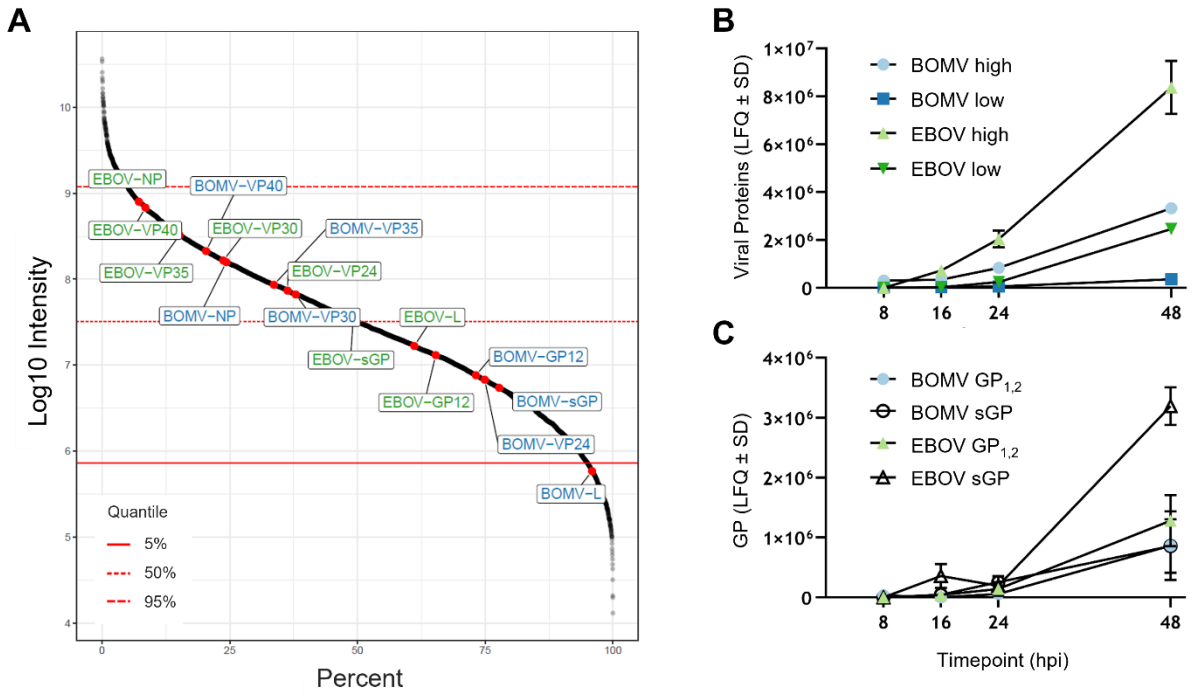

Figure 13: Expression of viral proteins during orthoebolavirus infection. Proteomes from BLaER1 cells infected with EBOV or BOMV were analyzed over 48 hours to quantify viral proteins. (A) The protein abundance ranking over all samples showing overall signal intensities, with the viral proteins highlighted in green for EBOV and blue for BOMV. (B, C) Average ± SD label-free quantification values of all viral proteins (B) and glycoproteins (GP, in C) during the infection time course with low (0.05) and high (0.5) multiplicity of infection.

Adaptation of BLaER1 transdifferentiation protocol

Our analysis of cellular proteomes revealed an unexpected response under control conditions. The standard transdifferentiation method was used as described previously (Gaidt *et al.*, 2018) to

generate BLaER1 macrophages by treating them with β-Estradiol, M-CSF and IL-3 for an infection on day 7 in supplemented RPMI (RPMIs, Figure 14A). Comparing the cellular proteome of mock-infected or untreated control samples still revealed the expression of proteins associated with immune cell activation after 24 and 48 hours (Figure 14B). Gene ontology (GO) analysis with proteins enriched after 48 hours supported this, by showing interleukin-signaling, MHC II-related, and antiviral biological processes (Supplementary Figure 8A). Within these, the pathway for negative regulation of viral processes (GO:0045071) contained various interferon-induced proteins, such as members of the 2'-5'-oligoadenylate synthase (OAS) and Interferon Induced proteins with tetratricopeptide repeats (IFIT) protein family. Due to this unexpected stress response, the transdifferentiation protocol was adapted to keep cells in a neutral state which allows to attribute any cellular reaction exclusively to the treatment. Therefore, various conditions were tested, resulting in a reduction of the transdifferentiation time to 5 days and continuous usage of transdifferentiation medium (TDM) for further treatment (Figure 14C). The proteomes from mock-treated cells that were generated with this approach showed a much lower overall difference between 8 and 48 hours without the enrichment of activation markers (Figure 14D). Supporting this, the GO analysis of significant proteins did not reveal the enrichment of the mentioned terms anymore (Supplementary Figure 8B). Therefore, the adapted protocol generated cells that remained in an unstimulated state, such that this protocol as applied in all further experiments.

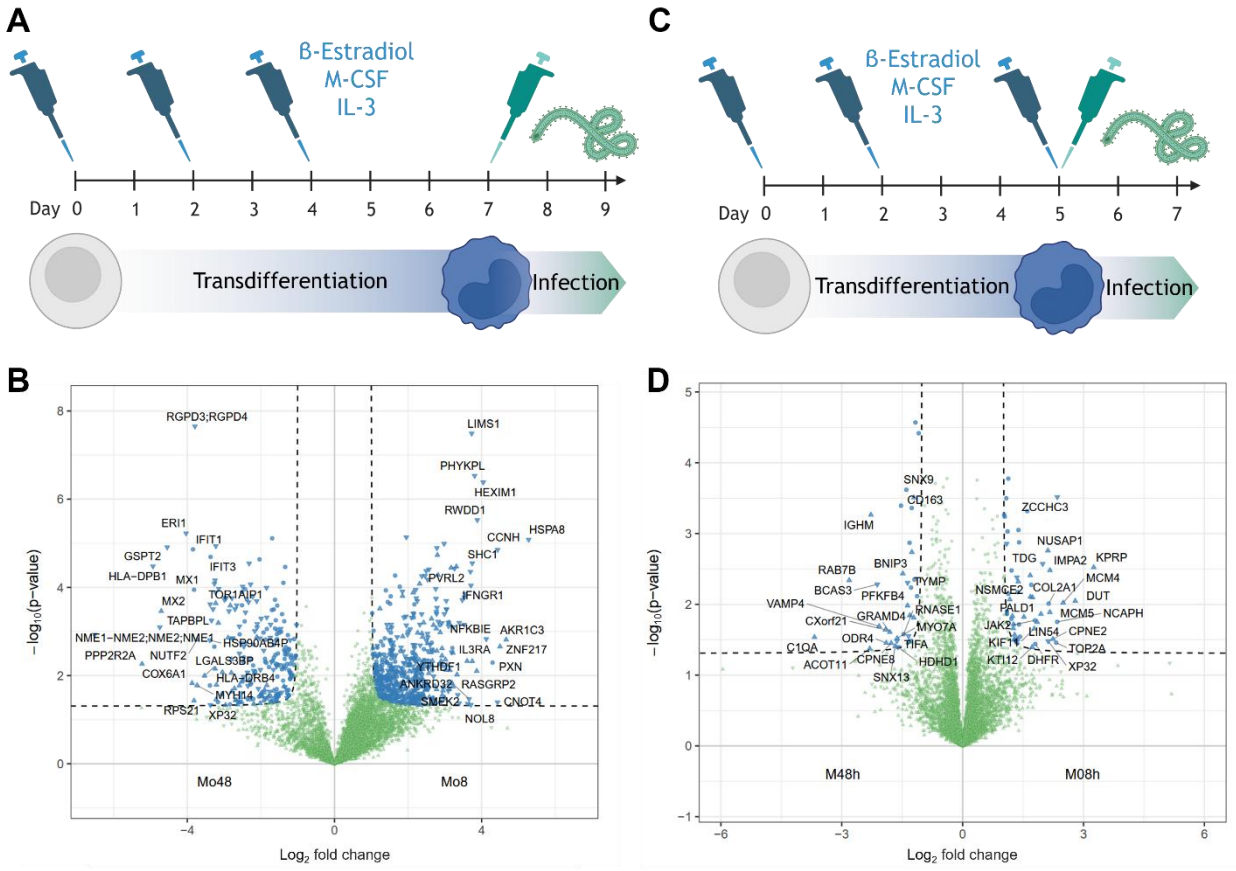

Figure 14: Optimization of the BLaER1 transdifferentiation protocol. (A) The original protocol for BLaER1 involved the addition of transdifferentiation medium (TMD) every 2 days to transform B cells into macrophage-like cells for infection experiments after 7 days in RPMIs. (B) Volcano plot comparing mock-infected samples after 8 (Mo8) and 48 hours (Mo48) using the original transdifferentiation protocol. (C) The adapted protocol with infection on day 5 in TDM. (D) Volcano plot comparing mock-infected samples after 8 (M08h) and 48 hours (M48h) using the adapted transdifferentiation protocol. Statistical analysis was performed with a Welch's t test for an enrichment threshold of fold change over 2 and p-value below 0.05. Figures (A, C) were created with BioRender.com.

EBOV infection time course for insight on host response

To generate a more reliable dataset for the proteome analysis of BLaER1 infection with orthoebolaviruses, the infection time course experiment was repeated with slight changes. The optimized transdifferentiation protocol was used for cell infection only with the high MOI of EBOV and BOMV and sample collection at 0, 1, 8, 16, 24 and 48 hpi. However, some samples showed an unusually high proportion of imputation. This was investigated by correlating the number of imputed values with the available amount of protein per sample (Figure 15A). This revealed a strong negative correlation between the number of imputed values and protein input, as the replicates from 16 and 24 hpi timepoints were affected above average. To ensure the quality of

the overall dataset analysis, all samples from these timepoints were classified as outliers and excluded them from further analysis. Next, the amount of viral protein for each timepoint was analyzed using LFQ values. A strong growth of EBOV was observed over time as seen previously, but an overall decrease of BOMV signal (Figure 15B). Because no growth of BOMV can be detected, subsequent analyses were performed exclusively with control and EBOV-infected samples.

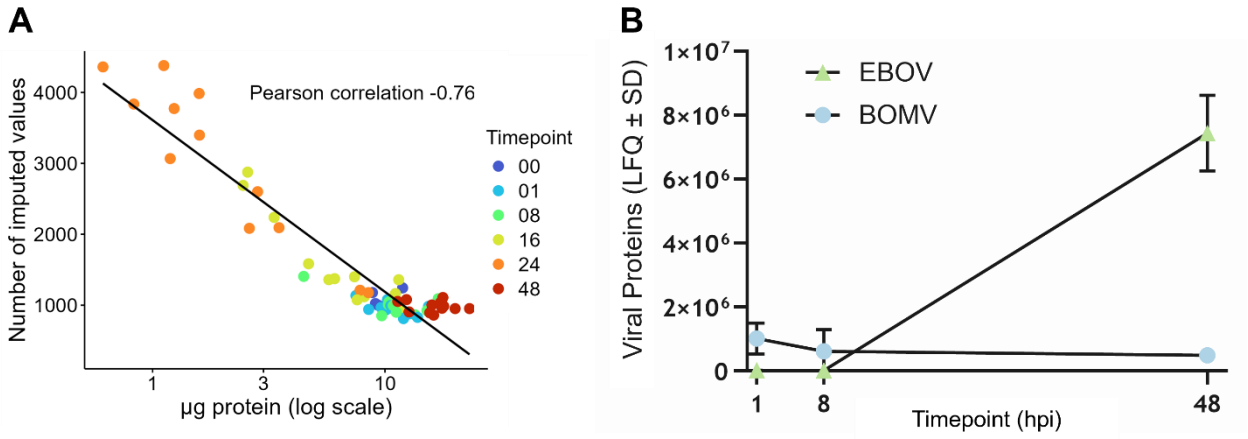

Figure 15*:* Proteome analysis from the optimized EBOV infection protocol. Proteome analysis of an infection time course at a multiplicity of infection of 0.5 from 0 to 48 hours post infection (hpi) was performed. (A) Correlation between the number of imputed values and the amount of available protein in the initial sample. (B) Average label-free quantification (LFQ) of all viral proteins during EBOV and BOMV infection at 1, 8, and 48 hpi with standard deviation (SD).

The host response to EBOV was further investigated by analysis of BLaER1 host proteomes during the infection. The RStudio package ComplexHeatmap (Zugang Gu) was used to generate heatmaps with protein clustering in an unsupervised manner. For this, the imputed LFQ intensities of the 0 hour control were used, as well as 1, 8, and 48 hpi samples from mock-treated or EBOV-infected cells. This revealed a complex map of 5,820 protein groups, that primarily showed a continuous protein expression in different experimental conditions and timepoints (Figure 16A). This included proteins with $\log_2$ LFQ intensities up to 24, while the lowest intensities around 14 were partly generated by imputation of missing values. For better comparison of detected proteins between samples, the $\log_2$ LFQ values were normalized using the 0 hour control and mock-treated samples. This resulted in 1,063 protein groups with a fold change over 2 at least once during EBOV infection. These were classified as proteins with a differential expression in response to EBOV infection. For the distinction of expression patterns, unsupervised clustering was performed with all differentially expressed proteins to generate a heatmap based on protein fold change. (Figure 16B). The heatmap revealed proteins with a fold change of up to 25 in comparison to mock-treated samples mainly at 48 hours, indicating their importance within the viral life cycle or an antiviral host response.

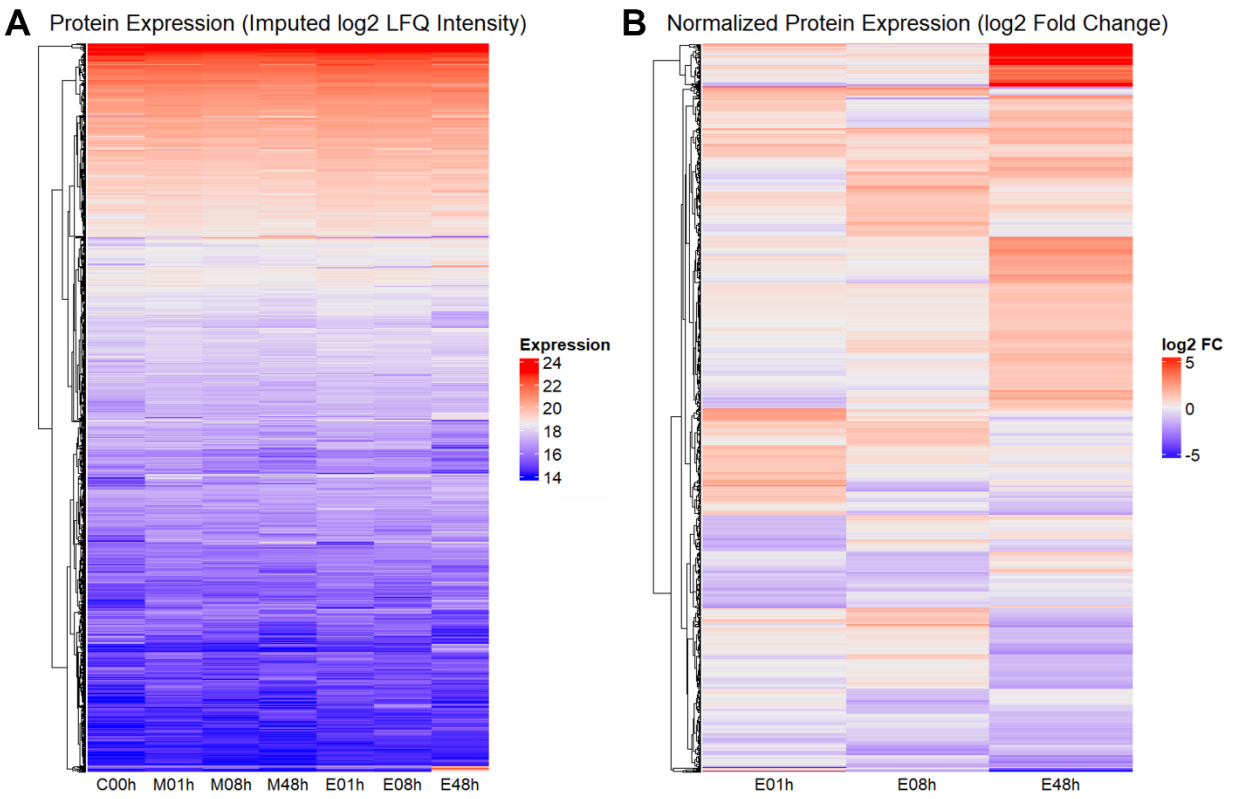

Figure 16: BLaER1 proteome during EBOV infection. (A) Heatmap displaying the expression profile of host and viral proteins over the course of the infection at 1, 8 and 48 hours (00h – 48h) for the control, mock-treated and EBOV infected (C, M, and E) samples after unsupervised clustering of the imputed log_2 label-free quantification (LFQ) intensity. (B) Log_2 LFQ intensity was normalized to the 0 hour control, and for infected samples the fold change (FC) was calculated in comparison to the mock treatment. From this, only proteins with a fold-change greater than two were used for the unsupervised clustering, shown in a heatmap.

To analyze major changes in the host proteome, protein groups were selected with signals showing a high fold change, and therefore a differential expression, compared to the control. Using the factoextra package (Alboukadel Kassambara) in RStudio, a specific number of distinct clusters were generated from the protein heatmap for further analysis. For this, the optimal number of clusters was determined first using the Elbow, Average Silhouette, and Gap statistic methods, which resulted in an average K-value of 6 clusters (Supplementary Figure 9). Subsequent clustering was performed and visualized in a heatmap to show proteins grouped by their log_2 fold change using K-means clustering. This revealed BLaER1 protein groups with distinct expression changes in response to EBOV infection (Figure 17A, Supplementary Table 1). To create a clear visual representation, the centroid of each cluster was calculated, such that six distinct profiles of host proteins over time were received (Figure 17B). Cluster 6 displayed a strong, and cluster 4 a moderate increase during infection compared to mock conditions. Furthermore, cluster 6

contained all viral proteins, highlighted in black. Conversely, proteins in clusters 1 and 5 displayed decreasing fold-changes approaching or dropping below 0.

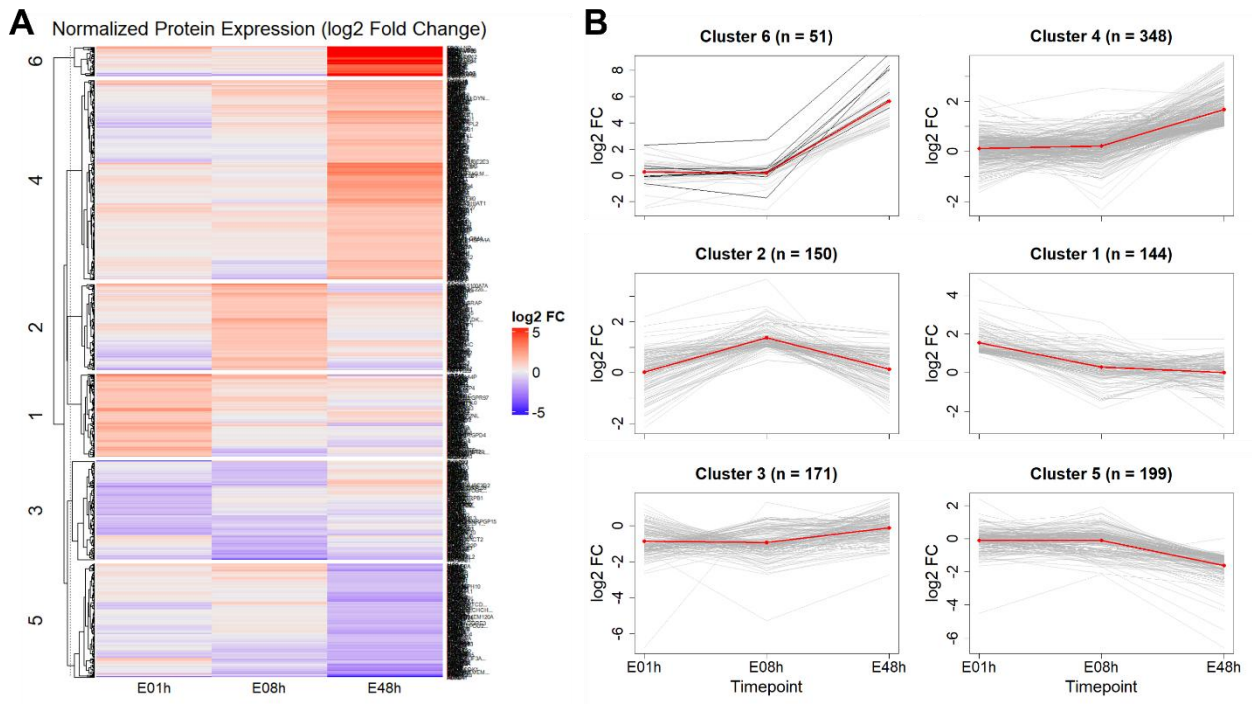

Figure 17: Clusters of host and viral proteins during EBOV infection. The proteomes of BLaER1 during EBOV infection were normalized for fold change (FC) and used for unsupervised K-means clustering. (A) Heatmap displaying clusters 1 – 6 for samples at 1, 8 and 48 hours post infection (E01h – E48h). (B) Cluster profiles showing the development of the $\log_2$ protein fold change of each protein(gray), of the centroid (red), and of EBOV proteins (black).

Some clusters displayed distinct development of host protein fold changes, such as clusters 6, 4, 1, and 5. This supports the hypothesis, that the proteins contained within these clusters specifically respond to EBOV infection. A notable observation was the grouping of all viral proteins into cluster 6. Therefore, the proteins from each cluster for GO enrichment were analyzed using the org.Hs.eg.db labeled human annotation database (Marc Carlson) and the clusterProfiler package (Guangchuang Yu) in RStudio for visualization. Cluster 4 showed an increasing fold change over time and revealed enhanced molecular functions related to MHC class I receptor and ubiquitin-related terms (Figure 18A, Supplementary Table 2). Cluster 6, which showed the largest increase over time, revealed enrichment for functions such as adenylyltransferase activity and dsRNA binding. Analysis of enriched biological processes revealed a decrease in DNA-related terms during the infection according to cluster 5 (Figure 18B, Supplementary Table 3). Clusters 4 and 6, which had an increasing expression over time, showed GO-terms that described various facets of the antiviral response, such as the regulation of viral processes, the antiviral innate immune response, and the defense against viruses. Additionally, cluster 6 displayed a much

stronger fold enrichment and lower p-values than cluster 4. This supports the assumption that cluster 6 contains genes that are strongly regulated and could play an important role in antiviral defense or the viral life cycle.

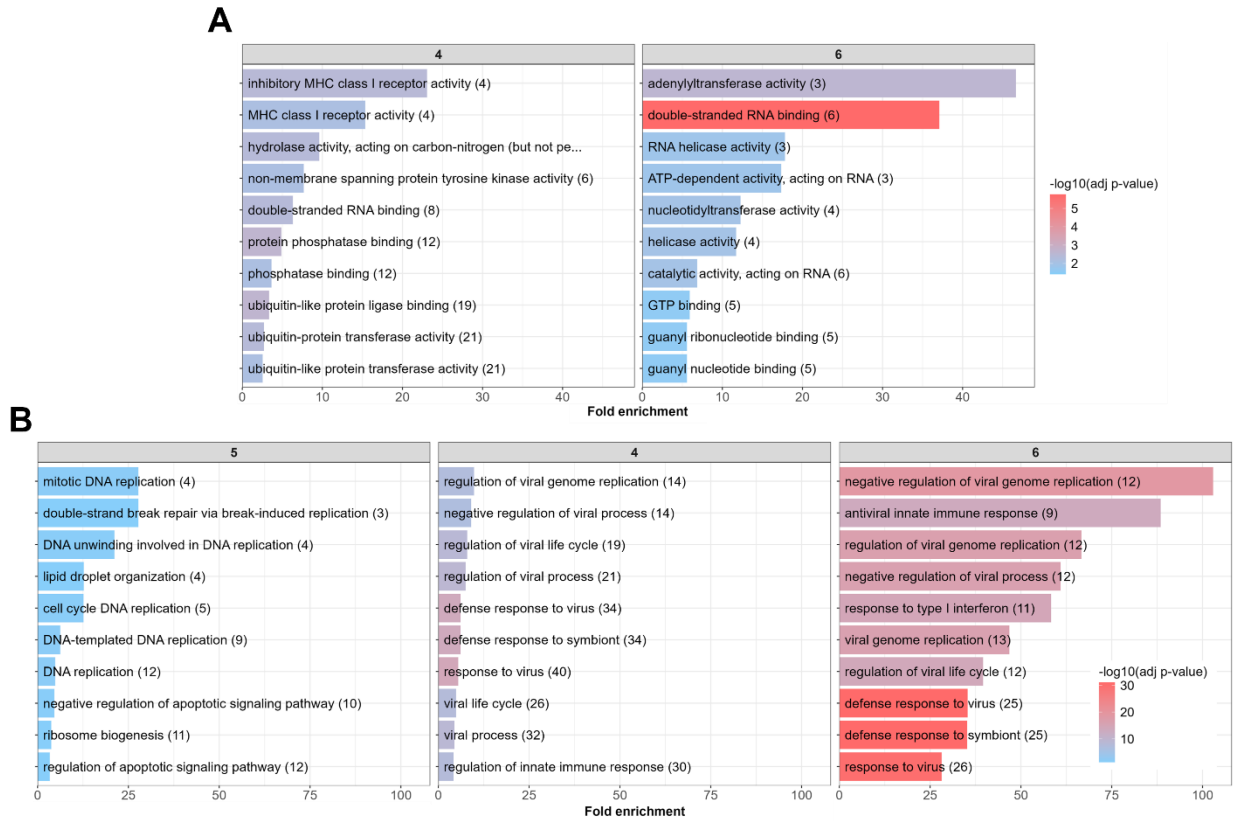

Figure 18: Gene ontology (GO) analysis of host proteins during EBOV infection. Host proteins were clustered according to their expression during an infection time course and analyzed for GO term enrichment. (A, B) Bar plots showing the fold enrichment of molecular functions from clusters 4 and 6 (A), as well as the enrichment of biological processes from clusters 5, 4, and 6 with the number of proteins for each term (B). Figure was generated using ShinyGO (Ge, Jung and Yao, 2020).

Due to the clear enrichment of antiviral GO terms in cluster 6, its 43 proteins were further analyzed to identify those known for their role in the antiviral response and to look for novel candidates. Therefore, an interaction network was generated based on the confidence of protein interactions using the STRING database (Szklarczyk *et al.*, 2023). The network showed a clear central cluster of proteins with strong interactions, while few or no interactions were found for others (Figure 19). The central cluster with high confidence interactions included the 2'-5'-oligoadenylate synthases OAS1 - 3 and interferon-induced proteins IFI27, IFI44, and IFIT1 - 3.

Meanwhile, GOLM1, UHRF1BP1, CACNA1A, and RIN2 did not show any interactions and may therefore be new, promising, host candidates that could affect EBOV infection.

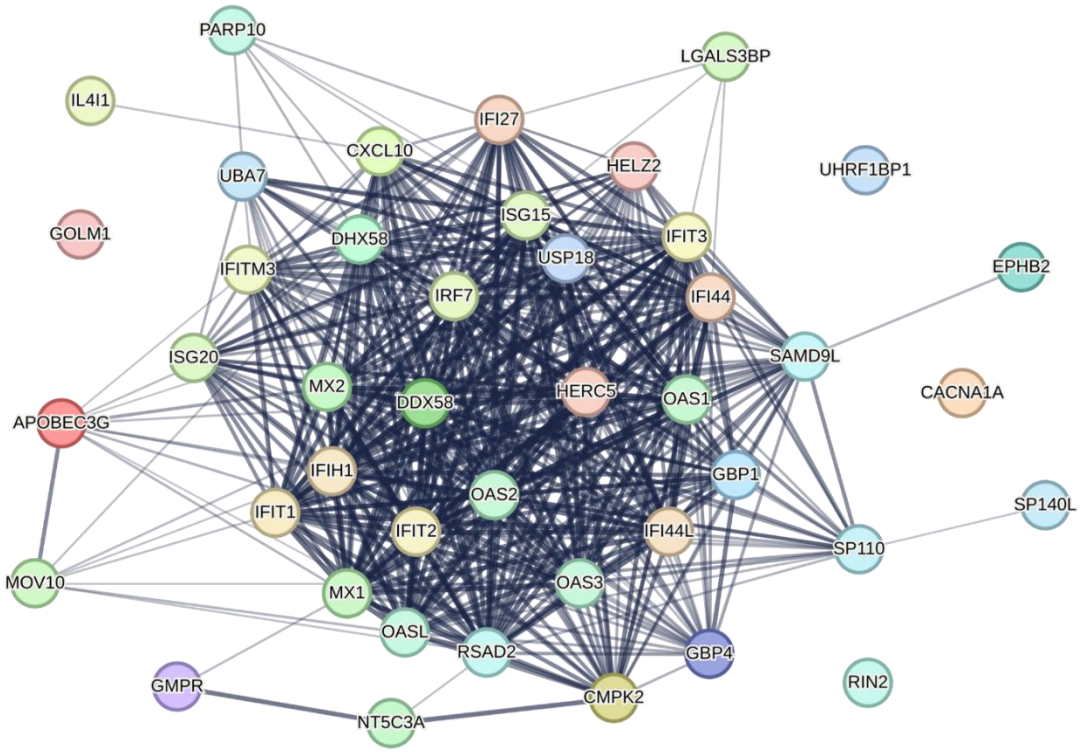

Figure 19: STRING network of proteins from cluster 6. Host proteins that showed increasing expression during EBOV infection were used for STRING network analysis to visualize interactions according to confidence. Network was generated using the string-db.org (Szklarczyk et al., 2023).

Development of secretome workflow

Since innate immune cells secrete specific proteins upon stimulation, the secretome of BLaER1 infection was analyzed during EBOV to evaluate cellular signaling response and release of viral proteins. The objective was to develop BSL-4-compatible workflow that would facilitate the analysis of the proteome from infected cells, as well as the secretome from the conditioned medium (Figure 20A). To determine the optimal conditions for secretome analyses, the usage of serum-free medium was tested in comparison to the conventional Fetal bovine serum (FBS)-containing medium. Additionally, the efficacy of sample preparation methods, namely in-solution digestion and SP3, was assessed, to identify the ideal workflow. Finally, a series of cell treatments were executed under BSL-2 conditions, which included non-treated controls and LPS stimulation, along with BSL-4 conditions, including EBOV and mock infection, to assess the broad applicability of the protocol. This approach unveiled substantial differences in the identification of proteins, as

evidenced by the proportion of imputed proteins in relation to the total number of proteins identified (Figure 20B). This revealed the lowest share of imputed values in the samples from the BSL-4 with FBS-containing medium and the SP3 workflow. Consequently, SP3 of conditioned medium with FBS was used in further experiments as the optimal approach. Using these conditions, the comparison of experiments with LPS stimulation and a control revealed the enrichment of few extracellular proteins, including Interleukin-1 receptor antagonist (IL1RN) and pentaxin-related protein 3 (PTX3), following LPS stimulation (Supplementary Figure 10). Furthermore, the analysis of gene ontology enrichment for cellular components exhibited a clear pattern towards terms related to the extracellular space, which verified the efficacy of the performed method for secretome analysis (Figure 20C, Supplementary Table 4).

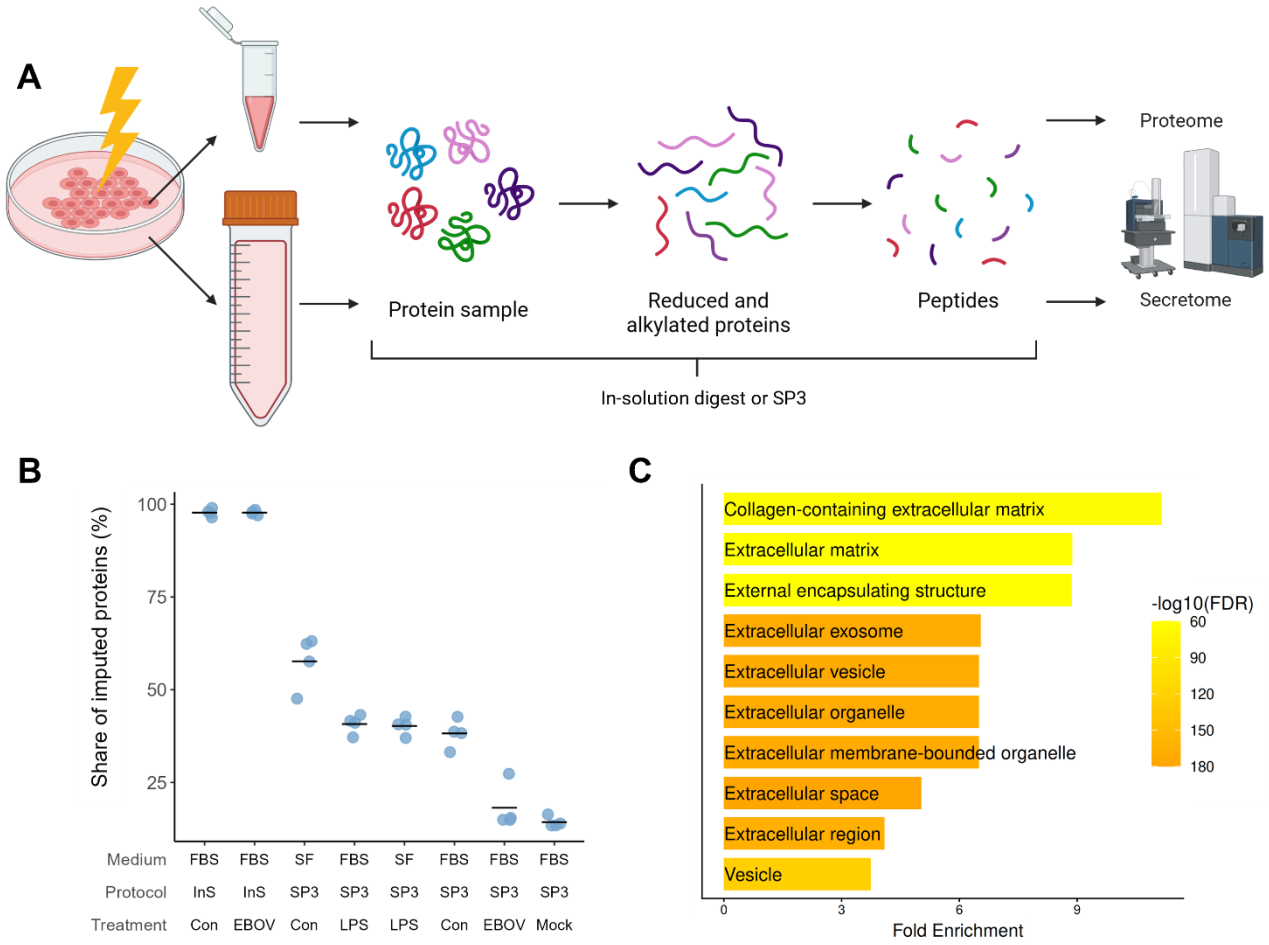

Figure 20: Method development for secretome analysis. (A) Secretome and proteome analysis workflow, from sample collection to processing and measurement. (B) Percentage of imputed proteins from various workflows in comparison using FBS-containing or serum-free (SF) medium, in-solution digest (InS) or single-pot, solid-phase-enhanced sample preparation (SP3) workflows, and treatment in BSL-2 with control (Con) and LPS stimulation, or in BSL-4 with EBOV or mock infection. (C) Gene ontology enrichment for cellular components using all proteins identified in the conditioned medium of experiments with FBS and SP3-treatment in BSL-4. Figure (C) was generated using ShinyGO (Ge, Jung and Yao, 2020).

Secretome analysis reveal release of novel host proteins

The established protocol for secretome analysis using FBS-containing medium and the SP3 protocol was applied to samples from BLaER1 infections with EBOV to compare the conditioned medium at 1 and 48 hpi with mock controls. The experimental conditions were directly compared to identify significant differences in protein secretion. This revealed an enrichment of viral proteins in the cellular medium at 48 hpi compared to the beginning of the infection (Figure 21A). The soluble GP was the most enriched viral protein, followed by VP40, VP35, and NP. Some host proteins also showed strong enrichment; therefore, a comparison of infected and mock-treated samples was performed at the same timepoint (Figure 21B). Again, viral protein enrichment was found in the conditioned medium from EBOV-infected cells after 48 hours, while also enriched host proteins were observed. Infection significantly lowered the glucose-6-phosphate isomerase (GPI) secretion compared to the mock, while infected cells released more phospholipid transfer protein (PLTP) and transforming growth factor beta (TGFB) at 48 hpi. This specificity in host protein secretion suggests that these proteins play a role in EBOV infection or the corresponding host response.

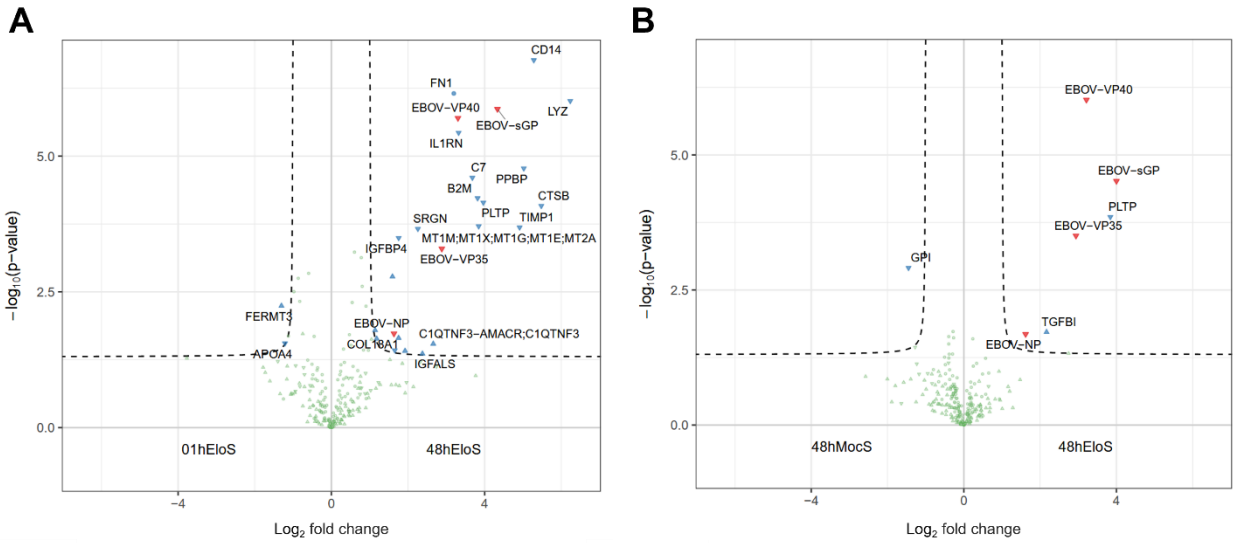

Figure 21: Secretion of host and viral proteins during EBOV infection. BLaER1 macrophages were infected with EBOV at a multiplicity of infection of 0.05, and the cellular supernatant was collected after 48 hours for secretome analysis. (A, B) Volcano plots comparing the secretomes of BLaER1 cells infected with EBOV after 48 hours (48hEloS) to those infected for 1 hour (01hEloS) (A) or to a mock-infected control (48hMocS) (B). Statistical analysis was performed with a Welch's t test for an enrichment threshold of fold change over 2 and p-value below 0.05.

Discussion

BLaER1 characterization during transdifferentiation

Flow cytometry reveals cell conversion after 48 hours

The BLaER1 B cell line contains a C/EBPα transcription factor, which enables the controlled transdifferentiation toward a macrophage-like phenotype that can be used for our research questions (Rapino *et al.*, 2013). To examine the transdifferentiation process, flow cytometric analysis of surface marker expression and proteome analyses were performed. During flow cytometry, live-dead staining revealed that dead cells in all stages lost the signal of the otherwise broadly expressed GFP. This conclusion aligns with previous publications, where lytic cell death was identified by loss of GFP via fluorescence microscopy due to the ubiquitous expression of the transduced C/EBPα-ER-IRES-GFP construct in BLaER1 (Gaidt *et al.*, 2018). Consequently, the live-dead staining was omitted and GFP was used to verify cell viability further on.

The investigation of cellular identity through the utilization of fluorescent antibodies in flow cytometry emerged half a century ago, when the distinction of multiple cell populations from a single suspension was initially demonstrated (Bonner *et al.*, 1972). For BLaER1 cells, this technique was previously employed with antibodies for CD19 as a B cell marker and macrophage-1 antigen (Mac-1) as a macrophage marker to track the transdifferentiation process over 7 days (Rapino *et al.*, 2013). The CD14-specific antibodies used as macrophage markers in this work were selected on the basis of the strong increase in expression over time demonstrated by numerous research groups (Rapino *et al.*, 2013; Schüssler *et al.*, 2023). BLaER1 flow cytometry revealed a continuous transdifferentiation of BLaER1 from CD19-positive B cells to CD14-positive macrophages, which is consistent with the results reported by Rapino *et al.* (2013). Intriguingly, over time, a subset of BLaER1 accumulated in a B cell state, while the majority of cells completed the full transdifferentiation process. This phenomenon can be explained by the post-mitotic state of BLaER1 macrophages, during while a small number of remaining BLaER1 B cells continue to proliferate and thus accumulate during the transdifferentiation period. A 4-fold increase in CD19+ B cells was observed from day 5 to day 7, and it can be assumed that this development would continue further. Therefore, subsequent experiments were conducted with BLaER1 transdifferentiation for a duration of only 5 days.

BLaER1 proteomes prove a rapid transition to a macrophage state

To date, there are no published proteome datasets for BLaER1; however, several transcriptome analyses are available, showing over 900 differentially expressed protein-coding genes that were likely involved in the process (Rapino *et al.*, 2013; Arnan *et al.*, 2022b). To address this gap in

knowledge and gain further insights into the molecular changes of BLaER1 cells during transdifferentiation, cell samples were taken during transdifferentiation for MS-based proteome analysis. The PCA revealed a clear development of proteomes over time until samples from days 4, 5, and 6 that did not exhibit significant development. Therefore, the changes along PC1 are interpreted as being caused by the adaptations of the cellular proteome from B cells to macrophage-like cells. Samples from day 7 did not align with this trend along PC2. One potential explanation for this phenomenon could be the enrichment of different BLaER1 cell populations over time, as demonstrated by the results of the flow cytometry analysis. While this has the potential to cause slight variations in the total proteome, the changes in PCA caused by a small cell populations around 1.4 % are unlikely to be the only explanation. As the reduction of complex data to few dimensions is the core principle of PCA, it can be adapted to support the detection of smaller subpopulations (Lall *et al.*, 2018). The more plausible explanation for the difference of samples from day 7 along PC2 is the prolonged incubation time and progressing decrease of nutrient concentrations affect the viability of the cells. This could cause the adaptation of transcriptome and proteome (Wei *et al.*, 2011; Gameiro and Struhl, 2018), leading to changes in the PCA.

For the analysis of BLaER1 proteomes during transdifferentiation, the selection of B cell markers was guided by prior transcriptome analyses (Rapino *et al.*, 2013). The results demonstrated that the development of B cell marker protein signals over time closely resembled the previous transcriptome data. The disappearance of B cell markers below the limit of detection after day 4 indicated a rapid conversion of a B cell-specific proteome in BLaER1 during transdifferentiation. Meanwhile, the expression of macrophage markers exhibited a notable increase, surpassing the limit of detection on day 2 and subsequently demonstrating a steady rise until day 7. An exception to this pattern is MMP9, which exhibited reduced LFQ signals after day 2. This discrepancy to previous transcriptome data can be explained by the continuous expression of the secretory MMP-9 in macrophages (Ariyoshi *et al.*, 2017). Consequently, MMP-9 expression could be strongly upregulated during transdifferentiation, but it subsequently shows a decline in signal within the cellular proteome due to its secretion.

In summary, the progression of cellular markers aligns with the flow cytometric data, with substantial alterations occurring around day 2 and the completion of transdifferentiation around day 5 on a proteome level. Therefore, BLaER1 cells were used following 5 days of transdifferentiation for later experiments, ensuring optimal cell conditions during stimulations or infections for experimental durations of up to 48 hours. Limitations of this approach include the categorization of BLaER1 cells primarily based on the expression of individual surface markers, which, particularly in genetically modified cells, is not guaranteed to be an exact indicator of cellular identity. However, the phenotypical changes and proteome data observed in this work support the generation of a suitable macrophage-like cellular model.

BLaER1 as suitable macrophage model

Alternative human macrophage models include primary cells that reflect *in vivo* processes best, but show limited availability, donor-specific variability, and complex requirements during preparation and cultivation (Garelnabi *et al.*, 2018; Ding *et al.*, 2025). Immortalized cell lines, such as those derived from cancerous samples, frequently exhibit altered properties that impede their capacity to accurately represent the behavior of macrophages in humans (Ding *et al.*, 2025).

Despite this, cell lines can model specific aspects of macrophage biology, making them valuable tools for the examination of the innate immune response. This includes the representation of primary M2 macrophages by U937 due to their expression profile, M1 macrophages by THP-1 with high phagocytotic activity, and complex immunological signaling pathways in BLaER1 (Gaidt *et al.*, 2016; Hoppenbrouwers *et al.*, 2022; Nascimento *et al.*, 2022). Furthermore, the proliferative B cell state of BLaER1 enables Cas9-mediated gene editing prior to the transdifferentiation to a post-mitotic macrophage phenotype (Volkmar *et al.*, 2024; Ding *et al.*, 2025). Even though a notable restriction of BLaER1 macrophages is the reduced functionality of the TLR4 signaling pathway in a subset of cells, which leads to an impaired LPS responsiveness, the examination of all cells revealed the anticipated response to specific stimulation of TLR7 and TLR8, thereby enabling the utilization of BLaER1 macrophages for the investigation of RNA-stimulation pathways (Wegner *et al.*, 2021).

Consequently, while BLaER1 cells are not fully representative of primary human macrophages, the possibility to generate KOs and to examine immune signaling pathways renders them a suitable model for the purposes of this work. Further analyses of interest include the direct comparison of the complete BLaER1 proteome during transdifferentiation with existing detailed transcriptome datasets to validate the results. Furthermore, a proteome comparison directly to primary human macrophages could facilitate a comprehensive evaluation of its usability as a macrophage model. Nevertheless, the evidence presented herein, in concert with previous studies on BLaER1 characterization, validates the cell line as a suitable model for the study of macrophage biology.

Impact of 2'-O-me on TLR8 stimulation

RNase6 is localized in the endolysosome

The detection of bacterial RNA in endolysosomes of macrophages depends on RNase-mediated digestion, which allows for TLR8 binding for pro-inflammatory signaling (Greulich *et al.*, 2019). While the role of RNase2 and RNaseT2 had previously been demonstrated, RNase6 could be involved in RNA processing upstream of TLR8 as well (Ostendorf *et al.*, 2020). Therefore, the

objective of this work was to examine the localization of RNase6 in the endolysosome, which would suggest a potential role upstream of TLR8.

To confirm the subcellular localization of RNase6 in the endolysosome, the present investigation was grounded in previous work regarding subcellular proteomics, wherein methods to specify the location of proteins within the cell have been described (Christopher *et al.*, 2021). In accordance with this concept, biochemical enrichment of organelles in fractions is performed to align the abundance profile of novel proteins with well-established organelle markers in line with de Duve's principle (de Duve *et al.*, 1955; Christopher *et al.*, 2021). Consequently, a sucrose density gradient was used to separate BLaER1 organelles and to assess protein content in each fraction via mass spectrometry. This resulted in a clear separation of organelle bands, which were enriched in endolysosomal or mitochondrial proteins according to proteome and subcellular annotation analysis. The distribution of endolysosomal proteins in the lighter fractions of the gradient could be attributed to the heterogeneity of endolysosomes, which have been observed to vary in size depending on the cellular state (Hipolito *et al.*, 2019). Consequently, smaller endolysosomes might have remained on top of the 25 % sucrose cushion throughout the ultracentrifugation process. However, the evident enrichment of mitochondria in F5 substantiated the methodology for the separation of subcellular organelles.

The distribution of RNase6 and RNaseT2 corresponded with the endolysosomal profile along the gradient. In accordance with de Duve's principle, this finding suggests that RNase6 is likely to be localized within the endolysosomes of BLaER1 macrophages. This is supported by previous results, which established the presence of RNase6 in lysosomal compartments (Sleat *et al.*, 2013). Furthermore, the enrichment of TLR7 in F3 of the density gradient demonstrated the expression of the receptor in BLaER1 cells, contradicting previous results that showed only traces of TLR8 mRNA signals (Hornung *et al.*, 2002). However, the expression and immunological signaling of TLR7 are well established in primary human macrophages, thereby supporting the usage of BLaER1 as an illustrative macrophage model (Gantier *et al.*, 2008; Simón-Fuentes *et al.*, 2023).

The precise generation of PNS and the elaborate preparation of the sucrose density gradient impede the replicability of this approach. As repeated experiments did not yield the desired separation of organelles, the presented results are based on two pooled gradients. However, the clear segregation of endolysosomal and mitochondrial proteins supported the validity of the approach, and consequently, the localization of RNase6 within the endolysosome. These results were part of a publication that will be discussed later in detail (Nunes *et al.*, 2024).

2'-O-me-dependend RNA binding protein TRMT61A

The stimulatory capacity of RNA is inhibited by the introduction of specific RNA modifications, such as 2'-O-methylation (2'-O-me), that modulate the immune response by a still unknown

mechanism (Freund *et al.*, 2019). To elucidate this process, 2'-O-me RNA baits were used in pull-down assays with BLaER1 protein extracts as described previously (Scherer *et al.*, 2020). The lack of enriched proteins from pull-downs with endolysosome-enriched protein extract can be attributed to the low protein concentration and potential decline in protein quality during the preparation process, which spanned multiple days. Comparable experiments with PNS revealed the tRNA methyltransferase heterotetramer complex, comprising TRMT61A and TRMT6, which exhibited increased binding affinity for unmodified RNA.

To further validate the RBP candidate, a second approach was employed, using a different RNA sequence for pull-downs and crosslinking with PNS. While the crosslinking step led to the identification of a higher number of proteins, the pull-downs resulted in a greater number of significantly enriched proteins overall, thereby supporting the successful performance of the protocols. However, the enriched proteins did not align with previous findings; a discrepancy that can be attributed to variations in sequence context and position of the modified nucleotide. This phenomenon is well explained by previous findings, that demonstrated the need of RBPs for specific RNA motifs to allow binding, which also includes modification-specific reader proteins (Taliaferro *et al.*, 2016; Fagre and Gilbert, 2024).

Consequently, TRMT61A was examined further as the strongest 2'-O-me-dependent candidate that could be responsible for the inhibition of TLR8 activity. Our working hypothesis for this phenomenon was a potential facilitation of RNA digestion or TLR8 detection through TRMT61A binding of unmodified RNA. As demonstrated previously, analogous functionalities have been reported for the RBP Roquin that lead to RNA degradation, or OAS binding of viral RNA that caused an induction of RNase activity (Leppek *et al.*, 2013). Consequently, the enhanced binding affinity of TRMT61A to unmodified RNA was substantiated through RNA pull-downs followed by Western blot analysis.

A limitation of the presented approach is the artificial setting *in vitro* with the use of protein extracts and the low variability of the synthesized RNA baits for investigation of protein binding. Potential alternatives for future research efforts include the performance of proximity-based biotin-labelling of proteins, such as the RNA-protein interaction detection (RaPID) approach, or the expression of tagged RNA for UV crosslinking and RNA purification to examine *in vivo* interactions (Tsai *et al.*, 2011; Ramanathan *et al.*, 2018). Nevertheless, TRMT61A was identified as a most confident 2'-O-me dependent RBP candidate that could be a potential regulator of RNA detection upstream of TLR8.

BLaER1 KO generation of TRMT61A

To validate the influence of TRMT61A on 2'-O-me-dependent TLR8-inhibition, a KO cell line was to be generated using a CRISPR-Cas9 expression plasmid with a TRMT61A-specific gRNA in the

proliferative BLaER1 B cell stage. Analysis via flow cytometry indicated the expression of the mCherry plasmid marker in 0.1 % of cells following lipofection. This phenomenon may be attributed to the suboptimal size profile of liposome-DNA complexes or the compromised cell viability resulting from toxic effects of the transfection process (Ross and Hui, 1999; Lonez, Vandenbranden and Ruysschaert, 2012). As demonstrated in prior publications, it has been shown that nucleofection exhibits superior transfection efficiency in comparison to lipofection (Cao *et al.*, 2010; Maurisse *et al.*, 2010). Consequently, the transfection approach was adapted.

Nucleofection was found to enhance transfection efficiencies from 0.1 % to 1.1 % and 8.0 % when the provided instructions were performed with the recommended, and with a higher number of cells. This may be associated to the direct delivery of DNA into the nucleus and the establishment of more reproducible conditions in suspension cells, as compared to chemical gene transfer by lipofection (Gresch *et al.*, 2004). The enhancement in nucleofection efficiency observed with a higher number of cells can be attributed to an optimized average distance of nucleic acids to cells for the applied pulse amplitude (Potočnik *et al.*, 2022). Furthermore, a higher cell density and the addition of conditioned medium from non-transfected cells could have supported the survival of transfected cells after the treatment (Brumatti, Salmanidis and Ekert, 2010).

The sequencing of clonal cells revealed clear mutations around the gRNA site within the genomic TRMT61A sequence following nucleofection. It can be assumed that the observed mutations were caused by the double-strand breaks introduced by Cas9, which lead to non-homologous end joining, microhomology-mediated end joining, or single-strand annealing (Xue and Greene, 2021). Due to the start of mutations upstream of the DSB-site in multiple clones, the performance of short-range end resection before the dsDNA break repair is likely (Xue and Greene, 2021). Depending on the efficiency of the repair, these mechanisms can introduce insertions or deletions causing frameshift during translation, which can in turn lead to nonsense-mediated RNA decay or the production of truncated proteins due to premature termination of translation (Tuladhar *et al.*, 2019). However, the validation of potential KO cell lines via Western blots for TRMT61A revealed a clear expression of the protein in all tested samples, which could be explained by silent mutations or heterozygous KO.

RNase6 is responsible for inhibited TLR8 stimulation due to 2'-O-me

Although the role of TRMT61A upstream of TLR8 could not definitively be established, parts of this research were published in collaboration with another group. The work demonstrated that 2’-O-me-dependent inhibition of TLR8 signaling is dependent upon RNase6-mediated RNA processing (Nunes *et al.*, 2024). Moreover, a comparable requirement for RNaseT2 and RNase6 in immune activation by foreign RNA was identified for TLR7 (Tong *et al.*, 2024). Mechanistically, RNase6 has been shown to digest bacterial RNA within the endolysosome, thereby generating

TLR8-stimulating fragments. However, 2'-O-me in a specific sequence context hinders RNase6-mediated digestion, thereby preventing the generation of RNA fragments capable of stimulating TLR8 (Nunes *et al.*, 2024).

A potential explanation for the absence of RNase6 enrichment during the presented RNA pull-downs is the transient nature of RNase-RNA interactions, along with the potential digestion of RNA baits. Furthermore, the recognition motif for RNase6 digestion was found to be UA, whereby a 2'-O-me of the U nucleotide inhibits RNase6 cleavage (Nunes *et al.*, 2024). Given that the RNA baits used in this work were deficient in the RNase6 recognition motif UA, and that the investigation focused on the consequences of a 2'-O-me G nucleotide, the absence of specific RNase6 binding to these sequences is a plausible outcome.

Orthoebolavirus infections of BLaER1

BLaER1 macrophages are permissive for EBOV

Filoviruses, such as EBOV, infect human macrophages and have caused numerous outbreaks with a frequently severe disease progression and high fatality rates over the past several decades (Mohd *et al.*, 2024; Bodmer *et al.*, 2025). The recent discovery of the non-pathogenic and closely related BOMV raises the question about the molecular causes for the high pathogenicity of EBOV. Therefore, the objective of this work was to establish BSL-4-compatible workflows to analyze the proteome and secretome of transdifferentiated BLaER1 macrophages infected with EBOV and BOMV, with the aim to determine host proteins that can be involved in orthoebolavirus pathogenicity.

Test infections of BLaER1 with a recombinant GFP-expressing EBOV confirmed the susceptibility and permissiveness of the cells. Although all BLaER1 cells exhibited a weak GFP signal, this phenomenon can be attributed to the stable transfection of BLaER1 with the C/EBPα-construct, which incorporates a GFP marker. Consequently, the generation of a recombinant virus that expresses a different fluorophore, such as mCherry to be used as a marker, would be advantageous and could facilitate the detailed surveillance of viral protein expression. However, there was a notable increase in fluorescence of specific cells, indicating the replication of the recombinant virus. This outcome was anticipated, given the inherent tropism of EBOV for monocytes and macrophages (Ströher *et al.*, 2001). Furthermore, the number of infected cells exhibiting strong GFP expression was found to be time- and dose-dependent, with the GFP signal increasing most significantly in cells infected with a high MOI after 48 hours. These results are consistent with previous literature on EBOV replication kinetics in cell culture (Liao *et al.*, 2020). A previously generated mathematical infection model based on *in vitro* data determines the eclipse phase at around 30 hpi, which describes the time from cell infection until virus production, and a strong increase in the number of secreted viruses up until 48 hpi (Liao *et al.*, 2020). This is

consistent with the finding of no significant increase in fluorescence in cells at 24 hpi, but a significant gain at 48 hpi.

EBOV replicates a tenfold faster than BOMV

The performance of a time-resolved BLaER1 infection experiment using EBOV and BOMV for quantitative mass spectrometry-based proteomics analysis allowed for the direct comparison of viral growth kinetics. The expression of EBOV proteins was found to be higher in all timepoints compared to BOMV, while both viruses exhibited a time- and MOI-dependent pattern. Due to the similar development of viral protein signals during the time course for EBOV at low MOI (0.05) and BOMV at high MOI (0.5), a tenfold higher replication efficiency of EBOV was hypothesized. This is further substantiated by prior findings in Vero cell culture, wherein EBOV infection resulted in tenfold increases in virus titers at 48 hpi in comparison to BOMV (Bodmer, Breithaupt, *et al.*, 2023).

The analysis of signals from EBOV GP revealed the amount of the soluble sGP to be approximately a twofold higher compared to the membrane-bound $GP_{1,2}$. This phenomenon can be explained by previous studies on the GP ORF, where transcriptional editing leads to a translation of sGP in 70 % and of $GP_{1,2}$ in 25 % of cases (Sanchez *et al.*, 1996; Mehedi *et al.*, 2011; Martin *et al.*, 2016). EBOV sGP has been shown to inhibit the activity of neutralizing antibodies directed against $GP_{1,2}$, thereby supporting the role of sGP in the evasion of the host immune defense (Ito *et al.*, 2001). Additionally, antigenic subversion of sGP during EBOV infection plays a significant role, which is defined as the redirection of antibodies against $GP_{1,2}$ towards shared epitopes with sGP, leading to antibody absorption (Mohan *et al.*, 2012). However, the absence of a comparable effect in BOMV, which exhibited the same signal intensity for sGP and $GP_{1,2}$ at 48 hpi, suggests that the mechanisms of immune evasion based on sGP are reduced or absent in BOMV. These results support further examination of BOMV sGP expression to elucidate the role of the potentially altered transcriptional editing for virus pathogenicity. Due to the natural secretion of sGP and the shown analysis of cellular proteomes during infection, the exploration of this phenomenon needs to be extended to secretome analyses, which would allow for a comparison of sGP secretion from EBOV and BOMV infected cells.

BLaER1 cells express activation markers in control conditions

The EBOV and BOMV infection experiments were performed in comparison to mock infected and untreated transdifferentiated BLaER1 macrophages as control conditions. However, control cells demonstrated proteins signals associated with a cellular activation after 48 hours. This impaired the ability to derive reliable conclusions from viral infection experiments, as it was presumed that antiviral pathways would exclusively be activated in infected cells.

The transdifferentiation protocol deployed in this work has been reported to generate a stable macrophage state within a period of 7 days, after which the transdifferentiation factors could be removed (Gaidt *et al.*, 2018). However, the exchange of the M-CSF-supplemented medium during transdifferentiation to infection in normal growth medium has the potential to reduce cell viability, thereby inducing a stress responses. This is supported by previous research, demonstrating that M-CSF promotes the survival of monocytes and macrophages (Wang *et al.*, 2011, 2013). An alternative explanation for the described phenomenon is the prolonged cultivation of transdifferentiated BLaER1 cells in the same dish, leading to overgrowth and nutrient depletion. This finding aligns with prior results in this work, as the transdifferentiation over a period of 7 days resulted in the gradual accumulation of proliferative BLaER1 B cells. Furthermore, a deficiency in nutrients can directly result in an adapted gene expression, including the translation of cytokines and inflammatory genes within a few hours (Gameiro and Struhl, 2018). Moreover, a small number of dying cells can release DAMPs via lytic pathways, which can result in the activation of macrophages, leading to an inflammatory response in a self-amplifying loop (Wang and Labzin, 2023; Wu *et al.*, 2025). Lastly, the basal production of IFN by macrophages could lead to an accumulation of the cytokine during prolonged cultivation and therefore lead to the activation of IFN-stimulated genes (Uccellini and García-Sastre, 2018; Willemsen *et al.*, 2022).

Therefore, BLaER1 cells were used after a transdifferentiation period of only 5 days. This is in alignment with previous flow-cytometry and proteomics results, which demonstrated that the cells employ a macrophage-like protein expression within a timeframe of 4 – 5 days. Furthermore, the medium supplementation with β-Estradiol, M-CSF, and IL-3 was maintained during infection experiments to minimize cellular stress.

BLaER1 homeostasis prevents BOMV replication

The adapted transdifferentiation protocol allowed for an improved time-resolved EBOV and BOMV infection experiment. Quality controls during data analysis revealed an inverse correlation between low protein input and high number of imputed values from most replicates of the 16 and 24 hpi timepoints. These results align with prior research, which demonstrated a negative correlation between the signal intensity and the rate of missing values (Shi *et al.*, 2025). The observed phenomenon may be attributed to potential variations in sample preparation during cell harvest, given that samples from both timepoints were collected simultaneously. Consequently, the exclusion of both timepoints was determined to ensure the integrity of the data quality for subsequent analyses.

The analysis of viral proteins between 1 and 48 hpi revealed a decline of BOMV signals in BLaER1 proteomes. This finding indicates the presence of the virus used during infection at the earliest timepoint within the cells. As demonstrated in earlier experiments, this phenomenon confirmed

the susceptibility, or ability of a virus to enter cells, of BLaER1 macrophages to BOMV. However, the decline in viral signals until 48 hpi indicated a problem within the BOMV life cycle and viral replication during this experiment. The same virus stock, reagents, and buffers as in the previous experiment were used, thus the major variation in comparison to the previous infection experiment was the adaptation of the BLaER1 transdifferentiation protocol. During the initial time course experiment, cells exhibited the expression of antiviral proteins in control conditions, likely resulting from prolonged cultivation and the absence of M-CSF supplementation. While the replication of BOMV exclusively in BLaER1 cells that were in a stressed, activated, and non-homeostatic state may appear counterintuitive, previous research could explain this phenomenon. For instance, specific interferon-stimulated genes have been observed to facilitate the replication of certain viruses (Schoggins and Rice, 2011; Wichit *et al.*, 2019). Additionally, the expression of the interferon-induced IFIT1 was shown to not affect EBOV replication (Pinto *et al.*, 2015). This observation led to a novel hypothesis, proposing that the expression of interferon-stimulated proteins in BLaER1 cells during the initial time course experiment was enhanced, but not to a sufficient level for BOMV inhibition. Moreover, the stressed cellular state of BLaER1 could have facilitated the replication of BOMV within the cells.

BOMV GP could lead to a decreased pathogenicity

The presented results reinforce the lower or missing pathogenicity of BOMV in humans compared to EBOV. While the data presented suggests the uptake of BOMV into BLaER1, this work demonstrated the lower or absent ability of BOMV to replicate within BLaER1 in comparison to EBOV and a decreased level of cellular sGP production. This phenomenon may be partially attributed to the decline in viral uptake efficiency with $GP_{1,2}$, as shown with transcription- and replication-competent virus-like particles (trVLP) equipped with BOMV $GP_{1,2}$ (Li *et al.*, 2024). The analyses with this model system revealed that the infectivity of BOMV $GP_{1,2}$ trVLPs was rescued to some extent by mutations in the NPC1-binding domain towards the amino acid sequence of EBOV $GP_{1,2}$. While the results presented in this work suggest BOMV entry into BLaER1, the observed difference in replication efficiency may be caused by deficiencies within the completion of the viral life cycle. To date, the reverse genetic systems to examine exclusively the replication of BOMV in a homologous sequence context have yet to be established. Nevertheless, previous heterologous studies with EBOV trVLPs and BOMV full-length genomes clearly demonstrated the reduced replication efficiency of BOMV (Bodmer, Breithaupt, *et al.*, 2023).

In addition to the ineffective viral entry and replication previously discussed, the functionality of BOMV immune-suppressing mechanisms are still a subject of debate. While EBOV VP24 has been demonstrated to impede the expression of interferon-activated genes, a similar effect was found for BOMV VP24 in a previous study (Khan *et al.*, 2023). However, a previous study showed the

EBOV $GP_{1,2}$-mediated IFN-λ1 promoter inhibition, while BOMV $GP_{1,2}$ did not exhibit an inhibitory effect (He *et al.*, 2022).

Finally, the reduced BOMV replication could be explained by the diminished production of BOMV sGP in comparison to EBOV sGP, as demonstrated in this work. While this effect has not been described for BOMV before, it could significantly impact the pathogenicity of the virus. This hypothesis is further substantiated by previous studies, which have demonstrated the vital role of sGP not only in immune evasion, but also in the efficient uptake of BOMV virus-like particles (VLPs) into the endosome of cells, a process that occurs prior to membrane fusion and viral entry (Mohan *et al.*, 2012; Furuyama *et al.*, 2021). Finally, the elimination of sGP production, accomplished through the generation of a mutated GP-ORF without transcriptional editing, was previously shown to cause an increase in cytopathy and accelerated cell death, possibly caused by the much higher expression of $GP_{1,2}$ (Volchkova *et al.*, 2015). Notably, this mutation led to a reduction in pathogenicity in guinea pigs due to the accelerated host response, along with a decrease in viral load in the blood serum (Volchkova *et al.*, 2015). This finding underscores the critical need for the precise regulation of sGP and $GP_{1,2}$ expression. The specific transcriptional editing site that is responsible for this phenomenon leads to polymerase stuttering at a poly-U repeat and an expression of sGP in 70 % of cases (Martin *et al.*, 2016). Interestingly, the genomic site of transcriptional editing seems to be highly conserved between the different orthoebolaviruses (Supplementary Figure 11). However, the single nucleotide exchanges between species could have an effect on sGP transcription and therefore must be examined further to confirm the cause for the low BOMV pathogenicity.

Proteomes uncover EBOV-related expression patterns

The infection of BLaER1 with EBOV in the adapted time course experiment revealed the significant increase of protein signals until 48 hpi. Further analyses were performed following a previously established method, using proteins exhibiting large fold changes for the subdivision into six clusters exhibiting specific expression patterns (Rahmatbakhsh, Gagarinova and Babu, 2021). The validity of this approach was substantiated by the observation that all viral proteins were assigned to cluster 6, which demonstrated the most significant increase in fold changes during the time course. As indicated by the differential fold change patterns over time in all clusters, it is plausible that the included host proteins play a significant role in the EBOV life cycle and antiviral host response.

The subsequent analysis of gene ontology for each cluster revealed the enrichment of molecular functions related to dsRNA binding, MHC class I activity and ubiquitin-protein transferase. These patterns are consistent with previous literature, as an increasing expression of MHC I genes during EBOV infection is known (Kotliar *et al.*, 2020). With regard to ubiquitin-protein transferases, the

ubiquitination of NP through the tripartite motif-containing protein (TRIM) 25 has been shown to result in a decrease in viral mRNA transcription (Galão *et al.*, 2022). Also the E3 ubiquitin ligase TRIM6 is involved in the EBOV life cycle, as it catalyzes the ubiquitination of viral VP35 and thereby facilitates efficient transcription and virus assembly (van Tol *et al.*, 2022). The examination of enriched biological processes within specific clusters revealed the rise of gene ontology terms related to antiviral processes and a defense response during EBOV infection. This finding aligns with previous studies, which demonstrated that macrophages detect viral infections through the recognition of GP or viral RNA by TLR4 or RIG-I, respectively, inducing an antiviral immune response (Habjan *et al.*, 2008; Okumura *et al.*, 2010; Bodmer *et al.*, 2025).

The generated cluster 5 contained proteins with decreasing expression over time and exhibited the enrichment of biological processes related to DNA replication. While previous studies concluded that actively proliferating cells were necessary for EBOV replication, in specific cell types the infection led to cell cycle arrest (Kota *et al.*, 2012). The reduced amount of DNA replication in BLaER1 cells provides support for the hypothesis that the macrophage model also exhibits this phenomenon and reduces cellular proliferation during EBOV infection.

In summary, the observed enrichment of antiviral processes in protein clusters demonstrated an increasing fold change throughout the infection experiment, substantiated the reliability of the performed analysis.

Protein network reveals novel host proteins involved in EBOV infection

The examination of proteins contained within the clusters that exhibited most pronounced trends over time could enhance our understanding of the host response to EBOV infection. Consequently, all proteins from cluster 6, which showed the most substantial increase in protein fold changes during the experiment, were examined further.

The central network of proteins, many of which are induced by interferon signaling, have known functions within the antiviral response and dominated the generated network. This includes members of the OAS family, which are known to be stimulated by viral dsRNA in the cytosol. The stimulation leads to the generation of messenger molecules and causes RNaseL dimerization for the digestion cytosolic RNA (Hornung *et al.*, 2014; Huang *et al.*, 2014). The group of IFN-induced proteins, including IFIH1, IFIT2, IFITM3, and IFI44, constituted another part of the central network. These proteins are known to be responsible for various antiviral mechanisms, including binding to viral RNA, inhibiting viral translation, and interfering with membrane fusion to prevent virus entry into the cytoplasm (Diamond and Farzan, 2013; Gómez-Herranz, Taylor and Sloan, 2023). Lastly, HERC5 was an additional central part of the network and has previously been identified as a factor contributing to the reduction of VP40-mRNA copies, thereby impeding viral assembly, (Paparisto *et al.*, 2021). In summary, a variety of IFN-stimulated proteins with known antiviral effects against

EBOV were found within the central network generated from cluster 6, which exhibited increasing expression during EBOV infection. The proteins identified in this work are consistent with those reported in previous literature, which validates the approach employed here.

However, the network also contained proteins not connected to the central cluster, which therefore are not known to be involved in an interferon-stimulated antiviral response. Consequently, the weakly or non-connected nodes may represent novel host proteins involved in the antiviral response to EBOV infection. This includes Interleukin 4 induced 1 (IL4I1), an oxidase secreted by macrophages that is responsible for the regulation of the adaptive immune response (Molinier-Frenkel, Prévost-Blondel and Castellano, 2019). It has been demonstrated that IL4I1 can drive macrophage polarization towards an anti-inflammatory phenotype and inhibit the activation of T-cells (Yue *et al.*, 2015; Aubatin *et al.*, 2018). These immunosuppressive functions could therefore support EBOV infection and pathogenicity.

A further candidate of interest is GOLM1, a known regulator of immunity that is upregulated by Hepatitis B and C virus or SARS-CoV-2 during viral infection to counteract the IFN-mediated innate immune response (Zhang *et al.*, 2017; Yang *et al.*, 2018; Wan *et al.*, 2022). To date, there have been no reports in the literature of an upregulation or functional role of GOLM during EBOV infection. The enhanced expression of GOLM1 during EBOV infection demonstrated in this work constitutes a potentially novel mechanism of immune evasion. Consequently, further validation of this phenomenon would be highly compelling.

The presented approach is limited due to the analysis of only few timepoints during EBOV infection. More data on protein expression over time could support the validity of novel candidates. Furthermore, there is a need for subsequent research on the novel host candidates to substantiate their role in EBOV infection and pathogenesis. Nevertheless, the identification of multiple known members of the antiviral response against EBOV renders the present dataset a promising resource for further studies on host factors affecting filovirus infection. The analysis of proteins in the various clusters demonstrating fluctuations in protein expression over time are particularly promising.

Optimization of secretome analysis workflows

The analysis of cellular proteomes during EBOV infection provided insights into the alterations in host protein expression and viral replication. However, macrophages and other immune cells frequently employ the secretion of signaling molecules in the form of proteins, which can be detected, quantified, and interpreted through secretome analyses (Wu and Krijgsveld, 2024). Furthermore, the secretion of sGP and the release of viral particles into the medium during EBOV infection were of particular interest. Consequently, a method for the analysis of secreted host and viral proteins was established and subsequently analyzed via mass spectrometry.

The preferred approach for secretome analyses is the utilization of serum-free medium for cultivated cells to circumvent the contamination of secreted cytokines with bovine serum proteins (Nonnis *et al.*, 2016; Knecht *et al.*, 2023). However, the absence of FBS supplementation in cell culture medium can result in starvation effects, causing substantial changes in the cellular proteome and secretome (Kulkarni and McCulloch, 1994; Shin *et al.*, 2019). In view of the previously observed sensitivity of transdifferentiated BLaER1 to alterations in the cultivation medium and the enhanced identification of proteins from conditioned medium containing FBS during test experiments, subsequent secretome analyses were conducted using serum-containing medium. Furthermore, the SP3 processing workflow exhibited a clear advantage over the in-solution approach and was consequently selected for the preparation of further secretome samples. The application of this workflow for the analysis of secretomes, following an exemplary LPS-stimulation, revealed an enrichment of few proteins, including IL1RN and PTX3. This phenomenon corresponds to former results, as the rapid secretion of the receptor antagonist IL1RN from macrophages upon LPS-stimulation was previously detected (Eichelbaum and Krijgsveld, 2014). Furthermore, PTX3 has already been identified within the response of various cell types, including macrophages, to LPS stimulation and is secreted as a single protein or in exosomes (Imamura *et al.*, 2007; Lin, Guo and Chen, 2021).

Although the secretome investigated in this work did not display the extensive array of all secreted proteins anticipated from LPS-stimulated cells, the identification of specific candidates in agreement with the literature validates the approach and proves the usability of the employed straightforward method. The optimized workflow described in this work resulted in the substantial enrichment of gene ontology terms associated with the extracellular space, thereby verifying the efficacy of the employed approach for subsequent analyses.

EBOV-infected cells secrete immune modulatory proteins

Detailed investigation of secretome samples from an EBOV infection experiment revealed the presence of viral proteins within the cellular medium at 48 hpi. The observed viral protein enrichment was largely consistent with previous research on the abundance of proteins within virions. The number of viral proteins in a single virus was previously approximated via densinometry at 3,600 for VP40, 2,686 of VP35, 833 for VP30, and 625 for NP, as well as lower values for the remaining proteins (Elliott, Kiley and McCormick, 1985). This data aligns with the observed enrichment of viral proteins in the secretome, with the exception of VP30, which was not detected. Collectively, these observations indicate the release of viral particles into the cellular medium and consequently the completion of the viral life cycle. Additionally, the substantial secretion of sGP within 48 hours was in accordance with the proteome results previously discussed. These findings are consistent with the available literature, which establishes that the

EBOV GP ORF is transcribed to sGP in 70 % of cases for secretion from the host cell (Mehedi *et al.*, 2011; Martin *et al.*, 2016).

The observed enrichment of host proteins during EBOV infection included an higher secretion of CD14, PLTP, and TGFβ1. Out of these candidates, CD14 has been identified as an innate immune co-receptor for various TLRs, and it has been demonstrated to be responsible for the activation of IFN expression upon ligand binding (Schilling *et al.*, 2022). Furthermore, EBOV infection in non-human primates has been shown to lead to an increase in CD14-positive hepatic macrophages, which in turn accelerates a pro-inflammatory response (Tseng *et al.*, 2023). Collectively, these results are consistent with the observed increase in CD14 secretion and further previously described mechanisms of EBOV to amplify the immune response.

For PLTP, an anti-inflammatory role has been established, as the protein is responsible for the regulation of Signal transducer and activator of transcription 3 (STAT3)- and NF-κB-mediated responses (Vuletic *et al.*, 2011). Strikingly, PLTP was previously discovered within EBOV virions, and a correlation between PLTP expression and survival of EBOV infection was observed in non-human primates (Spurgers *et al.*, 2010; Garamszegi *et al.*, 2014). Therefore, the presented evidence further supports the importance of the role of PLTP during Ebola virus disease (EVD), potentially through the control of an otherwise overly active immune response.

Finally, the transforming growth factor β (TGFβ) 1 has been shown to be secreted during EBOV infection of hepatocytes, leading to an increased virus replication and more severe pathology in a mouse model (Kindrachuk *et al.*, 2014). The increased expression was also found in an endothelial cell model, where TGFβ1 caused a cellular transition with accompanying changes in transcription and cell-cell adhesion (Ro and Patterson, 2022). Collectively, these studies substantiate the significance of TGFβ1 during EBOV infection, though the precise impact on macrophages and other immune cells remains to be clarified.

The secretome analyses conducted within this work collectively provide a compelling foundation for further exploration of macrophage secretion during EBOV infection. The simplicity of the applied method constitutes a limitation of this approach. Significant advancements can be anticipated from the optimization of workflows with the concentration or precipitation of secreted proteins, as recommended in the literature (Almeida-Marques *et al.*, 2024). Furthermore, while the use of FBS supplementation is essential considering the sensitivity of the cellular model, alternative solutions do exist, such as metabolic labelling of cellular proteins (Villarreal *et al.*, 2013; Knecht *et al.*, 2023). Additionally, adapting the measurement of samples to data-independent acquisition and to improved bioinformatic analysis has the potential to further improve the quality of future results (Shin *et al.*, 2015; Nakamura *et al.*, 2021).

Conclusion

In this work, I demonstrate that the BLaER1 macrophage model is a versatile and informative system for studying the innate immune response. Our successful optimization of the transdifferentiation workflow of BLaER1 cells from B cells to macrophage-like cells was supported by flow cytometric data and the first proteome analyses of the differentiation process. This data significantly improved our understanding of the cellular model and enhanced the applicability of BLaER1 cells for stimulation and infection experiments.

The usage of BLaER1 macrophages enabled the investigation of the processes preceding TLR8 activation by bacterial RNA in the endolysosome of macrophages, which is inhibited by 2'-O-methlation (2'-O-me) modifications. RNA pull-downs for mass spectrometry analysis allowed the identification of the RBP TRMT61A, which exhibited an increased binding affinity for unmodified RNA. We further pursued this finding with the subsequent generation of BLaER1 KO clones, aiming to verify the effect on 2'-O-me-mediated TLR8 inhibition. A further candidate with potential influence on RNA processing upstream of TLR8 is RNase6, which was examined with our collaborators. We determined the subcellular localization of RNase6 within the endolysosome using a subcellular fractionation and proteomics approach. This finding contributed to a paper, demonstrating the 2'-O-me-dependent processing of bacterial RNA by RNase6, which is essential for effective TLR8 stimulation (Nunes *et al.*, 2024).

Furthermore, the BLaER1 macrophage model was employed in the context of virological investigations concerning the group of highly pathogenic orthoebolaviruses. The susceptibility and permissiveness of BLaER1 for EBOV was determined, and workflows compatible with BSL-4 conditions were established to allow studying BLaER1 infections with orthoebolaviruses safely. Time-resolved infection experiments revealed a significantly higher growth rate of EBOV in comparison to BOMV, while the latter non-pathogenic virus was found to exclusively be able to replicate in non-homeostatic BLaER1 cells. This finding constitutes substantial evidence for the evaluation of BOMV pathogenicity. Furthermore, the analysis of proteomes and secretomes from EBOV-infected cells provides a comprehensive dataset for the identification of host factors that are important during pathogenesis, including novel host proteins that could be involved in the immune response or in viral immune modulation.

Our data highlights the role of BLaER1 as valuable macrophage model system for the examination of cell responses to specific stimulations, in addition to the investigation of cellular behavior during viral infections. The methods established in this work for proteome and secretome analyses using samples from a BSL-4 environment allow for further experiments to gain additional insights into the molecular processes of the innate immune response during infection. Moreover, the alignment of host proteins identified in this work in combination with the existing literature

substantiates the significance of this dataset for future research on novel host factors. Overall, these findings advance our understanding regarding the role of macrophages in infectious diseases and promote our understanding of EBOV pathogenicity, which ultimately lays the groundwork for the future development of therapeutic approaches.

Materials and Methods

Materials

Cell lines

Name	Origin
BLaER1 WT	Kind gift from Prof. Alexander Dalpke, University Hospital Heidelberg
BLaER1 TLR8KO	Kind gift from Prof. Alexander Dalpke, University Hospital Heidelberg

Viruses

Name	Origin
rgEBOV-WT 42MLS.AA.6	Generated by PD Dr. Thomas Hoenen, FLI, Greifswald
rgEBOV-iGFP 42.BB.AA.4	Generated by PD Dr. Thomas Hoenen, FLI, Greifswald
rgBOMV 42.BB.AJ.3.2	Generated by PD Dr. Thomas Hoenen, FLI, Greifswald

Plasmid

Name	Origin
pRP[CRISPR]-mCherry/Puro-hCas9 U6>hTRMT61A[gRNA#221] in VB UltraStable Amp	Plasmid termed pCas9-TRMT61A-gRNA was designed by Lan-Sun Chen, research group Alexander Dalpke, University Hospital Heidelberg and produced by VectorBuilder Inc.

Enzymes

Name	Product	Manufacturer
10 x HF-DNA Polymerase Buffer		IMB Protein Production Core Facility
HF-DNA Polymerase		IMB Protein Production Core Facility
Lysyl EndopeptidaseR, LysC	129-02541	Wako
Trypsin (porcine pancreas)	37286.03	Serva

Antibodies

Name	Product	Manufacturer
Goat anti-Mouse IRDye 680RD	926-68070	Li-cor
Goat anti-Rabbit IRDye 800CW	926-32211	Li-cor
Mouse anti-CD14 APC	367118 63D3	BioLegend, BIOZOL Diagnostica
Mouse anti-CD19 PE	392506 4G7	BioLegend, BIOZOL Diagnostica
Mouse anti-beta Actin	sc-47778	Santa Cruz Biotechnology
Rabbit anti-TRMT61A	orb411814	Biorbyt

Oligonucleotides

Name	Sequence	Manufacturer
RNA40 bait for PD	5'-GCCCGUCUGUUGUGUGACUC-biotin-3'	Biopolymers.net
RNA40mod bait for PD	5'-GCCCGUCUGmUUGUGUGACUC-biotin-3' Gm = 2'-O-me-G	Biopolymers.net
RNA_XLmod bait for XLink	5'-GmGCAAGUCCCUGUsUCGGGCGCCA-biotin-3' Us = 4-Thio-U and Gm = 2'-O-me-G	Both designed by Prof. Mark Helm, Johannes-Gutenberg University Mainz; synthesized by Dr. Timo Weinrich, Goethe University Frankfurt
RNA_XL bait for XLink	5'-GGCAAGUCCCUGUsUCGGGCGCCA-biotin-3' Us = 4-Thio-U	
TRMT61A_for DNA Primer	5'-CTCACTCCGGGAATCCTTGG-3'	Eurofins Genomics
TRMT61A_rev DNA Primer	5'-GTCAGTACCTAGGACAGCGC-3'	Eurofins Genomics

Cell media

Name	Product	Manufacturer
LB-Medium	X968.2	Carl Roth
RPMI 1640	31870-025	Gibco, Thermo Fisher Scientific
RPMI	ZB19d	Zellkulturbank FLI Riems
Opti-MEM 1x	11058-012	Gibco, Thermo Fisher Scientific

Prepared media

Name	Composition
RPMIs	RPMI 1640 10 % FBS 1 % Penicillin-Streptomycin 0.447 mg/ml L-Glutamine
TDM	RPMIs 10 ng/ml IL-3 10 ng/ml M-CSF 100 nM β-Estradiol
Cryomedium	RPMI 20 % FBS 10 % Dimethyl sulfoxide

Buffers

Purpose	Name	Composition
Electrophoresis	TBE, 10 x	0.9 M Trizma base 0.9 M boric acid 0.02 M $Na_2EDTA*H_2O$
Flow cytometry	FACS buffer	0.1% Sodium azide 0.1% BSA in PBS Buffer was a kind gift from Dr. Ulrike Blohm, Friedrich-Loeffler-Institute Greifswald
In-gel digestion	Destaining buffer	25 mM ABC 50 % ethanol
In-gel digestion	Reduction buffer	50 mM ABC 10 mM DTT
In-gel digestion	Alkylation buffer	50 mM ABC 50 mM IAA
In-gel digestion	Trypsin digestion buffer	50 mM ABC pH 8.0 1 µg trypsin per sample
Mass spectrometry	Buffer A	0.1 % formic acid
Mass spectrometry	Buffer B	80 % acetonitrile 0.1 % formic acid
Organelle fractionation	Hypoosmolar buffer	10 mM HEPES/KOH pH 7.6 1.5 mM $MgCl_2$, 10 mM KCl
Organelle fractionation	Lysis buffer	0.1 % Igepal CA-630 0.5 mM DTT 1 x cOmplete protease inhibitor cocktail

Purpose	Name	Composition
Organelle fractionation	PBB	150 mM NaCl 50 mM Tris/HCl pH 8.0 10 mM $MgCl_2$ for incomplete PBB, completed with 0.5 % Igepal CA-630 1 x cOmplete protease inhibitor cocktail
RNA pull-down	RNA binding buffer	100 mM NaCl 50 mM Hepes-KOH pH 7.6 0.5 % Igepal CA 630 10 mM $MgCl_2$
RNA pull-down	RNA wash buffer	250 mM NaCl 50 mM Hepes-KOH pH 7.6 0.5 % Igepal 10 mM $MgCl_2$
RNA pull-down	3 x Formamid buffer	10 mM Tris/HCl pH 7.5 0.25 % Formamid 0.25 % OrangeG
RNA pull-down	Sample buffer	1 x LDS 100 mM DTT
SP3	Reconstitution buffer	50 mM HEPES-NaOH pH8 10 mM NaCl 1 mM EDTA pH8 0.5 % Deoxycholic acid sodium salt 1 % Triton X-100
Western blot	Transfer buffer	14.4 g/l glycine 3.03 g/l Trizma base 20 % ethanol
Western blot	PBS-T	PBS 0.05 % Tween-20
Western blot	Blocking buffer	PBS 0.05 % Tween-20 10 % skim milk
Western blot and virus proteomes	1.5 % lysis buffer	1.5 % SDS
Virus secretomes	10 % lysis buffer	10 % SDS

Chemicals and reagents

Name	Product	Manufacturer
Acetonitrile (ACN) ≥ 99.9 %	83639.320	VWR International
Agarose Bioreagent	A9539-500G	Sigma-Aldrich

Name	Product	Manufacturer
Acetonitrile (ACN) ≥ 99.9 %	83639.320	VWR International
Agarose Bioreagent	A9539-500G	Sigma-Aldrich
Ammonium Bicarbonate (ABC) ≥ 99 %	A6141-500G	Sigma-Aldrich
Ampicillin sodium salt	K029.1	Carl Roth
Bovine Serum Albumin (BSA) Fraction V	292-322-5	Carl Roth
cOmplete, EDTA-free protease inhibitor cocktail	505648900 1	Roche
Coomassie 250 Brilliant Blue	9598.1	Carl Roth
Deoxycholic acid sodium salt ≥ 98 %	3484.2	Carl Roth
Dimethyl sulfoxide (DMSO) ≥ 99.7 %	D2650	Sigma-Aldrich
DL-Dithiothreitol (DTT) ≥ 98%	D0632-25G	Sigma-Aldrich
dNTP Bundle	NU-1005S	Jena Bioscience
Dulbecco's phosphate-buffered saline (DPBS) 1 x	14190-094	Gibco, Thermo Fisher Scientific
Dynabeads MyOne Streptavidin C1 Magnetic Beads	65002	Invitrogen, Thermo Fisher Scientific
Ethylenediamine tetraacetic acid (EDTA) ≥ 99 %	8040.2	Carl Roth
Ethanol (EtOH) gradient grade ≥ 99.9 %	111727250 0	LiChrosolv, Merck
Ethanol (EtOH) ROTIPURAN ≥ 99.8 %	9065.3	Carl Roth
Fetal Bovine Serum (FBS), qualified	10270-106	Gibco, Thermo Fisher Scientific
Formamide ≥ 99.5 %	F9037	Sigma-Aldrich
Formic Acid 98 - 100 %	131030.16 11	PanReac AppliChem, ITW Reagents
GeneRuler 1kb DNA Ladder	SM0311	Thermo Fisher Scientific
Glycerol puriss.	15523-1L-R	Honeywell
Glycine ≥ 99 %	3790.2	Carl Roth
HEPES ≥ 99.5 %	HN78.2	Carl Roth
Igepal CA-630	I8896	Sigma-Aldrich

Name	Product	Manufacturer
Iodoacetamide (IAA) ≥ 99 %	I6125	Sigma-Aldrich
L-Glutamine solution 200 mM	G7513-100ML	Sigma-Aldrich
LPS-EK from E. coli K12 – TLR4 Agonist	tlrl-peklps	InvivoGen
Magnesium chloride hexahydrate ($MgCl_2$) ≥ 99 %	M2670	Sigma-Aldrich
NuPAGE 4-12% Bis-Tris Gel 1.0 mm x 10-well	NP0321BOX	Invitrogen, Thermo Fisher Scientific
NuPAGE MES SDS Running Buffer 20x	NP0002	Life Technologies, Thermo Fisher Scientific
NuPAGE™ LDS Sample Buffer 4X	NP0008	Life Technologies, Thermo Fisher Scientific
Orange G	861286	Sigma-Aldrich
Paraformaldehyde (PFA) 16 %	043368.9M	Thermo Fisher Scientific
Penicillin-Streptomycin 100 x	P0781-100ML	Sigma-Aldrich
Ponceau S solution	A2935,0500	PanReac AppliChem, ITW Reagents
Potassium chloride (KCl) ≥ 99.5 %	6781.1	Carl Roth
Protein Assay Dye Reagent concentrate	#5000006	Bio-Rad
Recombinant Human IL-3	200-03-50UG	PeproTech
Recombinant Human M-CSF	300-25-100UG	PeproTech
Sera-Mag magnetic carboxylate modified particles (Hydrophobic)	GE44152105050250	Cytiva
Sera-Mag Magnetic carboxylate modified particles (Hydrophilic)	GE24152105050250	Cytiva
Skim milk powder	70166-500G	Sigma-Aldrich
Sodium chloride (NaCl) ≥ 99.5 %	71380	Sigma-Aldrich
Sodium lauryl sulphate (SDS) ≥ 99.5 %	4360.1	Carl Roth
Sucrose ≥ 99.5 %	S7908-250g	Sigma-Aldrich
Triton X-100	#X100	Sigma-Aldrich
Tris(2-carboxyethyl)phosphine hydrochloride (Tris/HCl)	C4706	Sigma-Aldrich

Name	Product	Manufacturer
Trizma Base ≥ 99.9 %	T1503-1KG	Sigma-Aldrich
Trypan Blue Solution 0.4 %	T8154-20 ml	Sigma-Aldrich
Tween 20	P7949-500ML	Sigma-Aldrich
UltraPure water	10977-035	Invitrogen, Thermo Fisher Scientific
Urea > 99.5 %	U1250-1KG	Sigma-Aldrich
Water HPLC grade	23595.328	VWR
yeast tRNA	15401-029	Invitrogen, Thermo Fisher Scientific
β-Estradiol	E2758-1G	Sigma-Aldrich

Commercial kits

Name	Product	Manufacturer
Amaxa P3 Primary Cell 4d-Nucleofector X Kit L	V4XP-3024	Lonza
DNeasy Blood & Tissue Kit	69504	Qiagen
e-Myco Mycoplasma PCR Detection Kit	25235	LiliF Diagnostics
Lipofectamine 3000 Transfection Kit	L3000001	Invitrogen
Monarch PCR & DNA Cleanup Kit	#T1030S	New England Biolabs
Pierce BCA Protein Assay Kit - Reducing Agent Compatible	23250	Thermo Fisher Scientific
Plasmid Midi Kit	12143	Qiagen
Qubit dsDNA High Sensitivity Assay-Kit	Q32851	Invitrogen
Zombie UV Fixable Viability Kit	77143	BioLegend

Other consumables

Name	Product	Manufacturer
13.2 mL, open-top thinwall ultra-clear tube, 14 x 89mm	344059	Beckman Coulter
96-well PCR Plate	710882	Biozym
Ambersham Protan 0.45 µm NC Nitrocellulose Blotting Membrane	10600002	GE Healthcare Life Sciences
Aurora Ultimate 25x75 Column	AUR3-25075C18	IonOpticks
CDS Analytical 2215 Empore™ C-18 disk	2215-C18	3M Purification Inc.
Costar 12-well clear TC-treated multiple well plates	3513	Corning Life Sciences
Costar 6-well clear TC-treated multiple well plates	3516	Corning Life Sciences
Dialysis tubing, benzoylated	D7884-5FT	Sigma-Aldrich
Falcon 100 mm TC-treated Cell Culture Dish	353003	Corning Life Sciences
Falcon 150 mm x 25 mm TC-treated Cell Culture Dish	353025	Corning Life Sciences
Falcon 24-well clear flat bottom TC-treated multiwell cell culture plate	353047	Corning Life Sciences
Fisherbrand sterile PES syringe filter	15206869	Thermo Fisher Scientific
Primaria 96-well clear flat bottom microtest microplate	353872	Corning Life Sciences
Protein LoBind tubes 1.5 mL	022431081	Eppendorf
ReproSil-Pur 120 C18-AQ, 75 um inner diameter	r119.aq.0001	Dr. Maisch
Safe-Lock Tubes 1.5 ml	0030 123.328	Eppendorf

Instruments

Name	Manufacturer
4D Nucleofector, Core and X Unit	Lonza
Bioruptor Plus sonicator	Diagenode
ChemiDoc Imaging System	Bio-Rad
CoolCell	Biozym
Easy-nLC 1000 and 1200 UHPLC	Thermo Fisher Scientific

Name	Manufacturer
Easy-nLC 1200 UHPLC	Thermo Fisher Scientific
Eclipse Ts2 Fluorescence Microscope	Nikon
FACSAria Fusion	BD Biosciences
FACSymphony A3	BD Biosciences
GloMax Discover Microplate Reader	Promega
Kimble Kontes Dounce Tissue Grinder 7 ml	DKW Life Sciences
nanoElute HPLC	Bruker
NanoPhotometer Pearl	Implen
Odysee CLx Imager	LI-COR
Optima XE-100 Ultracentrifuge	Beckman Coulter
Orbitrap Exploris 480 Mass Spectrometer	Thermo Fisher Scientific
Q Exactive Plus Mass Spectrometer	Thermo Fisher Scientific
Qubit 4 Fluorometer	Invitrogen
SW 41 TI Swinging bucket rotor	Beckman Coulter
TC20 automated cell counter	Bio-Rad
timsTOF Pro Mass Spectrometer	Bruker
UV Cross-Linker CL-508	UVItec

Software

Name	Version	Developer
BioRender		Science Suite Inc.
Clustal Omega Multiple Sequence Alignment	2.10.1+8ae38445	Fábio Madeira
ClusterProfiler R package	4.10.1	Guangchuang Yu
Compass HyStar	6.0	Bruker
ComplexHeatmap R package	2.18.0	Zugang Gu
Excel for Microsoft 365	2510	Microsoft
Factoextra R package	1.0.7	Alboukadel Kassambara

Name	Version	Developer
Fiji - ImageJ	1.54f	Wayne Rasband and contributors, National Institute of Health, USA
Geneious Prime	2025.1.3	Biomatters
GraphPad Prism	10.2.1	Dotmatics
org.Hs.eg.db R package	3.18.0	Marc Carlson
Image Studio	5.2	LI-COR
MaxQuant	2.1.0.0 and 2.4.2.0	Jürgen Cox Lab, Max Planck Institute of Biochemistry, Martinsried
PowerPoint for Microsoft 365	2510	Microsoft
RStudio	2023.06.1	The R foundation
ShinyGO	0.85	Ge SX, Jung D & Yao R
STRING database	12.0	String Consortium
timsControl	3.1	Bruker
Vectorbuilder		VectorBuilder Inc.
Word for Microsoft 365	2510	Microsoft
XCalibur	3.1	Thermo Fisher Scientific
Zotero	7.0.30	Digital Scholar

Biological Databases

Organism	Origin	Number
Bombali virus	FLI/Huh-7-rec/GER/2021/42BB.AJ.3	ON871047
Bundibugyo virus	BEI<USA>:NR_51692	MT583344.1
Homo sapiens	SwissProt database, 25,275 entries	UP000005640, v20200117
Homo sapiens	Trembl database, 54,436 entries	UP000005640, v20200117
Reston virus	RESTV/M.fascicularis-tc/PHL-USA/1996/Ferlite	JX477166.1
Sudan virus	H.sapiens-tc/SSD/1979/Maleo	KC242783.2
Taï Forest virus	H.sapiens-tc/CIV/1994/Pauleoula-CI	NC_014372.1
Ebola virus	rec/COD/1976/Mayinga-rgEBOV	KF827427.1

Artificial Intelligence Tools

Tool and Developer	Sections and Purpose of Usage	Date
Consensus.app Consensus NLP Inc.	Writing of introduction and literature research: generation of structured overviews for lists of relevant peer-reviewed references	10/25 – 02/26
DeepL.com/write DeepL SE	Writing of complete thesis: optimizing written text for language clarity and quality	06/25 – 02/26
Elicit.com Elicit Research, PBC	Writing of introduction and discussion: used for summaries on specific research questions and for finding peer-reviewed references	11/25 – 02/26
Julius.AI Caesar Labs Inc.	Data analysis: assistance for software development for analysis of proteome data	01/25 – 02/26
NotebookLM.google.com Google Labs	Writing of introduction and literature research: generation of structured overviews for lists of relevant peer-reviewed references	09.25 – 02/26

The listed artificial intelligence tools were used as described above and the output was checked for accuracy and content before usage within this work. I therefore assume full responsibility for this work.

Methods

Cell culture

BLaER1 cultivation

BLaER1 WT and TLR8KO cells (a kind gift from Prof. Alexander Dalpke, University Hospital Heidelberg, Germany) were cultivated according to protocols of Moritz Gaidt (Gaidt *et al.*, 2018). They were grown in RPMI 1640 medium (Gibco), supplemented with 10 % FBS (Gibco), 1 % Penicillin-Streptomycin (Sigma Aldrich) and 0.447 mg/ml L-Glutamine (Sigma Aldrich). The suspension of cells proliferating in their B cell state was split every 3 to 6 days by transferring 5.0E+05 cells to fresh 10 cm cell culture dishes (Corning Life Sciences). Cells were maintained under humid conditions at 5 % CO_2 and 37 °C. To rule out contamination, the cells were monitored every 6 months Mycoplasma PCR detection tests (LiliF Diagnostics) according to the manufacturer's instructions. Frozen cell stocks were produced by resuspending the cells in RPMI with 20 % FBS and 10 % dimethyl sulfoxide (DMSO, Sigma Aldrich) before cooling them at -1 °C per minute down to at -80 °C in a CoolCell (Biozym) and transfer to -150 °C for long-term storage. To reconstitute frozen cells, the cryovial was thawed in a 37 °C water bath. Then, the cryomedium was removed through centrifugation, before the cells were resuspended in RPMIs for cultivation.

BLaER1 transdifferentiation

The generation of postmitotic macrophage-like BLaER1 cells was performed according to the instructions of Moritz Gaidt (Gaidt *et al.*, 2018). In summary, the cells were harvested via centrifugation at 400 × g and counted with a TC20 automated cell counter (Bio-Rad) and 0.4 % Trypan Blue solution (Sigma Aldrich) before being resuspended in TDM. This medium was produced by supplementing RPMIs with 10 ng/ml IL-3 (PeproTech), 10 ng/ml M-CSF (PeproTech) and 100 nM β-Estradiol (Sigma-Aldrich). The cells were seeded with 5.0E+05 cells in each well of a 6-well plate (Corning Life Sciences) for infection or stimulation experiments. For large-scale experiments such as organelle gradients,1.0E+07 cells were seeded in a 15 cm dish (Corning Life Sciences). To increase the transdifferentiation efficiency, 50 % of TDM was replaced every 2 to 3 days during the incubation period of 5 to 7 days. During stimulation experiments of BLaER1 macrophages, lipopolysaccharide (LPS) was used as TLR4-ligand and as positive control for cell activation. For this purpose, 1 µg/ml LPS (InvivoGen) was dissolved in TDM for stimulation of 2.0E+05 transdifferentiated BLaER1 per 6-well in 2 ml of LPS-containing stimulation medium. Following incubation of 24 hours, cells were harvested and analyzed as for viral infection experiments.

Flow cytometry

BLaER1 transdifferentiation efficiency was determined via flow cytometry. The cells were harvested in RPMIs, centrifuged at 400 × g for 5 minutes and resuspended in Dulbecco's phosphate-buffered saline (DPBS) for counting. For each sample, 1.0E+06 cells were washed in Fluorescence-activated cell sorting (FACS) buffer and stained with a Zombie UV viability kit (BioLegend) according to the manufacturer's instructions. The cells were resuspended in FACS buffer and incubated with 5 µl of PE-conjugated CD19 (BioLegend) and APC-conjugated CD14 (BioLegend) antibodies for 15 minutes at 4 °C. After centrifugation, the supernatant was discarded, and the cells were washed in FACS buffer. Then, the cells were fixed in 4 % paraformaldehyde (Thermo Fisher Scientific) in DPBS for 30 minutes at room temperature. Finally, the cells were washed and resuspended in FACS buffer for analysis on a FACSymphony A3 Cell Analyzer (BD Biosciences). During measurement, single cells were selected using forward- and sideward-scatter area or width for analysis of GPF expression and comparison of CD19 PE and CD14 APC signals. According to previous publications, immunophenotyping was performed by assigning cells with CD19 expression to undifferentiated B cells, while cells with CD14 surface markers were classified as transdifferentiated macrophages (Schüssler *et al.*, 2023; Volkmar *et al.*, 2024).

Cas9 KO generation

Plasmid preparation

The plasmid pRP[CRISPR]-mCherry/Puro-hCas9 U6>hTRMT61A[gRNA#221] (hereafter termed pCas9-TRMT61A-gRNA) was designed by Lan-Sun Chen (research group Alexander Dalpke, University Hospital of Heidelberg) via VectorBuilder (VectorBuilder Inc.) to express Cas9 and a *TRMT61A*-specific gRNA. The VB UltraStable *E. coli* glycerol stock was inoculated in 50 ml of LB medium (Carl Roth) containing 100 µg/ml ampicillin (Carl Roth). After bacterial growth at 37 °C and 200 rpm overnight, the cells were harvested, and plasmid DNA was extracted using the Plasmid Midi Kit (Qiagen) according to the manufacturer's instructions. After the plasmid was resuspended, DNA concentration was determined using a Qubit 4 fluorometer (Invitrogen) with the dsDNA High Sensitivity Assay Kit (Invitrogen) following the standard procedure supplied with the kit. To confirm successful plasmid preparation, a 600 ng sample was sent for whole plasmid sequencing at Eurofins Genomics.

Transfection

To create KO cell lines, undifferentiated BLaER1 cells were transfected with pCas9-*TRMT61A*-gRNA via lipofection or nucleofection. For lipofection, the Lipofectamine 3000 Transfection Kit (Invitrogen) was used according to the manufacturer's instructions. In detail, 1.0E+06 cells were

seeded in a 6-well plate with 2 ml of RPMI in each well. A total of 3.75 µl Lipofectamine 3000 reagent was diluted in 125 µl of Opti-MEM (Gibco), and 4 µg of plasmid DNA was mixed with 125 µl of Opti-MEM and 8 µl of P3000 enhancer reagent. The lipofectamine and DNA mixtures were combined at a 1:1 ratio. They were incubated for 15 minutes, which enabled the formation of lipid-DNA complexes that were then added to the cells. After 6 hours, 2 ml of RPMIs was added to each well, and the cells were incubated for 48 hours.

Nucleofection was conducted with the Amaxa P3 Primary Cell Kit (Lonza) with a 4D Nucleofector (Lonza) following the manufacturer's instructions. After the growth medium was removed through centrifugation, 5.0E+05 and 1.0E+06 cells were resuspended in a mixture of 18 µl supplement and 82 µl N-solution for each reaction. Respectively, 1 and 2 µg of plasmid DNA were added to the mixture, which was transferred into nucleofection cuvettes. Nucleofection was carried out using the program E0-117 for human B cells, before the cells were resuspended in 1.5 ml of prewarmed RPMIs in a 12-well plate (Corning Life Sciences). To allow expression of the transfected plasmid before flow cytometry, the cells were then incubated for 48 hours.

Fluorescence-Activated Cell Sorting

To generate single-cell clones with a potential KO, BLaER1 cells expressing the plasmid marker mCherry were selected via FACS. For this purpose, 96-well plates (Corning Life Sciences) were prepared with 0.2 ml RPMIs per well and preheated to 37 °C. The cells were resuspended in 0.5 ml of RPMIs and sorted with a FACSAria Fusion Flow Cytometer (BD Biosciences). Individual cells showing GFP and mCherry expression were then incubated at 37 °C and 5 % CO_2. To support growth, 50 µl of conditioned medium from BLaER1 WT cultivation was added weekly. This medium had been filtered through 0.2 µm syringe filters (Thermo Fisher Scientific) beforehand. Cells with visible clonal expansion were transferred to 6-well plates and 10 cm dishes for expansion and further genotyping.

BLaER1 genotyping

To determine the genomic sequence of *TRMT61A* in potential KO cells, gDNA was extracted from each clone using the DNeasy Blood & Tissue Kit (Qiagen) according to the manufacturer's instructions. To amplify the genomic *TRMT61A* locus around the gRNA binding site, primers (#6265 TRMT61A_for: CTCACTCCGGGAATCCTTGG and #6266 TRMT61A_rev: GTCAGTACCTAGGACAGCGC) were designed in Geneious Prime (Dotmatics) as custom DNA oligonucleotides from Eurofins Genomics. PCR was performed with a HF-DNA Polymerase (IMB Protein Production Core Facility) following the supplied protocol with 100 ng gDNA. The reaction was performed with 35 cycles of an optimized PCR amplification protocol (10 seconds 98 °C denaturation, 30 seconds 70 °C annealing and 35 seconds 72 °C extension). Successful

amplification was confirmed by gel electrophoresis in 1 % agarose (Sigma Aldrich) and 1 × TBE (IMB Media Lab) at 100 V for 20 minutes. Then, the PCR product was purified using the Monarch PCR & DNA Cleanup Kit (New England Biolabs) as instructed by the manufacturer. The eluted gDNA concentration was measured with a Nanophotometer (Implen) and 50 ng gDNA were sent with 25 pmol TRMT61A_for primer for Sanger sequencing with LightRun Services by Eurofins Genomics. To find mutations that could lead to functional KO, the results were analyzed by assembling the sequences to the genomic reference of *TRMT61A* with Geneious Prime (version 2025.1.3, Biomatters).

Protein experiments

Protein extraction and subcellular organelle fractionation

To assess the subcellular localization of proteins and to generate an endolysosome (EL) enriched protein extract, a protocol by Lia Walker (Walker, Hussein and Akula, 2016) was adapted for the fractionation of BLaER1 organelles. BLaER1 cells were transdifferentiated in 150 mm TC-treated cell culture dishes (Corning Life Sciences) for 7 days. After discarding the BLaER1 cells suspended in the supernatant, 3.0E+08 adherent cells were harvested in DPBS (Gibco). The supernatant was discarded after centrifugation at 500 × g for 10 minutes. Then, the cell pellet was resuspended in 20 ml of RPMI (Gibco). The cells were cooled at 4 °C for 1 hour and washed three times in cold RPMI. For the following cell treatment and organelle separation, the cells were kept on ice or in precooled centrifuges at 4 °C. The cells were resuspended in hypoosmolar buffer at a 1:5 ratio of cell pellet to buffer volume. After incubation for 10 minutes, the cell suspension was centrifuged at 600 × g for 10 minutes, which allowed discarding of the supernatant above the soft cell pellet. The cells were mixed with freshly prepared lysis buffer containing a protease inhibitor cocktail (Roche) and homogenized with a Dounce tissue grinder (0.0171 mm clearance, DKW Life Sciences) using 12 strokes. To reduce the number of intact cells, nuclear proteins, and large cellular fragments, the homogenate was separated into a nuclear fraction and the PNS by centrifugation at 3,300 × g for 15 minutes. For RNA pull-down experiments with PNS, proteins were released from organelles via ultrasound by treating 300 µl of PNS in 1.5 ml tubes (Eppendorf) with sonification at a low setting for 15 seconds using a Bioruptor Plus (Diagenode). Alternatively, for the separation of cellular organelles, the PNS was adjusted to 150 mM NaCl (Sigma Aldrich), 1 mM Ethylenediamine tetraacetic acid (EDTA, Carl Roth) and 25 % sucrose (Sigma Aldrich). Sucrose solutions were prepared to generate two discontinuous density gradients for PNS separation. This was achieved through the careful layering of 3 ml 45 %, 4.1 ml 35 % and 3.8 ml 25 % cooled sucrose solutions from bottom to top in a 13.2 ml open-top thin wall ultra-clear tube (Beckman Coulter). Lastly, half of the adjusted PNS was layered on top to fill each tube up to 1 mm below the opening. This gradient was centrifuged at 4 °C and 100,000 × g for 1 hour in a precooled Optima XE-100 ultracentrifuge (Beckman Coulter) with a swinging bucket rotor SW 41 TI (Beckman Coulter). Afterward, the sucrose gradients containing the visible organelle bands were pooled from top to

bottom in 2 ml fractions. To assess organelle separation within the gradient, each fraction and a sample of the PNS were processed by in-gel digestion for Liquid chromatography-tandem mass spectrometry (LC-MS/MS) measurements.

To use the endolysosome-enriched fraction F3 in RNA pull-down experiments, dialysis was performed with the collected fraction to reduce the high sucrose concentration within the native protein sample. Therefore, samples were dialyzed through a membrane (Sigma Aldrich) using 2 l incomplete PBB dialysis buffer at 4 °C for 48 hours with buffer exchange after 24 hours. Afterward, PBB buffer in the samples was completed through the addition of protease inhibitor cocktail (Roche) and 0.5 % Igepal CA-630 (Sigma Aldrich). Finally, as described above, 15 seconds of sonication were performed to prepare the endolysosomal protein fraction for use in RNA pull-down experiments.

Protein concentration measurement

Concentrations of protein extracts were determined via Bradford assays with the Dye Reagent Concentrate (Bio-Rad) according to the manufacturer's instructions. In brief, 6.5 µl of the samples were mixed with 200 µl 1 x dye in 96-well plates (Biozym) for 5 minutes of incubation. The absorbance was measured at 595 nm using a GloMax Discover Microplate Reader (Promega). To determine the concentration, the absorbance of a sample buffer control was deducted from all measurements, and the sample absorbance was compared to the results from a standard row made from BSA (Carl Roth). For measurement of peptide concentration before LC-MS/MS or protein concentration in extracts containing SDS, a Pierce BCA protein assay kit (Thermo Fisher Scientific) was used because of its compatibility with reducing agents. The kit was used following the manufacturer's instructions by preparing 1 µl per sample for peptide and 2 µl per sample for protein measurement with 150 µl of working solution. Following incubation at 60 °C for 30 minutes in a 96-well plate, absorption was measured at 560 nm, and the concentration was determined with a standard row as described above.

Western blots

The amount of TRMT61A protein in samples was compared through Western blotting. For pull-downs, the complete eluted protein sample in LDS was used, while full-cell extracts were prepared by resuspending cells in 40 µl of UltraPure water (Invitrogen) and mixing with 120 µl of 1.5 % SDS lysis buffer for incubation at 70 °C and 300 rpm for 10 minutes. The samples were separated on a 4 - 12 % NuPAGE Bis-Tris gel (Thermo Fisher Scientific) using 1 x NuPAGE MES SDS buffer (Thermo Fisher Scientific) for 25 minutes at 180 V. For protein blotting, a transfer stack was prepared with the Bis-Tris gel and a nitrocellulose blotting membrane (GE Healthcare). The transfer was performed in precooled 1 x transfer buffer with 20 % ethanol (Carl Roth) at 300 mA for 60 minutes.

Then, the membrane was stained with Ponceau S (Applichem) for the visualization of the protein bands. The membrane was blocked in 10 % skim milk (Sigma Aldrich) in PBS-T as blocking buffer for 1 hour before primary antibody incubation using 1:500 dilutions of polyclonal TRMT61A rabbit antibody (Biorbyt) and monoclonal beta Actin mouse antibody (Santa Cruz Biotechnology). After incubating at 6 °C and 300 rpm overnight, the membrane was washed with PBS-T and incubated in blocking buffer with 1:15,000 dilutions of IRDye 800CW goat anti-rabbit (LI-COR) and IRDye 680RD goat anti-mouse (LI-COR) at room temperature for 1 hour. The membrane was washed in PBS-T to detect the fluorescence of secondary antibodies on an Odysee CLx Imager (LI-COR). Image Studio software (LI-COR, version 5.2) was used to scan the blots with 700 and 800 nm channels, and the fluorescence intensity was quantified for further analysis using a two-tailed unpaired t-test in GraphPad Prism (Dotmatics, version 10.2.1).

Identification of RNA-binding proteins

RNA pull-down

RBPs were identified using a pull-down protocol based on descriptions by Marion Scheibe (Scheibe *et al.*, 2013) in quadruplicates. For each reaction, 10 µg of biotinylated RNA oligonucleotides (Biopolymers), containing no (RNA40) or one 2'-O-me-G (RNA40mod), were used. RNA40 is an sequence fragment originating from the viral genome of the HIV, which is well-established for the induction of a TLR8-dependent immune response (Heil *et al.*, 2004b). To determine the amount of RNA to saturate Dynabeads MyOne Streptavidin C1 (Thermo Fisher Scientific), different RNA concentrations were incubated with 25 µl beads in RNA binding buffer. After collecting supernatant, beads were washed in RNA binding buffer and a 1 x formamide buffer was used to elute RNA from beads for electrophoresis in 3 % agarose (Sigma-Aldrich) and 1 x TBE (Sigma-Aldrich). For RNA pull-down experiments, the RNA was bound to 25 µl of beads in RNA binding buffer on a rotation wheel for 30 minutes at 4 °C. After the supernatant containing unbound RNA was discarded, the beads were washed with RNA wash buffer three times. The protein mixture was prepared with 200 µg of protein and 20 µg of yeast tRNA (Thermo Fisher Scientific) per reaction in 200 µl of PBB, which was added to the beads. Following incubation on a rotation wheel for 30 minutes at 4 °C, the supernatant was discarded, and the beads were washed three times with RNA wash buffer. To elute RNA-bound proteins, the beads were mixed vigorously with 25 µl 1 x LDS sample buffer containing 100 mM dithiothreitol (DTT) and incubated at 1400 rpm and 70 °C for 10 minutes. Afterward, the supernatant without beads was used for in-gel digestion and LC-MS/MS analysis.

RNA crosslinking experiment

To evaluate a second RNA sequence containing 2'-O-me and increase the number of proteins bound to RNA, oligonucleotides were designed by Prof. Mark Helm (Johannes-Gutenberg University, Mainz) and synthesized by Dr. Timo Weinrich (Goethe University, Frankfurt). The 3' biotinylated RNA_XLmod and RNA_XL both contained an additional 4-Thio modification to enable UV crosslinking to proteins (Favre *et al.*, 1986). Additionally, RNA_XLmod was modified with a 2'-O-me-G at the 5'-end, whereas RNA_XL contained an unmodified G. The experiment was performed like the RNA pull-down described above, with 2.5 µg of RNA per experiment and 200 µg of PNS as the protein extract. Additionally, after the protein was incubated with RNA bound to beads, the mixture was transferred to a 24-well plate, and a 10-minute crosslinking step was performed using 365 nm UV light in a CL-508 UV crosslinker (UVItec). Afterwards, the beads were washed three times in RNA wash buffer and eluted in LDS as described for RNA pull-down.

Viral infection

BLaER1 cells were infected in quadruplicates after 5 – 7 days of transdifferentiation (5.0E+05 cells per well) on 6-well plates (Corning Life Sciences) with recombinant orthoebolavirus in a BSL-4 laboratory. For this purpose, stocks of rgBOMV, rgEBOV-WT and rgEBOV-iGFP were diluted in TDM for tissue culture infective doses of 5.0E+05/ml and 5.0E+04/ml. Using these stocks, 1.0E+06 cells in each well were infected with 1 ml of the virus mixture at a high MOI of 0.5 and a low MOI of 0.05. The cells were incubated at 37 °C and 5 % CO_2 for 1 hour, and the supernatant was replaced with cell medium before further incubation. The infection with rgEBOV-iGFP allowed the documentation of virus infection via fluorescence microscopy, performed at 10 x magnification using an Eclipse Ts2 Fluorescence Microscope (Nikon) with 200 ms of exposure, while the gain was set to 2.4 for signal amplification. To collect samples, the supernatant was used to detach cells, which were collected by centrifugation at 1000 × g for 5 minutes. For secretome analysis, 300 µl of the supernatant was mixed with 40 µl 10 % SDS (Carl Roth) lysis buffer and incubated at 99 °C and 300 rpm for 10 minutes to inactivate the sample. The cells were washed in DPBS (Gibco), resuspended in 20 µl of UltraPure water (Invitrogen) for lysis and inactivated with 60 µl of 1.5 % SDS lysis buffer at 99 °C and 300 rpm for 10 minutes. Afterward, secretome and proteome samples were processed by in-gel digestion or SP3 for LC-MS/MS analysis.

Mass Spectrometry

Sample preparation

Protein samples were processed to peptides for MS measurement via an in-gel digestion, in-solution digestion, or SP3 workflow. In short, cell extracts or proteins eluted from RNA pull-downs were reduced and alkylated to break up bisulfide bonds and unfold proteins before tryptic digestion and peptide purification for LC-MS/MS analysis.

A previously described protocol was followed for in-gel digestion of proteins (Shevchenko *et al.*, 2006). Up to 20 µg of protein samples were denatured in 1 x NuPAGE LDS sample buffer (Thermo Fisher Scientific) at 70 °C for 10 minutes and separated at 180 V for 8 minutes on a 4 - 12 % NuPAGE Bis-Tris gel (Thermo Fisher Scientific) in 1 x NuPAGE MES SDS buffer (Thermo Fisher Scientific). For clear separation of samples, the gels were stained with Coomassie G 250 (Carl Roth) for imaging with a ChemiDoc (Bio-Rad). Each sample in the gel was minced for subsequent destaining in a destaining buffer containing 50 % ethanol (Carl Roth). After the gel was dehydrated in acetonitrile (ACN, VWR), peptides were reduced at 56 °C for 60 minutes in reduction buffer with 10 mM DTT (Sigma-Aldrich), and alkylation was performed for 45 minutes in alkylation buffer with 50 mM iodoacetamide (IAA, Sigma-Aldrich). For protein digestion, gel pieces were dehydrated in ACN and rehydrated in a digestion buffer containing 1 µg MS-grade trypsin (Serva) for incubation overnight at 37 °C. To recover peptides, 30 % and 100 % ACN solutions were used for extraction from the gel pieces, after which the organic solvent was evaporated. Peptides were first purified via stage tips with two layers of Empore C-18 material (3M Purification Inc.) and then eluted in buffer B containing 80 % ACN. The organic solvent was subsequently evaporated to yield peptides in buffer A made of 0.1 % formic acid (PanReac AppliChem) for LC–MS/MS measurement.

In-solution digestion was performed for the analysis of conditioned medium samples to investigate the secretome of BLaER1 cells during stimulation. The method is based on a previously described protocol and was performed as a single-pot approach at room temperature (Betancourt *et al.*, 2018). Utilizing 30 µl of an 8 M urea (Sigma-Aldrich) solution in 50 mM Ammonium bicarbonate (ABC, Sigma-Aldrich) 19 µl of the conditioned medium inactivated with 1 % SDS (Carl Roth) were incubated for 10 minutes. Following the addition of 10 µl 10 mM DTT (Sigma-Aldrich) and incubation for 30 minutes, 4 µl of 50 mM IAA were added for 20 minutes alkylation step. Proteins were digested with 1 µg of LysC (Wako) in 50 mM ABC for 3 hours, after which 150 µl 50 mM ABC were added with 0.5 µg of MS-grade trypsin (Serva) for incubation over night. This protocol was followed by stage tip purification as described previously before LC-MS/MS measurements.

Single-pot, solid-phase-enhanced sample preparation (SP3) is an alternative high-throughput protocol involving the same basic steps. It is based on protein-binding magnetic particles and was performed as described by Christopher Hughes (Hughes *et al.*, 2019) in a 96-well PCR plate (Biozym). In brief, 25 µg of proteins were diluted in reconstitution buffer containing 10 mM DTT

and incubated at 60 °C for 30 minutes before alkylation in 25 mM IAA for 25 minutes and quenching the remaining IAA with 10 mM DTT for 5 minutes. Proteins were bound to a 1:1 mixture of hydrophobic and hydrophilic magnetic carboxylated modified particles (Cytiva) by the addition of gradient-grade ethanol (Supelco) for a final ethanol concentration greater than 50%. After incubation for 15 minutes, the supernatant was removed with magnets, the beads were washed with 80 % ethanol three times and resuspended in 50 mM ABC at pH 8.0 with 500 ng of MS-grade trypsin (Serva) for digestion at 37 °C overnight. For sample collection, peptides were eluted by incubating the beads for 10 minutes in HPLC-grade water (VWR) with 0.5 % formic acid. The following peptide purification was performed with stage tips as described above before LC-MS/MS analysis.

Liquid chromatography-mass spectrometry

Generated peptides were analyzed via LC-MS/MS measurements using a Q Exactive Plus, Orbitrap Exploris 480 or timsTOF Pro mass spectrometer. Generally, up to 400 ng peptides were separated via C18 reverse-phase liquid chromatography before being sprayed onto a mass spectrometer with data-dependent acquisition for MS/MS scans.

For peptide measurements of pull-down samples on the Q Exactive Plus with XCalibur (Thermo Fisher), peptides were separated using an Easy-nLC 1000 (Thermo Fisher) with an in-house packed 20 cm ReproSil-Pur 120 C18 column (Dr. Maisch). With a flow rate of 225 nl/minute and a 2 hour gradient of 2 % to 40 % ACN with 0.1 % formic acid, the peptides were ionized and sprayed into the Q Exactive Plus. For each full MS scan, measurements were performed in a data-dependent acquisition mode with high-energy collisional dissociation (HCD) and 10 MS/MS scans.

Analyses on the Orbitrap Exploris 480 with XCalibur (Thermo Fisher) were conducted with the same LC gradient using an Easy-nLC 1200 (Thermo Fisher) and a 50 cm C18 column prepared in house (Dr. Maisch). For pull-down samples, the mass spectrometer was operated with HCD fragmentation for 15 MS/MS scans per full scan, while full proteomes were measured with 20 MS/MS scans.

The timsTOF Pro with timsControl (Bruker) was coupled to a nanoElute HPLC with Compass HyStar (Bruker) containing an Aurora Ultimate 25x75 column (IonOpticks) for a 100-minute gradient. It was performed to separate a maximum of 400 ng peptides at 300 nl per minute in 0.1 % formic acid with increasing concentration of ACN from 0 to 95 % (min 0 – 2 to 2 %, min 2 – 67 to 17 %, min 67 – 88 to 27 %, min 88 – 92 to 95 %, min 92 – 97 at 95 %, min 97 – 100 to 4%). The ionized peptides were analyzed in the timsTOF Pro through data-dependent acquisition in combination with a parallel accumulation serial fragmentation (PASEF) method and a 1.1 second cycle time.

Analysis of MS data

MaxQuant analysis

The measurement files from mass spectrometry were processed with MaxQuant version 2.1.0.0 for pull-down and organelle fractionation samples and with version 2.4.2.0 for proteomes to identify and quantify proteins using standard settings. As a base for peptide identification, the *Homo sapiens* SwissProt (UP000005640, v20200117) and trembl (UP000005640, v20200117) databases were used for in silico digestion to generate a peptide database with a minimum length of 7 amino acids. The analysis of measurements from viral infection samples was conducted with the databases from EBOV containing proteins based on KF827427.1, and Bombali virus FLI/Huh-7-rec/GER/2021/42BB.AJ.3 with proteins based on ON871047. For the analysis, methionine oxidation and protein N-acetylation were set as variable modifications, whereas cysteine carbamidomethylation was defined as a fixed modification to account for IAA treatment. Protein quantification was performed with a minimal ratio count of 2. Unique and razor peptides were used for quantification in pull-downs, whereas only unique peptides were used for proteome quantification. Additionally, Label free quantification (LFQ) values without fast LFQ and intensity based absolute quantification (iBAQ) values were generated.

Quality control and statistical analysis

Further bioinformatic analyses were conducted after excluding protein groups that are known contaminants, identified only by site without finding an unmodified version, or hits to the reverse decoy database from the MaxQuant output. Missing values were imputed for each replicate by generating a beta distribution based on the originally measured values at their detection limit. For imputation, all missing values were randomly assigned within this distribution. The imputed and $\log_2$-transformed LFQ values were subsequently used for detailed data analyses. To judge data quality, specific analysis was performed with each dataset using a script by Mario Dejung (Institute of Molecular Biology, Mainz, Germany) in RStudio. First, the measured intensity and LFQ intensity in each sample were compared to assess regularity between replicates and samples. Additionally, the number of imputed to originally measured values was compared, expecting a ratio of approximately or less than 1:4 for each replicate, to confirm consistent sample preparation and measurement. Finally, a principal component analysis (PCA) was performed to reduce the dimensionality of complex datasets to a two-dimensional scatterplot. The principal components represent the maximal data variance, such that clustering of replicates allowed evaluating the difference between experimental conditions. For a direct comparison between two experiments, volcano plots were generated by calculating the $\log_{10}$ p-value with a Welch t-test and plotting it over the $\log_2$ fold change between experiments. The threshold for statistically significant enrichment of proteins was set to p-values below 0.05 and fold changes over 2. The shape of proteins in the plot describes the imputation of protein signals, so a triangle shows proteins

measured at least once in both conditions, an inverted triangle represents proteins that were not detected in one condition, and proteins measured in all replicates are shown as circles. Furthermore, enriched proteins are depicted in blue, highlighted proteins in red and background proteins do not have a label and are shown in green.

Infection time course analysis

For the analysis of the EBOV infection time course, R-scripts were written in RStudio (The R foundation) with the assistance of Julius.AI (Caesar Labs Inc., 2025) for software development. The package ComplexHeatmap (Zugang Gu) was used to generate heatmaps based on unsupervised hierarchical clustering and the imputed $\log_2$ LFQ values. The same values were used to normalize to the 0 hour control and calculate the fold-change in infected samples compared to the mock control at the respective timepoint. Only proteins showing a fold change over 2 were investigated further in unsupervised K-means clustering. To determine the ideal number of clusters in an unbiased way, the Elbow, Average Silhouette, and Gap statistic methods were applied using the factoextra package (Alboukadel Kassambara). The resulting clusters were separated and analyzed for GO enrichment in different host protein expression patterns using the clusterProfiler package (Guangchuang Yu) and the human annotation database org.Hs.eg.db (Marc Carlson). Therefore, analyses with the GO biological processes, GO cellular component and GO molecular function human pathway databases were performed using standard settings (ShinyGO version 0.85, Ge, Jung and Yao, 2020). The ten most enriched terms were visualized with their fold-enrichment, adjusted p-value and number of proteins per term, respectively for each cluster. To visualize protein clusters, STRING network analyses were performed, using all interaction sources (textmining, experiments, databases, co-expression, neighborhood, gene fusion, and co-occurrence) and medium confidence to generate full networks without clustering (Szklarczyk *et al.*, 2023).

Appendix

Supplementary Figures

Supplementary Figure 1: BLaER1 live-dead staining. BLaER1 cells were incubated with zombie 510 live-dead-stain (BV510-A) for flow cytometry analysis in comparison to ubiquitous GFP expression.

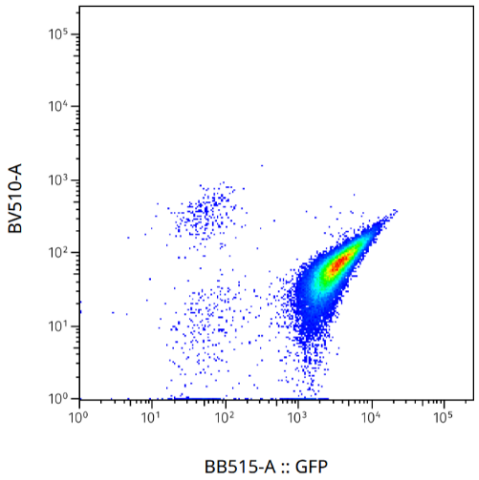

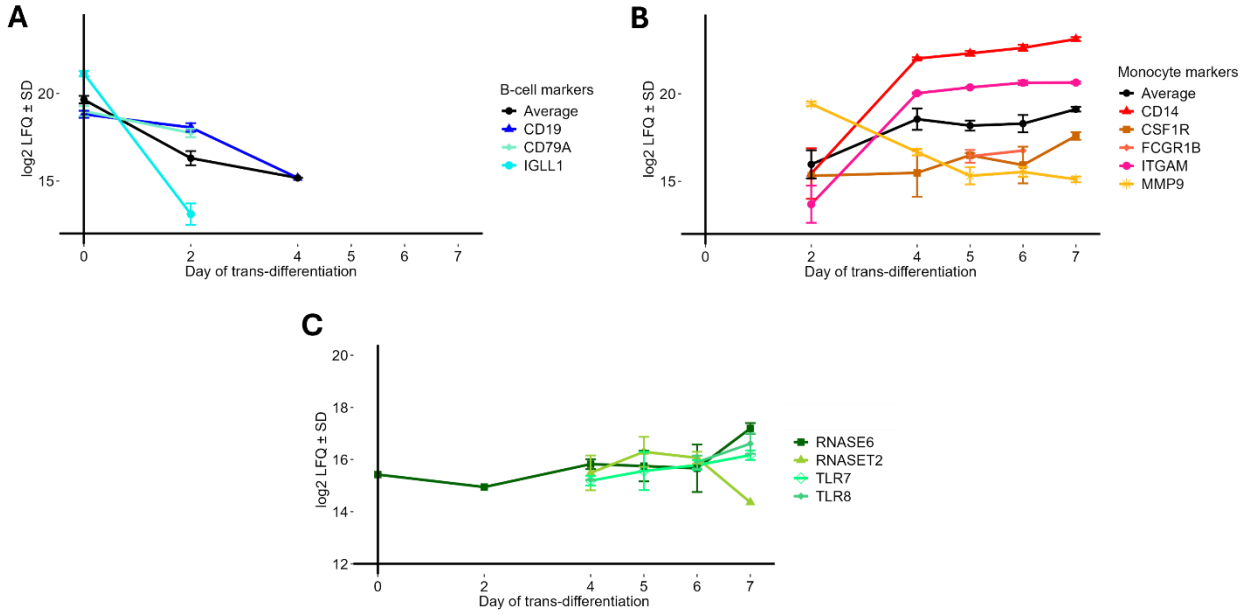

Supplementary Figure 2: Original BLaER1 proteome during transdifferentiation. (A - C) BLaER1 cells were transdifferentiated 7 days to analyze cellular proteomes. The non-imputed log_2 label-free quantification (LFQ) values of B cell (A), macrophage-markers (B), and proteins relevant to ssRNA recognition (C) are shown as average values ± SD.

Supplementary Figure 3 RNA40 binding test. RNA40 and RNA40mod were bound to 25 µg of beads using 1 – 10 µg, after which the supernatant was collected. In a 3 % agarose gel, 1 µg RNA, the amount of unbound RNA in the supernatant, and RNA eluted from beads was detected.

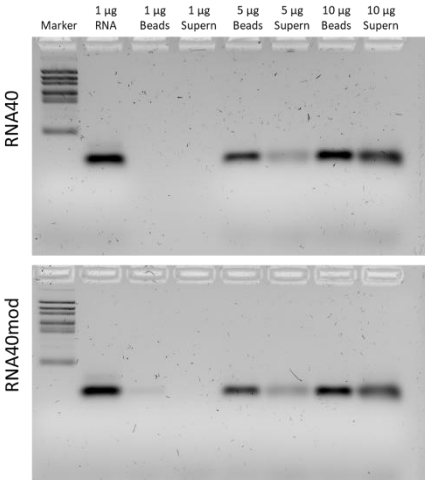

Supplementary Figure 4: RNA binding test for crosslinking. RNA_XLmod and RNA_XL were bound to 25 µg of beads using 1 – 5 µg, after which the supernatant was collected. In a 3 % agarose gel, 1 µg RNA, the amount of unbound RNA in the supernatant, and eluted from beads were detected.

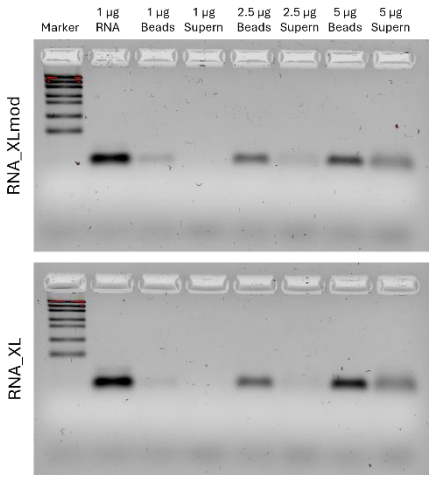

Supplementary Figure 5: TRMT61A Western blot to determine optimal protein concentration. BLaER1 protein extract ranging from 10 - 100 µg was used for Western blot with anti-beta Actin and anti-TRMT61A antibodies. Fluorescent secondary antibodies were used for detection with IRDye 680RD for beta Actin in red and IRDye 800CW for TRMT61A in green.

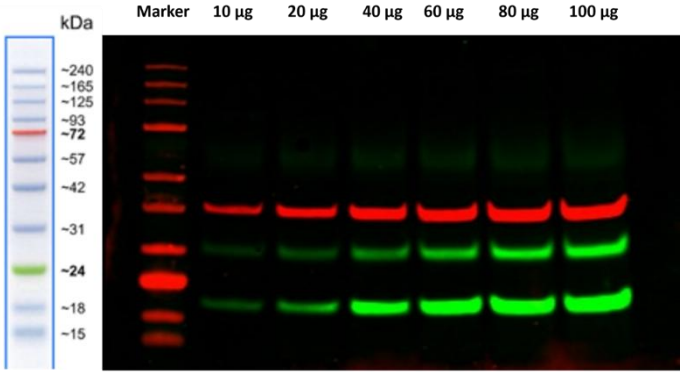

Supplementary Figure 6: Western blot of TRMT61A after RNA40 pull-down including beads-only control and input lane. The BLaER1 post-nuclear supernatant extract was used for RNA40 and RNA40mod pull-downs, which were then analyzed using a Western blot with primary TRMT61A-specific polyclonal and secondary IRDye antibodies. The fluorescence signal was quantified, and a statistical comparison was performed using a two-tailed unpaired t-test for a p-value of 0.0194.

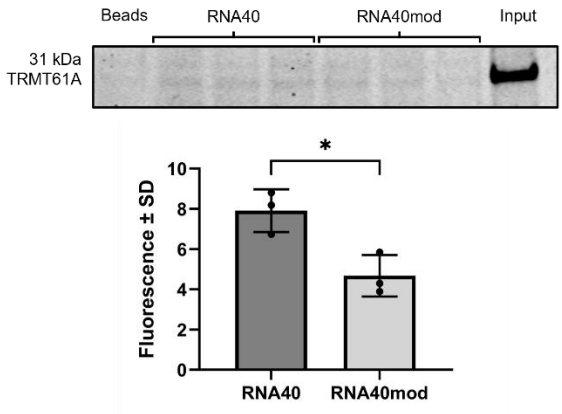

Supplementary Figure 7: Plasmid for the generation of BLaER1 TRMT61A KO cell lines. The 10.6 kbp pCas9-TRMT61A-gRNA sequence contained a TRMT61A gRNA for the encoded Cas9 nuclease and an mCherry selection marker. The plasmid was designed by Lan-Sun Chen (research group Alexander Dalpke, University Hospital of Heidelberg).

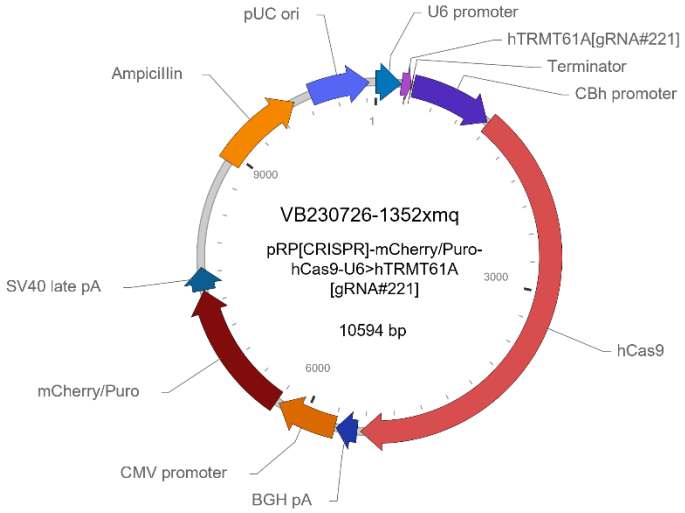

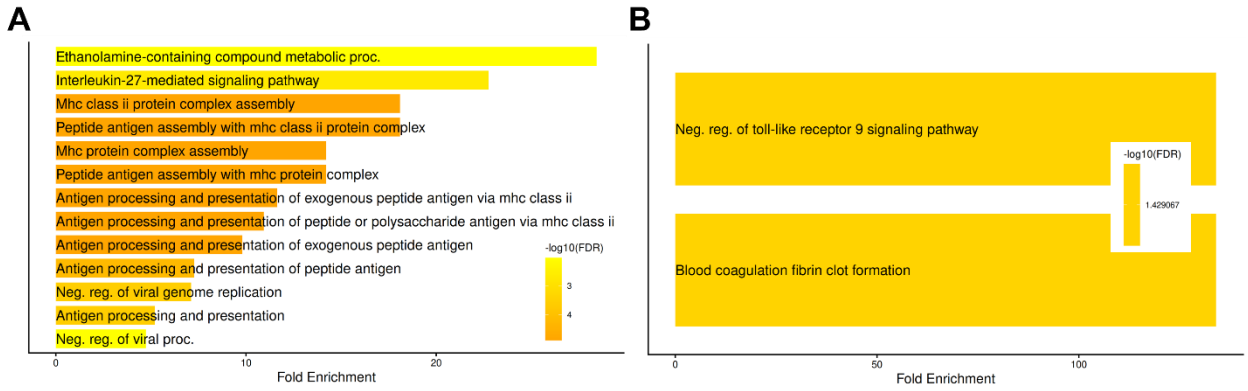

Supplementary Figure 8: Proteome analysis of BLaER1 during the original and optimized transdifferentiation protocols. (A, B) Gene ontology analysis of the proteins that were enriched in volcano plots after 48, showing the biological processes enriched by the original (C) and adapted (D) transdifferentiation protocols. Figure was generated using ShinyGO (Ge, Jung and Yao, 2020).

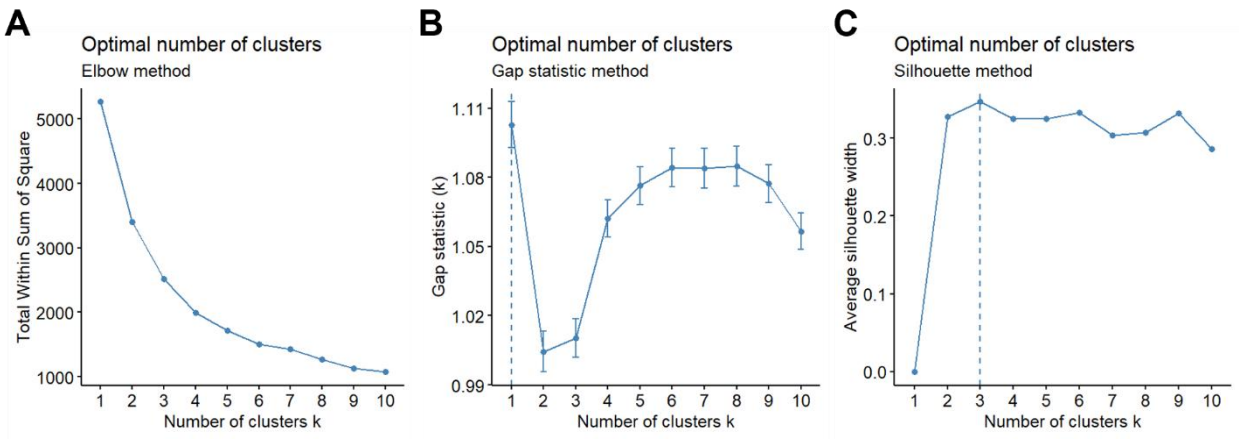

Supplementary Figure 9: Determination of the optimal number of clusters for K-means clustering. (A – C) The Elbow method (A), Average Silhouette method (B), and Gap Statistic method (C) were used with the factoextra package in RStudio to determine the ideal K-value.

Supplementary Figure 10: Volcano plot comparing the secretome of BLaER1 cells after LPS stimulation in comparison to a control using FBS-containing medium and SP3 processing. Statistical analysis was performed with a Welch's t test for an enrichment threshold of fold change over 2. and p-value below 0.05

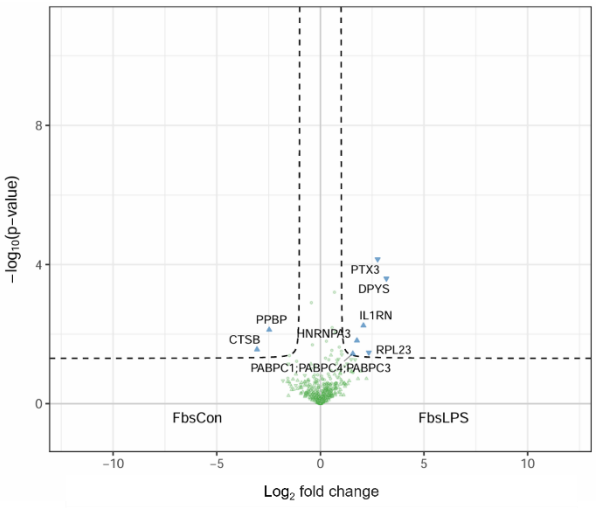

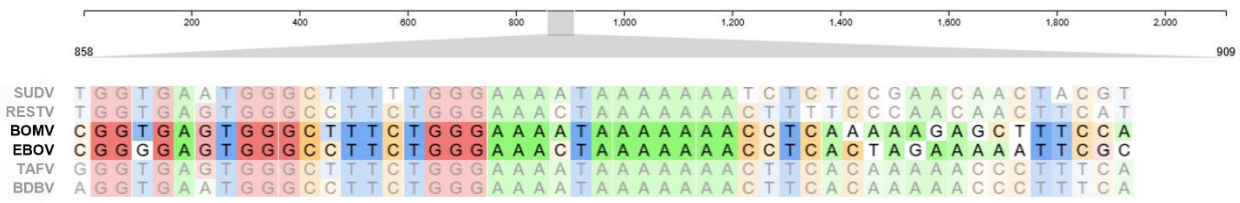

Supplementary Figure 11: Sequence alignment of orthoebolavirus GP ORFs. The nucleotide sequences of the transcriptional editing site in the GP ORF from different species is shown with emphasis on BOMV and EBOV. Figure was generated with Clustal Omega MSA (Madeira et al., 2024).

Supplementary Tables

Supplementary Table 1: Host and viral proteins in Clusters 1 – 6. The proteomes of BLaER1 during EBOV infection were normalized for fold change and used for unsupervised K-means clustering, table contains all proteins with fold changes over two sorted by cluster.

Cluster	Proteins
1 144 entries	A0A140T9L0, ADGRG3;GPR97, ANK2, APOH, ARID4A, ARRDC1, ATP11C, ATP6AP2, C1orf52, CA13, CASK, CASP6, CCDC134, CCNL1, CDC42EP4, CENPV, CMKLR1, CNOT8, CRELD1, CRYBB1, CTBS, CTTNBP2NL, CUX1, CYTIP, D2HGDH, DCAKD, DDB2, DOPEY2, DSG1, DSP, EMC8, EPS15L1, ERGIC2, FABP3, FAM126A, FAM206A, FAM32A, FASTKD2, FBXO7, FGL2, FLG, FLG2, FNTB, FXR1, GLS, GPT, GRAMD4, GSK3A, GSPT2, H2AFX;HIST2, HABP2, HAL, HIRIP3, HRNR, HSP90AA4P, ITFG3, JUP, KBTBD2, KCMF1, KIF3B, KLHDC3, KPRP, KRT1, KRT14, KRT16, KRT17, KRT6B, KRT9, KSR1, LARP4B, LIMK2, LLGL1, LSG1, MBP, MCTS1, MLYCD, MMAB, MORC2, MRPL10, MRPL23, MRPL27, MRPL41, MRPS28, N4BP2, NDC1, NEU1, NHS, NLRP3, NT5C3B, NUDT19, PARN, PFN2, PHLDB1, PIGN, PIK3R2, PMVK, POF1B, POM121C, PUM2, RAB11B, RAPGEF2, RBBP9, RGPD3;RGPD4, RHOC, RPS10, SCFD2, SEMA4B, SERPINB3, SF1, SLC25A4, SLC39A10, SLC44A2, SPI1, SPIN1, SPRR2E;SPRR, SRGAP1, STARD7, STIM2, STOM, SUMO3, TBK1, TEFM, TFEB;MITF, TMCO1, TRIM33, TRNT1, TTC39C, TXLNG, UBE2H, UHRF2, USF1, UTP11L, VLDLR, WASF1, WIBG, XP32, XPC, YIPF5, YTHDF3, ZDHHC17, ZNF24, ZNF706, ZNF800
2 150 entries	ABHD5, ACTR6, ADO, AFP, AGAP3, AKT3, ALG5, ANO10, ASCC1, ASH2L, ATG2B, ATXN2, BAZ2B, BCLAF1, BCS1L, C1QA, CACTIN, CBLL1, CCDC97, CCP110, CD200R1, CD46, CDC34, CERS6, CHD7, CHRAC1, CLASRP, CNPY2, CPNE8, CREG1, CST3, CTIF, CXorf21, CYB5B, DCUN1D5, DDX28, DGCR14, DGCR8, DGKZ, DHX37, DPP7, DSC1, EIF4E2, EIF4ENIF1, EPB41L1, ERAP2, FAM107B, FAM175A, FAM207A, FBXO28, FKBP11, GLO1, GRAPL;GRAP, GTF3C3, HDGFRP3, HECA, IGHG1, IGSF6, INPP5B, INTS5, ITGAV, ITIH4, IVL, KATNB1, KDM7A, KIAA1467;DK, KRT3, KRT6A, LENG1, LONP2, LUC7L, MAN1B1, MAPK12, MAX, MBD2, MCU, MERTK, METTL2B, MINPP1, MKRN1, MRPL55, MRPS33, MSH2, MTF1, MTUS1, MXD1, NAGPA, NAV1, NBR1, NDUFAF1, NDUFB7, NFIC, NOTCH2, NUDT18, ODR4, PALD1, PARG, PDCD6, PKP1, PLEKHM2, PRKRIR, PRPF18, PSMA3, PTAFR, PTDSS2, PUS7L, RAB29, RAP1B, RBM7, RETN, RETSAT, RINT1, RNF170, RNF34, RPL36AL, RPP38, S100A7;S100A7A, SCAMP4, SGTB, SIGLEC7, SLC36A1, SLC37A2, SPRYD4, STX10, SUDS3, SURF4, SYF2, TAF5L, TANGO2;C22o, TAPBPL, TCAF1, TDP1, TGM1, TMCO6, TMED8, TMEM14C, TMEM192, TMEM51, TMEM9B, TMSB10, TNRC6A, TPM4, TRAPPC1, TTI1, UCKL1, UQCC1, VWA8, YTHDC1, ZMYND8
3 171 entries	AGA, AIF1, AK1, ALG9, ANTXR2, ARHGAP10, ARID2, ATP5H, ATXN7L3B, BPHL, BRAT1, BRD8, C12orf29, C7orf50, CCDC43, CCNH, CCR1, CD151, CD300LF, CD53, CD68, CDIPT, CEPT1, CFAP58, CFDP1, CHMP1A, CHMP4A, CLEC3B, CLP1, CNN2, COPS8, COX5A, CPNE1, CPNE2, CSGALNACT2, CSNK1G2, CWC15, CYC1, DCTN5, DGAT1, DHPS, DRAM2, DVL3, DYNLT3, ECE1, EEF1E1;EEF1, EIF1AD, EIF3K, ELMOD2, ENDOG, ENO2, ENOPH1, EVI2A, EXOC6B, FAM76B, FNDC3A, FTO, FYTTD1, GABPA, GALNT14, GAN, GANC, GGA2, GNL3L, GNPTG, HAUS8, HEBP2, HNRNPA3, HSF1, HSP90AB2P, HSPE1-MOB4;, HSPG2, HTRA2, IKBKE, IL17RA, IMP4, IMPA2, IST1, JMJD6, KCNAB2, KRIT1, LIN54, LTF, LYN, MAT2B, METTL1, MFSD9, MOB2, MRPL28, MRPL46, MSH3, MSRB2, MT-CO3, MTPN, MYL1;MYL3, NADK, NCAPD3, NDRG3, NDUFA13, NOP9, NUP160, NUP35, PDHX, PGLS, PGRMC2, PHRF1, PIK3CA, PKNOX1, PLCL2, PPP1R12C, PPP3CC, PPP3R1, PRNP, PROCR, PSMG3, PWP2, PYCR1, RAB23, RAB33B, RABEP2, RAI1, RALY, REPS1, RFT1, RGS14, RNF149, RPA3, RPL39P5;RPL39, RPLP1, RPS15A, RRP9, SBF2, SCAF8, SCPEP1, SERF2, SERPIND1, SIRPA;SIRPB1, SLC38A9, SMARCD1, SNRPC, SNRPG;SNRPGP15, SNX12, STX8, SYNE2, SZRD1, TARBP2, TDG, TIA1, TLR1, TNFAIP8L2, TRAPPC2L, TRMT112, TSPO, UBAP2L, UBE2D3;UBE2D2, UBE2I, UBE2Q1, USP13, VAMP7, WDSUB1, WHSC1, WWP1, XXYLT1, YIPF3, ZAP70, ZBTB40, ZFC3H1, ZFPL1, ZMIZ1, ZNF512B, ZNF740
4 348 entries	A0A140T9I0, A0A140T9Y5, ABHD2, ABHD3, ACBD5, ACTR10, ACVRL1, ADARB1, ADCY7, ADD2, AGO4, AGPAT1, AGRN, ALCAM, AMBRA1, AMFR, AMPD3, ANKLE2, APOBEC3A, APOBEC3F, APOL2, APOL3, APOL6, ARGLU1, ARHGAP27, ARID1A, ATAD2B, ATG101, ATP13A2, B2M, BACH1, BAZ1A, BECN1, BRD2, BST2, C17orf75, C19orf66, C1GALT1, C1GALT1C1, C3orf38, C3orf58, C6orf47, C9, CALML5, CAP2, CASC3, CASP7, CBR1, CD38, CD40, CD48, CD86, CECR1, CEP350, CES1, CHD2, CHM, CLTCL1, CMTR1, CNP, COL1A1, COL2A1, COMP, COX5B, COX6B1, CSDE1, CSF1R, DAPK3, DAPP1, DCP1A, DDX60, DDX60L, DGKQ, DMD, DRAP1, DTX3L, DYNC1I1, DYNLRB1;DYN, EIF2AK2, ENC1, ENDOD1, EPSTI1, ETNK1, EVI5L, F5, FAM160B1, FBXO6, FCGBP, FCHSD1, FERMT3, FGD2, FGG, FLII, FMR1, FZR1, GABARAPL2, GAK, GAR1, GBP2, GBP7, GCH1, GCNT1, GEMIN4, GIMAP1-GIMA, GIMAP4, GIMAP6, GIMAP7, GIMAP8, GMFB, GPR180, GSDMD, GSTZ1, GTPBP1, GTPBP2, HEATR5A, HEBP1, HERC6, HIRA, HLA-DPB1, HNRNPLL, HSPA1B;HSPA1A, HSPBP1, IFI35, IFI6, IFIT5, IFITM2, IL1RN, IREB2, IRF5, IRF9, ISOC1, ITGA2, ITGB7, ITPA, JAK2, JAK3, KIAA0226, KIAA1551, KIAA2013, KIF16B, KLHL26, LACC1, LAMTOR2, LANCL1, LAP3, LAPTM5, LDLR, LGALS9, LILRA2, LILRA3, LILRA5, LILRB1, LIMS1, LRCH3, LRP10, LRSAM1, LYSMD2, LZTR1, MAGED2, MALT1, MAP1B, MAPK14, MAPRE2, MARCKS, MB21D1, MED13, MFSD12, MKL1;mkl1, MKLN1, MOB3C, MRPL18, MRPS10, MRPS24, MT2A;MT1G;M, MTG2, MTHFR, MYH11, MYOF, N4BP1, NAA30, NAGLU, NAPA, NCOA7, NDUFA4, NDUFB6, NDUFS8, NFKB2, NFX1, NFYA, NLN, NME3, NMI, NQO2, NSUN4, NUB1, NUCB1, OARD1, OPTN, OTUD4, P23497-4, P4HA1, PANX1, PARP12, PARP14, PARP9, PARVG, PDE1B, PDXDC1, PDXP, PEAK1, PEX3, PEX6, PHACTR4, PHF20L1, PI4K2B, PKM, PKN2, PLEC, PLEKHF1, PLEKHO1, PLSCR1, PNPT1, PPP6R3, PRIM2, PRKCE, PRRC2B, PSD4, PSMB10, PSMB9, PSMF1, PSMG1, PTK2B, PXDN, PYCARD, PYROXD1, RAD1, RASSF4, RBCK1, RBM42, RELB, RGL1, RICTOR, RIPK2, RIT1, RNASEL, RND3, RNF114, RNF138, RNF213, RNF31, RPL22L1, RPS6KB2, RTP4, SAMD9, SAP30BP, SCARF1, SCO2, SDSL, SEMA4D, SETX, SH2B2, SIDT2, SIGLEC1, SLC25A44, SLC35A3;HIAT1, SLC35B3, SLC38A2, SLC39A11, SLFN5, SMAD4, SMCHD1, SMG5, SMYD5, SNF8, SOAT1, SORBS3, SOS1, SPATS2L, STAT1, STAT2, STAT3, STAU1, SYNRG, TAF2, TAP1, TAP2, TAPBP, TBC1D1, TBC1D2B, TBC1D7, TBCEL, TCAF2, TDP2, TDRD7, TGFB1, TLE4;TLE1, TLK2, TLN2, TLR7, TMEM62, TMOD2, TMUB2, TNFSF10, TNS1, TOR1B, TP53I3, TRAFD1, TRANK1, TREX1, TRIM14, TRIM21, TRIM22, TRIM36, TRIM5, TRIM56, TRIP12, TRIP12, TRMT61B, TTC4, TUBB2A, TXNDC9, TYMP, UBE2E2;UBE2E3, UBE2K, UBE2L6, UBXN1,

	UCHL1, UNC119, UNC93B1, USP11, USP25, USP33, USP34, UVRAG, VAMP5, VNN1, VPS9D1, VRK2, WARS, XAF1, XPO6, XRN1, ZC3H7B, ZFYVE19, ZGPAT, ZNFX1, ZSWIM8
5 199 entries	AGPAT5, AMDHD2, AMICA1, ANKH, APH1A, APLP2, APOA1BP, ASF1A, ASF1B, ATP13A3, ATP5J, ATP5J2-PTCD, ATPAF2, AUP1, BASP1, BCKDHA, BCKDK, C12orf43, C2orf47, C5AR1, C9orf114, CAP1, CD163L1, CD248, CD36, CD47, CDC2;CDK1, CEBPB, CEP128, CEP164, CETN2, CHCHD2;CHCH, CHMP2B, CIAPIN1, CLCN3, CLEC4E, CPM, CTDSP1, DAXX, DHFR, DHX32, DIMT1, DIRC2, DNM1L, DOCK5, DUT, EED, EEF2K, EMR3;ADGRE3, EXOSC6, FABP5, FAM101B, FAM192A, FAM20C, FAM210A, FAM84B, FANCM, FGB, FPGT, FYN, GGT5, GLIPR1, GRK6, GRWD1, GTF3C2, H3F3B;H3F3A, HERC1, HGF, HLA-DRB5, HMGA1, HNRNPA3, HNRNPDL, IGHM, IL10RB, IL1RAP, ILF3, ITGA6, ITGAX, KDM4B, KIAA0430, KMT2C, KRR1, KRT5, LIG1, LIMA1, LMAN2, LRRC41, LTV1, MAD2L1, MARCO, MBD4, MCM2, MCM3, MCM6, METTL7A, MFF, MFSD1, MICU1, MKI67, MPEG1, MPHOSPH10, MRPL47, MRPS15, MRPS23, NAPG, NBEA, NCAM1, NCAPH, NDE1, NDUFS7, NOL8, NUMA1, NUPL1, PGBD5, PGM3, PHKG2, PLCD1, PLXDC2, PLXNC1, PNPLA2, POLD3, POSTN, POU2F1;POU2, PPAT, PPBP, PPIA, PPIH, PRKAR2B, PRPF38B, PSEN1, PTGFRN, RABL3, RBM6, RHOT1, RMDN3, RNASE6, RNF146, RNF169, RPS6KB1, RRM2, RSL24D1, SELL, SERPINA1, SERPINF1, SETDB1, SFN, SFT2D2, SFXN4, SH3BP2, SLA, SLC16A7, SLC37A4, SLC38A7, SLC7A7, SORT1, SRPK1, STK17B, SUGP1, SULF2, SUMF1, SYTL3, SZT2, TBCC, TBCK, TGFBR1, THBD, TIAM1, TIMM21, TIMP1, TMC6, TMED3, TMEM104, TMEM55B, TMPIT;TMEM120A, TMPO, TNFAIP8, TYK2, TYMS, UBE2V1;TMEM, UBQLN1, UBXN7, UHRF1, UTP6, VNN2, VPS52, VRK1, WDR46, WDR74, WDR77, WFS1, WHSC1L1, ZAK, ZDHHC20, ZFAND6, ZMYND11, ZNF316, ZPR1
6 51 entries	CACNA1A, CMPK2, CXCL10, DDX58, DHX58, EBOV-GP12, EBOV-L, EBOV-NP, EBOV-sGP, EBOV-VP24, EBOV-VP30, EBOV-VP35, EBOV-VP40, EPHB2, GBP1, GBP4, GMPR, GOLM1, HELZ2, HERC5, IFI27, IFI44, IFI44L, IFIH1, IFIT1, IFIT2, IFIT3, IFITM3, IL4I1, IRF7, ISG15, ISG20, LGALS3BP, MOV10, MX1, MX2, NT5C3A, OAS1, OAS2, OAS3, OASL, PARP10, RIN2, RSAD2, SAMD9L, SP110, SP140L, UBA7, UHRF1BP1, USP18

Supplementary Table 2: Gene Ontology Enrichment for molecular function. Host proteins were clustered according to their expression during an infection time course and analyzed for GO term enrichment.

ID	Description	Gene Ratio	Bg Ratio	pvalue	p. adjust	qvalue	count	cluster
GO:0019903	protein phosphatase binding	12/321	142/18496	7.06E-06	0.002118284	0.0018024	12	4
GO:0044389	ubiquitin-like protein ligase binding	19/321	327/18496	4.81E-06	0.002118284	0.0018024	19	4
GO:0032396	inhibitory MHC class I receptor activity	4/321	10/18496	1.72E-05	0.003443638	0.0029030113	4	4
GO:0016814	hydrolase activity, acting on carbon-nitrogen (but not peptide) bonds, in cyclic amidines	6/321	36/18496	3.27E-05	0.003986034	0.0033091625	6	4
GO:0003725	double-stranded RNA binding	8/321	73/18496	3.81E-05	0.003986034	0.0033091625	8	4
GO:0004842	ubiquitin-protein transferase activity	21/321	448/18496	3.99E-05	0.003986034	0.0033091625	21	4
GO:0032393	MHC class I receptor activity	4/321	15/18496	0.000104483	0.007206088	0.0061031496	4	4
GO:0004715	non-membrane spanning protein tyrosine kinase activity	6/321	45/18496	0.000120101	0.007206088	0.0061031496	6	4
GO:0019902	phosphatase binding	12/321	189/18496	0.00011945	0.007206088	0.0061031496	12	4
GO:0019787	ubiquitin-like protein transferase activity	21/321	477/18496	9.73E-05	0.007206088	0.0061031496	21	4
GO:0003725	double-stranded RNA binding	6/41	73/18496	1.24E-08	1.74E-06	1.35E-06	6	6
GO:0070566	adenylyltransferase activity	3/41	29/18496	3.55E-05	0.002502079	0.0019042637	3	6
GO:0140098	catalytic activity, acting on RNA	6/41	395/18496	0.000218183	0.010254604	0.0079061768	6	6
GO:0016779	nucleotidyltransferase activity	4/41	147/18496	0.000308594	0.010385217	0.0080063177	4	6
GO:0004386	helicase activity	4/41	154/18496	0.00036827	0.010385217	0.0080063177	4	6
GO:0003724	RNA helicase activity	3/41	76/18496	0.000635201	0.013803565	0.0107017214	3	6
GO:0008186	ATP-dependent activity, acting on RNA	3/41	78/18496	0.000685283	0.013803565	0.0107017214	3	6
GO:0005525	GTP binding	5/41	382/18496	0.001488536	0.026235449	0.0203069441	5	6

GO:0019001	guanyl nucleotide binding	5/41	403/18496	0.001882707	0.026546174	0.020610691	5	6
GO:0032561	guanyl ribonucleotide binding	5/41	403/18496	0.001882707	0.026546174	0.020610691	5	6

Supplementary Table 3: Gene Ontology Enrichment for biological processes. Host proteins were clustered according to their expression during an infection time course and analyzed for GO term enrichment.

ID	Description	Gene Ratio	Bg Ratio	pvalue	p. adjust	qvalue	count	cluster
GO:0009615	response to virus	40/315	436/18870	1.49E-18	5.51E-15	4.64E-15	40	4
GO:0051607	defense response to virus	34/315	334/18870	2.79E-17	3.77E-14	3.18E-14	34	4
GO:0140546	defense response to symbiont	34/315	335/18870	3.06E-17	3.77E-14	3.18E-14	34	4
GO:0050792	regulation of viral process	21/315	168/18870	7.59E-13	7.01E-10	5.91E-10	21	4
GO:0016032	viral process	32/315	432/18870	1.82E-12	1.35E-09	1.14E-09	32	4
GO:1903900	regulation of viral life cycle	19/315	143/18870	3.20E-12	1.97E-09	1.66E-09	19	4
GO:0045088	regulation of innate immune response	30/315	425/18870	3.11E-11	1.57E-08	1.32E-08	30	4
GO:0019058	viral life cycle	26/315	321/18870	3.39E-11	1.57E-08	1.32E-08	26	4
GO:0045069	regulation of viral genome replication	14/315	85/18870	1.28E-10	5.26E-08	4.43E-08	14	4
GO:0048525	negative regulation of viral process	14/315	93/18870	4.44E-10	1.64E-07	1.38E-07	14	4
GO:0006260	DNA replication	12/170	278/18870	8.55E-06	0.013556642	0.012501962	12	5
GO:1902969	mitotic DNA replication	4/170	16/18870	1.06E-05	0.013556642	0.012501962	4	5
GO:0006261	DNA-templated DNA replication	9/170	161/18870	1.56E-05	0.013556642	0.012501962	9	5
GO:0006268	DNA unwinding involved in DNA replication	4/170	21/18870	3.38E-05	0.021936886	0.020203057	4	5
GO:0044786	cell cycle DNA replication	5/170	44/18870	4.57E-05	0.023768686	0.021919887	5	5
GO:2001234	negative regulation of apoptotic signaling pathway	10/170	243/18870	7.31E-05	0.031679312	0.029215202	10	5
GO:0000727	double-strand break repair via break-induced replication	3/170	12/18870	0.000148877	0.049029917	0.045216225	3	5
GO:0042254	ribosome biogenesis	11/170	325/18870	0.000181415	0.049029917	0.045216225	11	5
GO:0034389	lipid droplet organization	4/170	35/18870	0.000267716	0.049029917	0.045216225	4	5
GO:2001233	regulation of apoptotic signaling pathway	12/170	398/18870	0.000269367	0.049029917	0.045216225	12	5
GO:0051607	defense response to virus	25/40	334/18870	2.03E-34	8.99E-32	7.00E-32	25	6
GO:0140546	defense response to symbiont	25/40	335/18870	2.19E-34	8.99E-32	7.00E-32	25	6
GO:0009615	response to virus	26/40	436/18870	2.35E-33	6.43E-31	5.00E-31	26	6
GO:0045071	negative regulation of viral genome replication	12/40	55/18870	5.45E-22	1.12E-19	8.70E-20	12	6
GO:0045069	regulation of viral genome replication	12/40	85/18870	1.57E-19	2.57E-17	2.00E-17	12	6
GO:0019079	viral genome replication	13/40	131/18870	4.85E-19	5.76E-17	4.48E-17	13	6

GO:0048525	negative regulation of viral process	12/40	93/18870	4.91E-19	5.76E-17	4.48E-17	12	6
GO:0034340	response to type I interferon	11/40	89/18870	2.80E-17	2.88E-15	2.24E-15	11	6
GO:1903900	regulation of viral life cycle	12/40	143/18870	1.05E-16	9.53E-15	7.42E-15	12	6
GO:0140374	antiviral innate immune response	9/40	48/18870	5.19E-16	4.26E-14	3.31E-14	9	6

Supplementary Table 4: Gene Ontology Enrichment for cellular components. Analysis of secretome samples using all proteins identified in the conditioned medium of experiments with FBS and SP3-treatment in BSL-4.

Enrichment FDR	nGenes	Pathway Genes	Fold Enrichment	Pathway
4.53E-61	88	448	10.19762436	GO:0062023 Collagen-containing extracellular matrix
1.22E-56	94	594	8.215533309	GO:0031012 Extracellular matrix
1.29E-56	94	595	8.20172569	GO:0030312 External encapsulating structure
6.23E-165	281	2349	6.210372575	GO:0070062 Extracellular exosome
1.66E-165	283	2382	6.167924238	GO:1903561 Extracellular vesicle
1.66E-165	283	2383	6.165335936	GO:0043230 Extracellular organelle
1.66E-165	283	2383	6.165335936	GO:0065010 Extracellular membrane-bounded organelle
1.10E-159	323	3619	4.633490654	GO:0005615 Extracellular space
9.32E-144	340	4675	3.775649351	GO:0005576 Extracellular region
3.92E-120	315	4571	3.577615675	GO:0031982 Vesicle

References

Aderem, A. and Underhill, D.M. (1999) “MECHANISMS OF PHAGOCYTOSIS IN MACROPHAGES,” *Annual Review of Immunology*, 17(Volume 17, 1999), pp. 593–623. Available at: https://doi.org/10.1146/annurev.immunol.17.1.593.

Adu-Gyamfi, E. *et al.* (2012) “Single-Particle Tracking Demonstrates that Actin Coordinates the Movement of the Ebola Virus Matrix Protein,” *Biophysical Journal*, 103(9), pp. L41–L43. Available at: https://doi.org/10.1016/j.bpj.2012.09.026.

Adu-Gyamfi, E. *et al.* (2013) “The Ebola Virus Matrix Protein Penetrates into the Plasma Membrane,” *The Journal of Biological Chemistry*, 288(8), pp. 5779–5789. Available at: https://doi.org/10.1074/jbc.M112.443960.

Akira, S. and Takeda, K. (2004) “Toll-like receptor signalling,” *Nature Reviews Immunology*, 4(7), pp. 499–511. Available at: https://doi.org/10.1038/nri1391.

Alexopoulou, L. *et al.* (2001) “Recognition of double-stranded RNA and activation of NF-κB by Toll-like receptor 3,” *Nature*, 413(6857), pp. 732–738. Available at: https://doi.org/10.1038/35099560.

Almeida-Marques, C. *et al.* (2024) “Secretome processing for proteomics: A methods comparison,” *PROTEOMICS*, 24(7), p. 2300262. Available at: https://doi.org/10.1002/pmic.202300262.

Amos, H. and Korn, M. (1958) “5-Methyl cytosine in the RNA of *Escherichia coli*,” *Biochimica et Biophysica Acta*, 29(2), pp. 444–445. Available at: https://doi.org/10.1016/0006-3002(58)90214-2.

Arango Duque, G. and Descoteaux, A. (2014) “Macrophage Cytokines: Involvement in Immunity and Infectious Diseases,” *Frontiers in Immunology*, 5, p. 491. Available at: https://doi.org/10.3389/fimmu.2014.00491.

Ariyoshi, W. *et al.* (2017) “Mechanisms involved in enhancement of matrix metalloproteinase-9 expression in macrophages by interleukin-33,” *Journal of Cellular Physiology*, 232(12), pp. 3481–3495. Available at: https://doi.org/10.1002/jcp.25809.

Arnan, C. *et al.* (2022a) “Paired guide RNA CRISPR-Cas9 screening for protein-coding genes and lncRNAs involved in transdifferentiation of human B-cells to macrophages,” *BMC Genomics*, 23, p. 402. Available at: https://doi.org/10.1186/s12864-022-08612-7.

Arnan, C. *et al.* (2022b) “Paired guide RNA CRISPR-Cas9 screening for protein-coding genes and lncRNAs involved in transdifferentiation of human B-cells to macrophages,” *BMC Genomics*, 23, p. 402. Available at: https://doi.org/10.1186/s12864-022-08612-7.

Arnold, C.E. *et al.* (2014) “A critical role for suppressor of cytokine signalling 3 in promoting M1 macrophage activation and function in vitro and in vivo,” *Immunology*, 141(1), pp. 96–110. Available at: https://doi.org/10.1111/imm.12173.

Arzumanian, V.A. *et al.* (2022) “Epitranscriptome: Review of Top 25 Most-Studied RNA Modifications,” *International Journal of Molecular Sciences*, 23(22). Available at: https://doi.org/10.3390/ijms232213851.

Asano, K. *et al.* (2011) “CD169-Positive Macrophages Dominate Antitumor Immunity by Crosspresenting Dead Cell-Associated Antigens,” *Immunity*, 34(1), pp. 85–95. Available at: https://doi.org/10.1016/j.immuni.2010.12.011.

Aubatin, A. *et al.* (2018) “IL4-induced gene 1 is secreted at the immune synapse and modulates TCR activation independently of its enzymatic activity,” *European Journal of Immunology*, 48(1), pp. 106–119. Available at: https://doi.org/10.1002/eji.201646769.

Auffray, C. *et al.* (2007) “Monitoring of Blood Vessels and Tissues by a Population of Monocytes with Patrolling Behavior,” *Science*, 317(5838), pp. 666–670. Available at: https://doi.org/10.1126/science.1142883.

Austermann, J., Roth, J. and Barczyk-Kahlert, K. (2022) “The Good and the Bad: Monocytes’ and Macrophages’ Diverse Functions in Inflammation,” *Cells*, 11(12), p. 1979. Available at: https://doi.org/10.3390/cells11121979.

Avelino, C.D. and Montenegro, Y.H.A. (2025) “The Role of Innate Immune System: A Crosstalk between Invertebrates and Humans,” *Journal of Cellular Immunology*, Volume 7(Issue 3), pp. 116–121. Available at: https://doi.org/10.33696/immunology.7.230.

Bachellerie, J.-P. and Cavaillé, J. (1998) “Small Nucleolar RNAs Guide the Ribose Methylations of Eukaryotic rRNAs,” *Modification and Editing of RNA*. John Wiley & Sons, Ltd, pp. 255–272. Available at: https://doi.org/10.1128/9781555818296.ch13.

Balka, K.R. and De Nardo, D. (2019) “Understanding early TLR signaling through the Myddosome,” *Journal of Leukocyte Biology*, 105(2), pp. 339–351. Available at: https://doi.org/10.1002/JLB.MR0318-096R.

Barrangou, R. *et al.* (2007) “CRISPR provides acquired resistance against viruses in prokaryotes,” *Science*, 315(5819), pp. 1709–1712. Available at: https://doi.org/10.1126/science.1138140.

Barreat, J.G.N. and Katzourakis, A. (2023) “A billion years arms-race between viruses, virophages, and eukaryotes,” *eLife*, 12, p. RP86617. Available at: https://doi.org/10.7554/eLife.86617.

Barton, G.M. and Kagan, J.C. (2009) “A cell biological view of Toll-like receptor function: regulation through compartmentalization,” *Nature reviews. Immunology*, 9(8), pp. 535–542. Available at: https://doi.org/10.1038/nri2587.

Becknell, B. *et al.* (2015) “Ribonucleases 6 and 7 have antimicrobial function in the human and murine urinary tract,” *Kidney international*, 87(1), pp. 151–161. Available at: https://doi.org/10.1038/ki.2014.268.

Bergstrøm, B. *et al.* (2015) “TLR8 Senses Staphylococcus aureus RNA in Human Primary Monocytes and Macrophages and Induces IFN-β Production via a TAK1–IKKβ–IRF5 Signaling Pathway,” *The Journal of Immunology*, 195(3), pp. 1100–1111. Available at: https://doi.org/10.4049/jimmunol.1403176.

Bernheim, A., Cury, J. and Poirier, E.Z. (2024) “The immune modules conserved across the tree of life: Towards a definition of ancestral immunity,” *PLoS biology*, 22(7), p. e3002717. Available at: https://doi.org/10.1371/journal.pbio.3002717.

Betancourt, L.H. *et al.* (2018) “Quantitative Assessment of Urea In-Solution Lys-C/Trypsin Digestions Reveals Superior Performance at Room Temperature over Traditional Proteolysis at 37 °C,” *Journal of Proteome Research*, 17(7), pp. 2556–2561. Available at: https://doi.org/10.1021/acs.jproteome.8b00228.

Bharat, T.A.M. *et al.* (2012) “Structural dissection of Ebola virus and its assembly determinants using cryo-electron tomography,” *Proceedings of the National Academy of Sciences of the United States of America*, 109(11), pp. 4275–4280. Available at: https://doi.org/10.1073/pnas.1120453109.

Bian, F. *et al.* (2023) “A Biological Perspective of TLR8 Signaling in Host Defense and Inflammation,” *Infectious Microbes & Diseases*, 5(2), p. 44. Available at: https://doi.org/10.1097/IM9.0000000000000119.

Biedenkopf, N. *et al.* (2023) “Renaming of genera Ebolavirus and Marburgvirus to Orthoebolavirus and Orthomarburgvirus, respectively, and introduction of binomial species names within family Filoviridae,” *Archives of Virology*, 168(8), p. 220. Available at: https://doi.org/10.1007/s00705-023-05834-2.

Bodmer, B.S., Vallbracht, M., *et al.* (2023) “Ebola virus inclusion bodies are liquid organelles whose formation is facilitated by nucleoprotein oligomerization,” *Emerging Microbes & Infections*, 12(2), p. 2223727. Available at: https://doi.org/10.1080/22221751.2023.2223727.

Bodmer, B.S., Breithaupt, A., *et al.* (2023) “In vivo characterization of the novel ebolavirus Bombali virus suggests a low pathogenic potential for humans,” *Emerging Microbes & Infections*, 12(1), p. 2164216. Available at: https://doi.org/10.1080/22221751.2022.2164216.

Bodmer, B.S. *et al.* (2025) “Antiviral defense against filovirus infections: targets and evasion mechanisms,” *Future Microbiology*, 20(7–9), pp. 573–587. Available at: https://doi.org/10.1080/17460913.2025.2501924.

Bodmer, B.S., Hoenen, T. and Wendt, L. (2024) “Molecular insights into the Ebola virus life cycle,” *Nature Microbiology*, 9(6), pp. 1417–1426. Available at: https://doi.org/10.1038/s41564-024-01703-z.

Bonner, W.A. *et al.* (1972) “Fluorescence activated cell sorting,” *The Review of Scientific Instruments*, 43(3), pp. 404–409. Available at: https://doi.org/10.1063/1.1685647.

Bowen, E.T. *et al.* (1977) “Viral haemorrhagic fever in southern Sudan and northern Zaire. Preliminary studies on the aetiological agent,” *Lancet*, 1(8011), pp. 571–573. Available at: https://doi.org/10.1016/s0140-6736(77)92001-3.

Brancewicz, J. *et al.* (2025) “The Multifaceted Role of Macrophages in Biology and Diseases,” *International Journal of Molecular Sciences*, 26(5). Available at: https://doi.org/10.3390/ijms26052107.

Bray, M. and Geisbert, T.W. (2005) “Ebola virus: The role of macrophages and dendritic cells in the pathogenesis of Ebola hemorrhagic fever,” *The International Journal of Biochemistry & Cell Biology*, 37(8), pp. 1560–1566. Available at: https://doi.org/10.1016/j.biocel.2005.02.018.

Brumatti, G., Salmanidis, M. and Ekert, P.G. (2010) “Crossing paths: interactions between the cell death machinery and growth factor survival signals,” *Cellular and Molecular Life Sciences: CMLS*, 67(10), pp. 1619–1630. Available at: https://doi.org/10.1007/s00018-010-0288-8.

Bulletin of the World Health Organization (1978a) “Ebola haemorrhagic fever in Sudan, 1976,” 56(2), pp. 247–270.

Bulletin of the World Health Organization (1978b) “Ebola haemorrhagic fever in Zaire, 1976,” 56(2), pp. 271–293.

Bussmann, L.H. *et al.* (2009) “A Robust and Highly Efficient Immune Cell Reprogramming System,” *Cell Stem Cell*, 5(5), pp. 554–566. Available at: https://doi.org/10.1016/j.stem.2009.10.004.

Cai, M. *et al.* (2013) “The Herpes Simplex Virus 1-Encoded Envelope Glycoprotein B Activates NF-κB through the Toll-Like Receptor 2 and MyD88/TRAF6-Dependent Signaling Pathway,” *PLoS ONE*. Edited by J.C. Glorioso, 8(1), p. e54586. Available at: https://doi.org/10.1371/journal.pone.0054586.

Cao, F. *et al.* (2010) “Comparison of Gene-Transfer Efficiency in Human Embryonic Stem Cells,” *Molecular Imaging and Biology*, 12(1), pp. 15–24. Available at: https://doi.org/10.1007/s11307-009-0236-x.

Cao, Z. *et al.* (2023) “Ebola virus VP35 perturbs type I interferon signaling to facilitate viral replication,” *Virologica Sinica*, 38(6), pp. 922–930. Available at: https://doi.org/10.1016/j.virs.2023.10.004.

Cárdenas, W.B. *et al.* (2006) “Ebola Virus VP35 Protein Binds Double-Stranded RNA and Inhibits Alpha/Beta Interferon Production Induced by RIG-I Signaling,” *Journal of Virology*, 80(11), pp. 5168–5178. Available at: https://doi.org/10.1128/JVI.02199-05.

Chandran, K. *et al.* (2005) “Endosomal Proteolysis of the Ebola Virus Glycoprotein Is Necessary for Infection,” *Science (New York, N.Y.)*, 308(5728), pp. 1643–1645. Available at: https://doi.org/10.1126/science.1110656.

Chaplin, D.D. (2010) “Overview of the Immune Response,” *The Journal of allergy and clinical immunology*, 125(2 Suppl 2), pp. S3-23. Available at: https://doi.org/10.1016/j.jaci.2009.12.980.

Chen, R. *et al.* (2025) “Pattern recognition receptors: function, regulation and therapeutic potential,” *Signal Transduction and Targeted Therapy*, 10(1), p. 216. Available at: https://doi.org/10.1038/s41392-025-02264-1.

Chen, S., Zhu, H. and Jounaidi, Y. (2024) “Comprehensive snapshots of natural killer cells functions, signaling, molecular mechanisms and clinical utilization,” *Signal Transduction and Targeted Therapy*, 9(1), p. 302. Available at: https://doi.org/10.1038/s41392-024-02005-w.

Cheng, N. *et al.* (2025a) “Global distribution and genetic diversity of orthoebolaviruses: Mapping and evolutionary analysis,” *One Health*, 21, p. 101236. Available at: https://doi.org/10.1016/j.onehlt.2025.101236.

Cheng, N. *et al.* (2025b) “Global distribution and genetic diversity of orthoebolaviruses: Mapping and evolutionary analysis,” *One Health*, 21, p. 101236. Available at: https://doi.org/10.1016/j.onehlt.2025.101236.

Christopher, J.A. *et al.* (2021) “Subcellular proteomics,” *Nature Reviews. Methods Primers*, 1, p. 32. Available at: https://doi.org/10.1038/s43586-021-00029-y.

Cline, M.J. and Moore, M.A.S. (1972) “Embryonic Origin of the Mouse Macrophage,” *Blood*, 39(6), pp. 842–849. Available at: https://doi.org/10.1182/blood.V39.6.842.842.

Cohn, W.E. and Volkin, E. (1951) “Nucleoside-5’-Phosphates from Ribonucleic Acid,” *Nature*, 167(4247), pp. 483–484. Available at: https://doi.org/10.1038/167483a0.

Coulborn, R.M. *et al.* (2024) “Case fatality risk among individuals vaccinated with rVSVΔG-ZEBOV-GP: a retrospective cohort analysis of patients with confirmed Ebola virus disease in the Democratic Republic of the Congo,” *The Lancet Infectious Diseases*, 24(6), pp. 602–610. Available at: https://doi.org/10.1016/S1473-3099(23)00819-8.

Coutinho, A. and Meo, T. (1978) “Genetic basis for unresponsiveness to lipopolysaccharide in C57BL/10Cr mice,” *Immunogenetics*, 7(1), pp. 17–24. Available at: https://doi.org/10.1007/BF01843983.

Daffis, S. *et al.* (2010) “2’-O methylation of the viral mRNA cap evades host restriction by IFIT family members,” *Nature*, 468(7322), pp. 452–456. Available at: https://doi.org/10.1038/nature09489.

Dahlmann, F. *et al.* (2015) “Analysis of Ebola Virus Entry Into Macrophages,” *The Journal of Infectious Diseases*, 212(Suppl 2), pp. S247–S257. Available at: https://doi.org/10.1093/infdis/jiv140.

Dalpke, A.H. and Helm, M. (2012) “RNA mediated toll-like receptor stimulation in health and disease,” *RNA Biology*, 9(6), pp. 828–842. Available at: https://doi.org/10.4161/rna.20206.

Das, D.K. *et al.* (2020) “Conformational changes in the Ebola virus membrane fusion machine induced by pH, Ca2+, and receptor binding,” *PLoS Biology*, 18(2), p. e3000626. Available at: https://doi.org/10.1371/journal.pbio.3000626.

Das, S. *et al.* (2014) “Immune subversion by Mycobacterium tuberculosis through CCR5 mediated signaling: involvement of IL-10,” *PloS One*, 9(4), p. e92477. Available at: https://doi.org/10.1371/journal.pone.0092477.

Davis, D.R. (1995) “Stabilization of RNA stacking by pseudouridine.,” *Nucleic Acids Research*, 23(24), pp. 5020–5026. Available at: https://doi.org/10.1093/nar/23.24.5020.

Davis, F.F. and Allen, F.W. (1957) “Ribonucleic acids from yeast which contain a fifth nucleotide,” *The Journal of Biological Chemistry*, 227(2), pp. 907–915.

Delaunay, S., Helm, M. and Frye, M. (2024) “RNA modifications in physiology and disease: towards clinical applications,” *Nature Reviews Genetics*, 25(2), pp. 104–122. Available at: https://doi.org/10.1038/s41576-023-00645-2.

Diamond, M.S. and Farzan, M. (2013) “The broad-spectrum antiviral functions of IFIT and IFITM proteins,” *Nature Reviews. Immunology*, 13(1), pp. 46–57. Available at: https://doi.org/10.1038/nri3344.

Dietsch, G.N. *et al.* (2016) “Coordinated Activation of Toll-Like Receptor8 (TLR8) and NLRP3 by the TLR8 Agonist, VTX-2337, Ignites Tumoricidal Natural Killer Cell Activity,” *PLoS ONE*, 11(2), p. e0148764. Available at: https://doi.org/10.1371/journal.pone.0148764.

Ding, T. *et al.* (2025) “Comprehensive review of macrophage models: primary cells and immortalized lines across species,” *Frontiers in Immunology*, 16. Available at: https://doi.org/10.3389/fimmu.2025.1640935.

Disease Outbreak News; Ebola virus disease in the Democratic Republic of the Congo (2025). World Health Organization. Available at: https://www.who.int/emergencies/disease-outbreak-news/item/2025-DON589 (Accessed: January 28, 2026).

Doherty, G.J. and McMahon, H.T. (2009) “Mechanisms of endocytosis,” *Annual Review of Biochemistry*, 78, pp. 857–902. Available at: https://doi.org/10.1146/annurev.biochem.78.081307.110540.

Dolnik, O., Gerresheim, G.K. and Biedenkopf, N. (2021) “New Perspectives on the Biogenesis of Viral Inclusion Bodies in Negative-Sense RNA Virus Infections,” *Cells*, 10(6), p. 1460. Available at: https://doi.org/10.3390/cells10061460.

Dong, C. *et al.* (2013) “RNA sequencing and transcriptomal analysis of human monocyte to macrophage differentiation,” *Gene*, 519(2), pp. 279–287. Available at: https://doi.org/10.1016/j.gene.2013.02.015.

Doron, S. *et al.* (2018) “Systematic discovery of anti-phage defense systems in the microbial pan-genome,” *Science (New York, N.Y.)*, 359(6379), p. eaar4120. Available at: https://doi.org/10.1126/science.aar4120.

Doyle, S.E. *et al.* (2004) “Toll-like receptors induce a phagocytic gene program through p38,” *The Journal of Experimental Medicine*, 199(1), pp. 81–90. Available at: https://doi.org/10.1084/jem.20031237.

Duan, T. *et al.* (2022) “Toll-Like Receptor Signaling and Its Role in Cell-Mediated Immunity,” *Frontiers in Immunology*, 13. Available at: https://doi.org/10.3389/fimmu.2022.812774.

de Duve, C. *et al.* (1955) “Tissue fractionation studies. 6. Intracellular distribution patterns of enzymes in rat-liver tissue,” *Biochemical Journal*, 60(4), pp. 604–617. Available at: https://doi.org/10.1042/bj0600604.

Ebert, R.H. and Florey, H.W. (1939) “The Extravascular Development of the Monocyte Observed In vivo,” *British Journal of Experimental Pathology*, 20(4), pp. 342–356.

Eichelbaum, K. and Krijgsveld, J. (2014) “Rapid Temporal Dynamics of Transcription, Protein Synthesis, and Secretion during Macrophage Activation*,” *Molecular & Cellular Proteomics*, 13(3), pp. 792–810. Available at: https://doi.org/10.1074/mcp.M113.030916.

Eigenbrod, T. *et al.* (2015) “TLR8 Senses Bacterial RNA in Human Monocytes and Plays a Nonredundant Role for Recognition of Streptococcus pyogenes,” *The Journal of Immunology*, 195(3), pp. 1092–1099. Available at: https://doi.org/10.4049/jimmunol.1403173.

Elias, P.M. (2007) “The skin barrier as an innate immune element,” *Seminars in Immunopathology*, 29(1), pp. 3–14. Available at: https://doi.org/10.1007/s00281-007-0060-9.

Elliott, L.H., Kiley, M.P. and McCormick, J.B. (1985) “Descriptive analysis of Ebola virus proteins,” *Virology*, 147(1), pp. 169–176. Available at: https://doi.org/10.1016/0042-6822(85)90236-3.

Fagre, C. and Gilbert, W. (2024) “Beyond reader proteins: RNA binding proteins and RNA modifications in conversation to regulate gene expression,” *Wiley interdisciplinary reviews. RNA*, 15(2), p. e1834. Available at: https://doi.org/10.1002/wrna.1834.

Fang, J. *et al.* (2023) “Spatial and functional arrangement of Ebola virus polymerase inside phase-separated viral factories,” *Nature Communications*, 14(1), p. 4159. Available at: https://doi.org/10.1038/s41467-023-39821-7.

Favre, A. *et al.* (1986) “4-Thiouridine photosensitized RNA-protein crosslinking in mammalian cells,” *Biochemical and Biophysical Research Communications*, 141(2), pp. 847–854. Available at: https://doi.org/10.1016/s0006-291x(86)80250-9.

Flannagan, R.S., Jaumouillé, V. and Grinstein, S. (2012) “The cell biology of phagocytosis,” *Annual Review of Pathology*, 7, pp. 61–98. Available at: https://doi.org/10.1146/annurev-pathol-011811-132445.

Formenty, P. *et al.* (1999) “Human infection due to Ebola virus, subtype Côte d’Ivoire: clinical and biologic presentation,” *The Journal of Infectious Diseases*, 179 Suppl 1, pp. S48-53. Available at: https://doi.org/10.1086/514285.

Freeley, S., Kemper, C. and Le Friec, G. (2016) “The ‘Ins and Outs’ of complement-driven immune responses,” *Immunological reviews*, 274(1), pp. 16–32. Available at: https://doi.org/10.1111/imr.12472.

Freund, I. *et al.* (2019) “RNA Modifications Modulate Activation of Innate Toll-Like Receptors,” *Genes*, 10(2), p. 92. Available at: https://doi.org/10.3390/genes10020092.

van Furth, R. and Cohn, Z.A. (1968) “THE ORIGIN AND KINETICS OF MONONUCLEAR PHAGOCYTES,” *The Journal of Experimental Medicine*, 128(3), pp. 415–435. Available at: https://doi.org/10.1084/jem.128.3.415.

Furuyama, W. *et al.* (2021) “The Ebola virus soluble glycoprotein contributes to viral pathogenesis by activating the MAP kinase signaling pathway,” *PLOS Pathogens*, 17(9), p. e1009937. Available at: https://doi.org/10.1371/journal.ppat.1009937.

Gaidt, M.M. *et al.* (2016) “Human Monocytes Engage an Alternative Inflammasome Pathway,” *Immunity*, 44(4), pp. 833–846. Available at: https://doi.org/10.1016/j.immuni.2016.01.012.

Gaidt, M.M. *et al.* (2018) “Modeling Primary Human Monocytes with the Trans-Differentiation Cell Line BLaER1,” *Methods in Molecular Biology (Clifton, N.J.)*, 1714, pp. 57–66. Available at: https://doi.org/10.1007/978-1-4939-7519-8_4.

Galão, R.P. *et al.* (2022) “TRIM25 and ZAP target the Ebola virus ribonucleoprotein complex to mediate interferon-induced restriction,” *PLoS Pathogens*, 18(5), p. e1010530. Available at: https://doi.org/10.1371/journal.ppat.1010530.

Gameiro, P.A. and Struhl, K. (2018) “Nutrient Deprivation Elicits a Transcriptional and Translational Inflammatory Response Coupled to Decreased Protein Synthesis,” *Cell Reports*, 24(6), pp. 1415–1424. Available at: https://doi.org/10.1016/j.celrep.2018.07.021.

Gantier, M.P. *et al.* (2008) “TLR7 Is Involved in Sequence-Specific Sensing of Single-Stranded RNAs in Human Macrophages,” *The Journal of Immunology*, 180(4), pp. 2117–2124. Available at: https://doi.org/10.4049/jimmunol.180.4.2117.

Gao, D. and Li, W. (2017) “Structures and recognition modes of toll-like receptors,” *Proteins: Structure, Function, and Bioinformatics*, 85(1), pp. 3–9. Available at: https://doi.org/10.1002/prot.25179.

Garamszegi, S. *et al.* (2014) “Transcriptional Correlates of Disease Outcome in Anticoagulant-Treated Non-Human Primates Infected with Ebolavirus,” *PLoS Neglected Tropical Diseases*, 8(7), p. e3061. Available at: https://doi.org/10.1371/journal.pntd.0003061.

Garelnabi, M. *et al.* (2018) “Quantifying donor-to-donor variation in macrophage responses to the human fungal pathogen Cryptococcus neoformans,” *PLoS ONE*, 13(3), p. e0194615. Available at: https://doi.org/10.1371/journal.pone.0194615.

Ge, S.X., Jung, D. and Yao, R. (2020) “ShinyGO: a graphical gene-set enrichment tool for animals and plants,” *Bioinformatics*, 36(8), pp. 2628–2629. Available at: https://doi.org/10.1093/bioinformatics/btz931.

Gehrig, S. *et al.* (2012a) “Identification of modifications in microbial, native tRNA that suppress immunostimulatory activity,” *The Journal of Experimental Medicine*, 209(2), pp. 225–233. Available at: https://doi.org/10.1084/jem.20111044.

Gehrig, S. *et al.* (2012b) “Identification of modifications in microbial, native tRNA that suppress immunostimulatory activity,” *The Journal of Experimental Medicine*, 209(2), pp. 225–233. Available at: https://doi.org/10.1084/jem.20111044.

Geisbert, T.W. *et al.* (2003) “Pathogenesis of Ebola Hemorrhagic Fever in Cynomolgus Macaques,” *The American Journal of Pathology*, 163(6), pp. 2347–2370. Available at: https://doi.org/10.1016/S0002-9440(10)63591-2.

Goldstein, T. *et al.* (2018) “Discovery of a new ebolavirus (Bombali virus) in molossid bats in Sierra Leone.,” *Nature microbiology*, 3(10), pp. 1084–1089. Available at: https://doi.org/10.1038/s41564-018-0227-2.

Goldstein, T. *et al.* (2020) “Spillover of ebolaviruses into people in eastern Democratic Republic of Congo prior to the 2018 Ebola virus disease outbreak,” *One Health Outlook*, 2, p. 21. Available at: https://doi.org/10.1186/s42522-020-00028-1.

Gómez-Herranz, M., Taylor, J. and Sloan, R.D. (2023) “IFITM proteins: Understanding their diverse roles in viral infection, cancer, and immunity,” *Journal of Biological Chemistry*, 299(1), p. 102741. Available at: https://doi.org/10.1016/j.jbc.2022.102741.

Gordon, S. and Taylor, P.R. (2005) “Monocyte and macrophage heterogeneity,” *Nature Reviews Immunology*, 5(12), pp. 953–964. Available at: https://doi.org/10.1038/nri1733.

Gresch, O. *et al.* (2004) “New non-viral method for gene transfer into primary cells,” *Methods*, 33(2), pp. 151–163. Available at: https://doi.org/10.1016/j.ymeth.2003.11.009.

Greulich, W. *et al.* (2019) “TLR8 is a sensor of RNase T2 degradation products,” *Cell*, 179(6), pp. 1264-1275.e13. Available at: https://doi.org/10.1016/j.cell.2019.11.001.

Groseth, A. and Hoenen, T. (2024) “Novel filoviruses: indication of a global threat or cause to reassess our risk perception?,” *npj Viruses*, 2(1), p. 38. Available at: https://doi.org/10.1038/s44298-024-00050-4.

Guan, F. *et al.* (2025) “Tissue macrophages: origin, heterogenity, biological functions, diseases and therapeutic targets,” *Signal Transduction and Targeted Therapy*, 10(1), p. 93. Available at: https://doi.org/10.1038/s41392-025-02124-y.

Habjan, M. *et al.* (2008) “Processing of Genome 5′ Termini as a Strategy of Negative-Strand RNA Viruses to Avoid RIG-I-Dependent Interferon Induction,” *PLoS ONE*, 3(4), p. e2032. Available at: https://doi.org/10.1371/journal.pone.0002032.

Han, D. *et al.* (2025) “Cell-Autonomous Immunity: From Cytosolic Sensing to Self-Defense,” *International Journal of Molecular Sciences*, 26(9), p. 4025. Available at: https://doi.org/10.3390/ijms26094025.

Hashimoto, D. *et al.* (2013) “Tissue resident macrophages self-maintain locally throughout adult life with minimal contribution from circulating monocytes,” *Immunity*, 38(4), p. 10.1016/j.immuni.2013.04.004. Available at: https://doi.org/10.1016/j.immuni.2013.04.004.

Hayashi, F. *et al.* (2001) “The innate immune response to bacterial flagellin is mediated by Toll-like receptor 5,” *Nature*, 410(6832), pp. 1099–1103. Available at: https://doi.org/10.1038/35074106.

He, F.B. *et al.* (2022) “Filovirus VP24 Proteins Differentially Regulate RIG-I and MDA5-Dependent Type I and III Interferon Promoter Activation,” *Frontiers in Immunology*, 12, p. 694105. Available at: https://doi.org/10.3389/fimmu.2021.694105.

Heil, F. *et al.* (2004a) “Species-Specific Recognition of Single-Stranded RNA via Toll-like Receptor 7 and 8,” *Science*, 303(5663), pp. 1526–1529. Available at: https://doi.org/10.1126/science.1093620.

Heil, F. *et al.* (2004b) “Species-specific recognition of single-stranded RNA via toll-like receptor 7 and 8,” *Science*, 303(5663), pp. 1526–1529. Available at: https://doi.org/10.1126/science.1093620.

Helm, M. (2006) “Post-transcriptional nucleotide modification and alternative folding of RNA,” *Nucleic Acids Research*, 34(2), pp. 721–733. Available at: https://doi.org/10.1093/nar/gkj471.

Hemmi, H. *et al.* (2000) “A Toll-like receptor recognizes bacterial DNA,” *Nature*, 408(6813), pp. 740–745. Available at: https://doi.org/10.1038/35047123.

Henao-Restrepo, A.M. *et al.* (2015) “Efficacy and effectiveness of an rVSV-vectored vaccine expressing Ebola surface glycoprotein: interim results from the Guinea ring vaccination cluster-randomised trial,” *The Lancet*, 386(9996), pp. 857–866. Available at: https://doi.org/10.1016/S0140-6736(15)61117-5.

Hensley, L.E. *et al.* (2002) “Proinflammatory response during Ebola virus infection of primate models: possible involvement of the tumor necrosis factor receptor superfamily,” *Immunology Letters*, 80(3), pp. 169–179. Available at: https://doi.org/10.1016/S0165-2478(01)00327-3.

Herb, M. and Schramm, M. (2021) “Functions of ROS in Macrophages and Antimicrobial Immunity,” *Antioxidants*, 10(2), p. 313. Available at: https://doi.org/10.3390/antiox10020313.

Hipolito, V.E.B. *et al.* (2019) “Enhanced translation expands the endo-lysosome size and promotes antigen presentation during phagocyte activation,” *PLoS Biology*, 17(12), p. e3000535. Available at: https://doi.org/10.1371/journal.pbio.3000535.

Hoeffel, G. and Ginhoux, F. (2015) “Ontogeny of Tissue-Resident Macrophages,” *Frontiers in Immunology*, 6, p. 486. Available at: https://doi.org/10.3389/fimmu.2015.00486.

Hoenen, T. *et al.* (2012) “Inclusion Bodies Are a Site of Ebolavirus Replication,” *Journal of Virology*, 86(21), pp. 11779–11788. Available at: https://doi.org/10.1128/JVI.01525-12.

Hoenen, T. *et al.* (2013) “A novel Ebola virus expressing luciferase allows for rapid and quantitative testing of antivirals,” *Antiviral research*, 99(3), pp. 207–213. Available at: https://doi.org/10.1016/j.antiviral.2013.05.017.

Höfler, S. and Carlomagno, T. (2020) “Structural and functional roles of 2’-*O*-ribose methylations and their enzymatic machinery across multiple classes of RNAs,” *Current Opinion in Structural Biology*, 65, pp. 42–50. Available at: https://doi.org/10.1016/j.sbi.2020.05.008.

Hoppenbrouwers, T. *et al.* (2022) “Functional differences between primary monocyte-derived and THP-1 macrophages and their response to LCPUFAs,” *PharmaNutrition*, 22, p. 100322. Available at: https://doi.org/10.1016/j.phanu.2022.100322.

Hornung, V. *et al.* (2002) “Quantitative Expression of Toll-Like Receptor 1–10 mRNA in Cellular Subsets of Human Peripheral Blood Mononuclear Cells and Sensitivity to CpG Oligodeoxynucleotides1,” *The Journal of Immunology*, 168(9), pp. 4531–4537. Available at: https://doi.org/10.4049/jimmunol.168.9.4531.

Hornung, V. *et al.* (2014) “OAS proteins and cGAS: unifying concepts in sensing and responding to cytosolic nucleic acids,” *Nature Reviews Immunology*, 14(8), pp. 521–528. Available at: https://doi.org/10.1038/nri3719.

Hounmenou, C.G. *et al.* (2024) “Ebola virus circulation in a non-epidemic Guinean rural area: A mixed-method approach to assessing endemicity,” *International Journal of Infectious Diseases*, 146. Available at: https://doi.org/10.1016/j.ijid.2024.107129.

Huang, H. *et al.* (2014) “Dimeric Structure of Pseudokinase RNase L Bound to 2-5A Reveals a Basis for Interferon-Induced Antiviral Activity,” *Molecular Cell*, 53(2), pp. 221–234. Available at: https://doi.org/10.1016/j.molcel.2013.12.025.

Hughes, C.S. *et al.* (2019) “Single-pot, solid-phase-enhanced sample preparation for proteomics experiments,” *Nature Protocols*, 14(1), pp. 68–85. Available at: https://doi.org/10.1038/s41596-018-0082-x.

Imamura, M. *et al.* (2007) “Lipopolysaccharide induced expression of pentraxin 3 in human neutrophils and monocyte-derived macrophages,” *Cellular Immunology*, 248(2), pp. 86–94. Available at: https://doi.org/10.1016/j.cellimm.2007.09.003.

Ito, H. *et al.* (2001) “Ebola Virus Glycoprotein: Proteolytic Processing, Acylation, Cell Tropism, and Detection of Neutralizing Antibodies,” *Journal of Virology*, 75(3), pp. 1576–1580. Available at: https://doi.org/10.1128/JVI.75.3.1576-1580.2001.

Janeway, C.A. (1989a) “Approaching the asymptote? Evolution and revolution in immunology,” *Cold Spring Harbor Symposia on Quantitative Biology*, 54 Pt 1, pp. 1–13. Available at: https://doi.org/10.1101/sqb.1989.054.01.003.

Janeway, C.A. (1989b) “Approaching the asymptote? Evolution and revolution in immunology,” *Cold Spring Harbor Symposia on Quantitative Biology*, 54 Pt 1, pp. 1–13. Available at: https://doi.org/10.1101/sqb.1989.054.01.003.

Janeway, C.A. and Medzhitov, R. (2002) “Innate immune recognition,” *Annual Review of Immunology*, 20, pp. 197–216. Available at: https://doi.org/10.1146/annurev.immunol.20.083001.084359.

Jöckel, S. *et al.* (2012) “The 2’-O-methylation status of a single guanosine controls transfer RNA-mediated Toll-like receptor 7 activation or inhibition,” *The Journal of Experimental Medicine*, 209(2), pp. 235–241. Available at: https://doi.org/10.1084/jem.20111075.

Karikó, K. *et al.* (2004) “mRNA Is an Endogenous Ligand for Toll-like Receptor 3*,” *Journal of Biological Chemistry*, 279(13), pp. 12542–12550. Available at: https://doi.org/10.1074/jbc.M310175200.

Karikó, K. *et al.* (2005) “Suppression of RNA recognition by Toll-like receptors: the impact of nucleoside modification and the evolutionary origin of RNA,” *Immunity*, 23(2), pp. 165–175. Available at: https://doi.org/10.1016/j.immuni.2005.06.008.

Kärre, K. *et al.* (1986) “Selective rejection of H–2-deficient lymphoma variants suggests alternative immune defence strategy,” *Nature*, 319(6055), pp. 675–678. Available at: https://doi.org/10.1038/319675a0.

Kawai, T. *et al.* (2024) “Decoding Toll-like receptors: Recent insights and perspectives in innate immunity,” *Immunity*, 57(4), pp. 649–673. Available at: https://doi.org/10.1016/j.immuni.2024.03.004.

Khan, H. *et al.* (2023) “VP24 matrix proteins of eight filoviruses downregulate innate immune response by inhibiting the interferon-induced pathway,” *Journal of General Virology*, 104(8), p. 001888. Available at: https://doi.org/10.1099/jgv.0.001888.

Kindrachuk, J. *et al.* (2014) “Ebola Virus Modulates Transforming Growth Factor β Signaling and Cellular Markers of Mesenchyme-Like Transition in Hepatocytes,” *Journal of Virology*, 88(17), pp. 9877–9892. Available at: https://doi.org/10.1128/JVI.01410-14.

Klatt, A.-B. *et al.* (2023) “CLEC12A Binds to Legionella pneumophila but Has No Impact on the Host’s Antibacterial Response,” *International Journal of Molecular Sciences*, 24(4), p. 3891. Available at: https://doi.org/10.3390/ijms24043891.

Knecht, S. *et al.* (2023) “An Introduction to Analytical Challenges, Approaches, and Applications in Mass Spectrometry–Based Secretomics,” *Molecular & Cellular Proteomics*, 22(9), p. 100636. Available at: https://doi.org/10.1016/j.mcpro.2023.100636.

Kota, K.P. *et al.* (2012) “High Content Image Based Analysis Identifies Cell Cycle Inhibitors as Regulators of Ebola Virus Infection,” *Viruses*, 4(10), pp. 1865–1877. Available at: https://doi.org/10.3390/v4101865.

Kotliar, D. *et al.* (2020) “Single-Cell Profiling of Ebola Virus Disease *In Vivo* Reveals Viral and Host Dynamics,” *Cell*, 183(5), pp. 1383-1401.e19. Available at: https://doi.org/10.1016/j.cell.2020.10.002.

Kulkarni, G.V. and McCulloch, C.A. (1994) “Serum deprivation induces apoptotic cell death in a subset of Balb/c 3T3 fibroblasts,” *Journal of Cell Science*, 107 (Pt 5), pp. 1169–1179. Available at: https://doi.org/10.1242/jcs.107.5.1169.

Lall, S. *et al.* (2018) “Structure-Aware Principal Component Analysis for Single-Cell RNA-seq Data,” *Journal of Computational Biology*, 25(12), pp. 1365–1373. Available at: https://doi.org/10.1089/cmb.2018.0027.

Latz, E. *et al.* (2004) “TLR9 signals after translocating from the ER to CpG DNA in the lysosome,” *Nature Immunology*, 5(2), pp. 190–198. Available at: https://doi.org/10.1038/ni1028.

Lawrence, P. *et al.* (2017) “Human transmission of Ebola virus,” *Current Opinion in Virology*, 22, pp. 51–58. Available at: https://doi.org/10.1016/j.coviro.2016.11.013.

Lee, B.L. and Barton, G.M. (2014) “Trafficking of endosomal Toll-like receptors,” *Trends in cell biology*, 24(6), pp. 360–369. Available at: https://doi.org/10.1016/j.tcb.2013.12.002.

Lendeckel, U., Venz, S. and Wolke, C. (2022) “Macrophages: shapes and functions,” *ChemTexts*, 8(2), p. 12. Available at: https://doi.org/10.1007/s40828-022-00163-4.

Leppek, K. *et al.* (2013) “Roquin promotes constitutive mRNA decay via a conserved class of stem-loop recognition motifs,” *Cell*, 153(4), pp. 869–881. Available at: https://doi.org/10.1016/j.cell.2013.04.016.

Leroy, E.M. *et al.* (2005) “Fruit bats as reservoirs of Ebola virus,” *Nature*, 438(7068), pp. 575–576. Available at: https://doi.org/10.1038/438575a.

Lesbats, J. *et al.* (2025) “Macrophages recycle phagocytosed bacteria to fuel immunometabolic responses,” *Nature*, 640(8058), pp. 524–533. Available at: https://doi.org/10.1038/s41586-025-08629-4.

Li, D. and Wu, M. (2021) “Pattern recognition receptors in health and diseases,” *Signal Transduction and Targeted Therapy*, 6(1), p. 291. Available at: https://doi.org/10.1038/s41392-021-00687-0.

Li, K. and Underhill, D.M. (2025) “Phagocytosis: a process that shapes immune responses to engulfed meals,” *Nature Reviews Immunology*, pp. 1–14. Available at: https://doi.org/10.1038/s41577-025-01231-9.

Li, L. *et al.* (2024) “Assessing risk of Bombali virus spillover to humans by mutagenesis analysis of viral glycoprotein,” *hLife*, 2(1), pp. 32–42. Available at: https://doi.org/10.1016/j.hlife.2023.11.003.

Li, T. *et al.* (2019) “An endosomal LAPF is required for macrophage endocytosis and elimination of bacteria,” *Proceedings of the National Academy of Sciences*, 116(26), pp. 12958–12963. Available at: https://doi.org/10.1073/pnas.1903896116.

Li, X.X. and Woodruff, T.M. (2025) “The complement system: Biology, pathology, and therapeutic interventions,” *Pharmacological Reviews*, 77(5), p. 100079. Available at: https://doi.org/10.1016/j.pharmr.2025.100079.

Liao, L.E. *et al.* (2020) “Quantification of Ebola virus replication kinetics in vitro,” *PLOS Computational Biology*, 16(11), p. e1008375. Available at: https://doi.org/10.1371/journal.pcbi.1008375.

Licata, J.M. *et al.* (2004) “Contribution of Ebola Virus Glycoprotein, Nucleoprotein, and VP24 to Budding of VP40 Virus-Like Particles,” *Journal of Virology*, 78(14), pp. 7344–7351. Available at: https://doi.org/10.1128/JVI.78.14.7344-7351.2004.

Lin, T.-Y., Guo, H. and Chen, X. (2021) “Unraveling mechanisms of pentraxin 3 secretion in adipocytes during inflammation,” *Journal of Molecular Endocrinology*, 67(3), pp. 55–69. Available at: https://doi.org/10.1530/JME-21-0026.

Lin, Y.-S. *et al.* (2025) “Involvement of nucleic acid-sensing toll-like receptors in human diseases and their controlling mechanisms,” *Journal of Biomedical Science*, 32(1), p. 56. Available at: https://doi.org/10.1186/s12929-025-01151-9.

Liu, G. *et al.* (2018) “Nuclear-resident RIG-I senses viral replication inducing antiviral immunity,” *Nature Communications*, 9, p. 3199. Available at: https://doi.org/10.1038/s41467-018-05745-w.

Lonez, C., Vandenbranden, M. and Ruysschaert, J.-M. (2012) “Cationic lipids activate intracellular signaling pathways,” *Advanced Drug Delivery Reviews*, 64(15), pp. 1749–1758. Available at: https://doi.org/10.1016/j.addr.2012.05.009.

Luzio, J.P. *et al.* (2014) “The Biogenesis of Lysosomes and Lysosome-Related Organelles,” *Cold Spring Harbor Perspectives in Biology*, 6(9), p. a016840. Available at: https://doi.org/10.1101/cshperspect.a016840.

Madeira, F. *et al.* (2024) “The EMBL-EBI Job Dispatcher sequence analysis tools framework in 2024,” *Nucleic acids research*, 52(W1), pp. W521–W525. Available at: https://doi.org/10.1093/nar/gkae241.

Mahanty, S. and Bray, M. (2004) “Pathogenesis of filoviral haemorrhagic fevers,” *The Lancet Infectious Diseases*, 4(8), pp. 487–498. Available at: https://doi.org/10.1016/S1473-3099(04)01103-X.

Martin, B. *et al.* (2016) “Filovirus proteins for antiviral drug discovery: A structure/function analysis of surface glycoproteins and virus entry,” *Antiviral Research*, 135, pp. 1–14. Available at: https://doi.org/10.1016/j.antiviral.2016.09.001.

Martines, R.B. *et al.* (2015) “Tissue and cellular tropism, pathology and pathogenesis of Ebola and Marburg viruses,” *The Journal of Pathology*, 235(2), pp. 153–174. Available at: https://doi.org/10.1002/path.4456.

Martinon, F., Burns, K. and Tschopp, J. (2002) “The Inflammasome: A Molecular Platform Triggering Activation of Inflammatory Caspases and Processing of proIL-β,” *Molecular Cell*, 10(2), pp. 417–426. Available at: https://doi.org/10.1016/S1097-2765(02)00599-3.

Matzinger, P. (1994) “Tolerance, danger, and the extended family,” *Annual Review of Immunology*, 12, pp. 991–1045. Available at: https://doi.org/10.1146/annurev.iy.12.040194.005015.

Matzinger, P. (2002) “The Danger Model: A Renewed Sense of Self,” *Science*, 296(5566), pp. 301–305. Available at: https://doi.org/10.1126/science.1071059.

Matziol, T. *et al.* (2025) “Structure-guided approaches to modulate endosomal toll-like receptors TLR7, TLR8 and TLR9: advances, challenges and therapeutic promise,” *Drug Discovery Today*, 30(11), p. 104495. Available at: https://doi.org/10.1016/j.drudis.2025.104495.

Maurisse, R. *et al.* (2010) “Comparative transfection of DNA into primary and transformed mammalian cells from different lineages,” *BMC Biotechnology*, 10(1), p. 9. Available at: https://doi.org/10.1186/1472-6750-10-9.

McCown, P.J. *et al.* (2020) “Naturally occurring modified ribonucleosides,” *WIREs RNA*, 11(5), p. e1595. Available at: https://doi.org/10.1002/wrna.1595.

Mechnikov, I.I. (1988) “Immunity in infective diseases. By Il’ia Il’ich Mechnikov, 1905,” *Reviews of Infectious Diseases*, 10(1), pp. 223–227.

Medzhitov, R. (2009) “Approaching the Asymptote: 20 Years Later,” *Immunity*, 30(6), pp. 766–775. Available at: https://doi.org/10.1016/j.immuni.2009.06.004.

Medzhitov, R., Preston-Hurlburt, P. and Janeway, C.A. (1997) “A human homologue of the Drosophila Toll protein signals activation of adaptive immunity,” *Nature*, 388(6640), pp. 394–397. Available at: https://doi.org/10.1038/41131.

Mehedi, M. *et al.* (2011) “A New Ebola Virus Nonstructural Glycoprotein Expressed through RNA Editing ▿ ,” *Journal of Virology*, 85(11), pp. 5406–5414. Available at: https://doi.org/10.1128/JVI.02190-10.

Meyer, K.D. and Jaffrey, S.R. (2017) “Rethinking m6A Readers, Writers, and Erasers,” *Annual review of cell and developmental biology*, 33, pp. 319–342. Available at: https://doi.org/10.1146/annurev-cellbio-100616-060758.

Mildner, A., Kim, K.-W. and Yona, S. (2024) “Unravelling monocyte functions: from the guardians of health to the regulators of disease,” *Discovery Immunology*, 3(1), p. kyae014. Available at: https://doi.org/10.1093/discim/kyae014.

Mills, C.D. *et al.* (2000) “M-1/M-2 Macrophages and the Th1/Th2 Paradigm1,” *The Journal of Immunology*, 164(12), pp. 6166–6173. Available at: https://doi.org/10.4049/jimmunol.164.12.6166.

Mohan, G.S. *et al.* (2012) “Antigenic Subversion: A Novel Mechanism of Host Immune Evasion by Ebola Virus,” *PLoS Pathogens*, 8(12), p. e1003065. Available at: https://doi.org/10.1371/journal.ppat.1003065.

Mohd, O.B. *et al.* (2024) “The Development of Ebola Virus Outbreaks: A Review of Epidemiological Trends, Clinical Features, and Treatment Advances,” *Cureus*, 16(11), p. e74078. Available at: https://doi.org/10.7759/cureus.74078.

Molinier-Frenkel, V., Prévost-Blondel, A. and Castellano, F. (2019) “The IL4I1 Enzyme: A New Player in the Immunosuppressive Tumor Microenvironment,” *Cells*, 8(7). Available at: https://doi.org/10.3390/cells8070757.

Motorin, Y. and Helm, M. (2011) “RNA nucleotide methylation,” *Wiley interdisciplinary reviews. RNA*, 2(5), pp. 611–631. Available at: https://doi.org/10.1002/wrna.79.

Mujal, A.M., Delconte, R.B. and Sun, J.C. (2021) “Natural Killer Cells: From Innate to Adaptive Features,” *Annual Review of Immunology*, 39(Volume 39, 2021), pp. 417–447. Available at: https://doi.org/10.1146/annurev-immunol-101819-074948.

Munk, M. *et al.* (2022) “Differential expression of the three independent CaM genes coding for an identical protein: Potential relevance of distinct mRNA stability by different codon usage,” *Cell Calcium*, 107, p. 102656. Available at: https://doi.org/10.1016/j.ceca.2022.102656.

Murray, P.J. and Wynn, T.A. (2011) “Protective and pathogenic functions of macrophage subsets,” *Nature reviews. Immunology*, 11(11), pp. 723–737. Available at: https://doi.org/10.1038/nri3073.

Nahrendorf, M., Ginhoux, F. and Swirski, F.K. (2025) “Immune System Influence on Physiology,” *Science (New York, N.Y.)*, 389(6760), pp. 594–599. Available at: https://doi.org/10.1126/science.adx4380.

Nakamura, R. *et al.* (2021) “A Simple Method for In-Depth Proteome Analysis of Mammalian Cell Culture Conditioned Media Containing Fetal Bovine Serum,” *International Journal of Molecular Sciences*, 22(5). Available at: https://doi.org/10.3390/ijms22052565.

Nanbo, A. *et al.* (2013) “The spatio-temporal distribution dynamics of Ebola virus proteins and RNA in infected cells,” *Scientific Reports*, 3, p. 1206. Available at: https://doi.org/10.1038/srep01206.

Nanduri, R., Furusawa, T. and Bustin, M. (2020) “Biological Functions of HMGN Chromosomal Proteins,” *International Journal of Molecular Sciences*, 21(2), p. 449. Available at: https://doi.org/10.3390/ijms21020449.

Nascimento, C.R. *et al.* (2022) “Comparison of monocytic cell lines U937 and THP-1 as macrophage models for in vitro studies,” *Biochemistry and Biophysics Reports*, 32, p. 101383. Available at: https://doi.org/10.1016/j.bbrep.2022.101383.

Natchiar, S.K. *et al.* (2018) “Visualizing the Role of 2’-OH rRNA Methylations in the Human Ribosome Structure,” *Biomolecules*, 8(4). Available at: https://doi.org/10.3390/biom8040125.

Nilsen, K.E. *et al.* (2022) “TIRAP/Mal Positively Regulates TLR8-Mediated Signaling via IRF5 in Human Cells,” *Biomedicines*, 10(7). Available at: https://doi.org/10.3390/biomedicines10071476.

Nonnis, S. *et al.* (2016) “Effect of fetal bovine serum in culture media on MS analysis of mesenchymal stromal cells secretome,” *EuPA Open Proteomics*, 10, pp. 28–30. Available at: https://doi.org/10.1016/j.euprot.2016.01.005.

Nunes, I.V. *et al.* (2024) “Bacterial RNA sensing by TLR8 requires RNase 6 processing and is inhibited by RNA 2’O-methylation,” *EMBO reports*, 25(11), pp. 4674–4692. Available at: https://doi.org/10.1038/s44319-024-00281-9.

Okumura, A. *et al.* (2010) “Interaction between Ebola Virus Glycoprotein and Host Toll-Like Receptor 4 Leads to Induction of Proinflammatory Cytokines and SOCS1,” *Journal of Virology*, 84(1), pp. 27–33. Available at: https://doi.org/10.1128/JVI.01462-09.

Olejnik, J. *et al.* (2017) “Ebolaviruses Associated with Differential Pathogenicity Induce Distinct Host Responses in Human Macrophages,” *Journal of Virology*, 91(11), p. e00179. Available at: https://doi.org/10.1128/JVI.00179-17.

O’Neill, L.A.J. (2003) “The role of MyD88-like adapters in Toll-like receptor signal transduction,” *Biochemical Society Transactions*, 31(3), pp. 643–647. Available at: https://doi.org/10.1042/bst0310643.

Ontiveros, R.J., Stoute, J. and Liu, K.F. (2019) “The chemical diversity of RNA modifications,” *Biochemical Journal*, 476(8), pp. 1227–1245. Available at: https://doi.org/10.1042/BCJ20180445.

Ostendorf, T. *et al.* (2020) “Immune Sensing of Synthetic, Bacterial, and Protozoan RNA by Toll-like Receptor 8 Requires Coordinated Processing by RNase T2 and RNase 2,” *Immunity*, 52(4), pp. 591-605.e6. Available at: https://doi.org/10.1016/j.immuni.2020.03.009.

Osterholm, M.T. *et al.* (2015) “Transmission of Ebola Viruses: What We Know and What We Do Not Know,” *mBio*, 6(2), pp. e00137-15. Available at: https://doi.org/10.1128/mBio.00137-15.

Ozanick, S. *et al.* (2005) “The bipartite structure of the tRNA m1A58 methyltransferase from S. cerevisiae is conserved in humans,” *RNA (New York, N.Y.)*, 11(8), pp. 1281–1290. Available at: https://doi.org/10.1261/rna.5040605.

Paparisto, E. *et al.* (2021) “Interferon-Induced HERC5 Inhibits Ebola Virus Particle Production and Is Antagonized by Ebola Glycoprotein,” *Cells*, 10(9), p. 2399. Available at: https://doi.org/10.3390/cells10092399.

Pattyn, S. *et al.* (1977) “Isolation of Marburg-like virus from a case of haemorrhagic fever in Zaire,” *Lancet*, 1(8011), pp. 573–574. Available at: https://doi.org/10.1016/s0140-6736(77)92002-5.

Pichlmair, A. *et al.* (2006) “RIG-I-Mediated Antiviral Responses to Single-Stranded RNA Bearing 5’-Phosphates,” *Science*, 314(5801), pp. 997–1001. Available at: https://doi.org/10.1126/science.1132998.

Pinto, A.K. *et al.* (2015) “Human and Murine IFIT1 Proteins Do Not Restrict Infection of Negative-Sense RNA Viruses of the Orthomyxoviridae, Bunyaviridae, and Filoviridae Families,” *Journal of Virology*, 89(18), pp. 9465–9476. Available at: https://doi.org/10.1128/JVI.00996-15.

Pisapia, R. *et al.* (2025) “Clinical features of Marburg virus disease: a review of all reported patients since 1967,” *eClinicalMedicine*, 89, p. 103581. Available at: https://doi.org/10.1016/j.eclinm.2025.103581.

Poltorak, A. *et al.* (1998) “Defective LPS signaling in C3H/HeJ and C57BL/10ScCr mice: mutations in Tlr4 gene,” *Science*, 282(5396), pp. 2085–2088. Available at: https://doi.org/10.1126/science.282.5396.2085.

Potočnik, T. *et al.* (2022) “Effect of Experimental Electrical and Biological Parameters on Gene Transfer by Electroporation: A Systematic Review and Meta-Analysis,” *Pharmaceutics*, 14(12). Available at: https://doi.org/10.3390/pharmaceutics14122700.

Pujol, N. *et al.* (2008) “Anti-Fungal Innate Immunity in C. elegans Is Enhanced by Evolutionary Diversification of Antimicrobial Peptides,” *PLoS Pathogens*, 4(7), p. e1000105. Available at: https://doi.org/10.1371/journal.ppat.1000105.

Rahmatbakhsh, M., Gagarinova, A. and Babu, M. (2021) “Bioinformatic Analysis of Temporal and Spatial Proteome Alternations During Infections,” *Frontiers in Genetics*, 12. Available at: https://doi.org/10.3389/fgene.2021.667936.

Ramanathan, M. *et al.* (2018) “RNA–protein interaction detection in living cells,” *Nature methods*, 15(3), pp. 207–212. Available at: https://doi.org/10.1038/nmeth.4601.

Ramanathan, P. *et al.* (2023) “Ebolavirus Species-Specific Interferon Antagonism Mediated by VP24,” *Viruses*, 15(5), p. 1075. Available at: https://doi.org/10.3390/v15051075.

Rapino, F. *et al.* (2013) “C/EBPα Induces Highly Efficient Macrophage Transdifferentiation of B Lymphoma and Leukemia Cell Lines and Impairs Their Tumorigenicity,” *Cell Reports*, 3(4), pp. 1153–1163. Available at: https://doi.org/10.1016/j.celrep.2013.03.003.

Rapino, F. *et al.* (2017) “C/EBPα Induces Highly Efficient Macrophage Transdifferentiation of B Lymphoma and Leukemia Cell Lines and Impairs Their Tumorigenicity,” *Cell Reports*, 19(6), p. 1281. Available at: https://doi.org/10.1016/j.celrep.2017.04.072.

Reid, St.P. *et al.* (2006) “Ebola Virus VP24 Binds Karyopherin α1 and Blocks STAT1 Nuclear Accumulation,” *Journal of Virology*, 80(11), pp. 5156–5167. Available at: https://doi.org/10.1128/JVI.02349-05.

Reynard, S. *et al.* (2019) “Immune parameters and outcomes during Ebola virus disease,” *JCI Insight*, 4(1), p. e125106. Available at: https://doi.org/10.1172/jci.insight.125106.

Ricklin, D. *et al.* (2010) “Complement - a key system for immune surveillance and homeostasis,” *Nature immunology*, 11(9), pp. 785–797. Available at: https://doi.org/10.1038/ni.1923.

Rimbach, K. *et al.* (2015) “2’-O-Methylation within Bacterial RNA Acts as Suppressor of TLR7/TLR8 Activation in Human Innate Immune Cells,” *Journal of Innate Immunity*, 7(5), pp. 482–493. Available at: https://doi.org/10.1159/000375460.

Ro, Y.-T. and Patterson, J.L. (2022) “Transcriptional induction of TGF-β1 and endothelial-to-mesenchymal transition cell markers in human umbilical vein endothelial cells by Ebola virus infection,” *Genes & Genomics*, 44(12), pp. 1499–1507. Available at: https://doi.org/10.1007/s13258-022-01333-x.

Rosenberg, H.F. and Dyer, K.D. (1996) “Molecular cloning and characterization of a novel human ribonuclease (RNase k6): increasing diversity in the enlarging ribonuclease gene family.,” *Nucleic Acids Research*, 24(18), pp. 3507–3513. Available at: https://doi.org/10.1093/nar/24.18.3507.

Rosetto, M. *et al.* (1995) “Signals from the IL-1 Receptor Homolog, Toll, Can Activate an Immune Response in a *Drosophila* Hemocyte Cell Line,” *Biochemical and Biophysical Research Communications*, 209(1), pp. 111–116. Available at: https://doi.org/10.1006/bbrc.1995.1477.

Ross, P.C. and Hui, S.W. (1999) “Lipoplex size is a major determinant of in vitro lipofection efficiency,” *Gene Therapy*, 6(4), pp. 651–659. Available at: https://doi.org/10.1038/sj.gt.3300863.

Ruiz-Rosado, J. de D. *et al.* (2023) “Human Ribonuclease 6 Has a Protective Role during Experimental Urinary Tract Infection,” *Journal of Innate Immunity*, 15(1), pp. 865–875. Available at: https://doi.org/10.1159/000534736.

Saeed, M.F. *et al.* (2010) “Cellular Entry of Ebola Virus Involves Uptake by a Macropinocytosis-Like Mechanism and Subsequent Trafficking through Early and Late Endosomes,” *PLoS Pathogens*, 6(9), p. e1001110. Available at: https://doi.org/10.1371/journal.ppat.1001110.

Sanchez, A. *et al.* (1993) “Sequence analysis of the Ebola virus genome: organization, genetic elements, and comparison with the genome of Marburg virus,” *Virus Research*, 29(3), pp. 215–240. Available at: https://doi.org/10.1016/0168-1702(93)90063-S.

Sanchez, A. *et al.* (1996) “The virion glycoproteins of Ebola viruses are encoded in two reading frames and are expressed through transcriptional editing.,” *Proceedings of the National Academy of Sciences of the United States of America*, 93(8), pp. 3602–3607. Available at: https://doi.org/10.1073/pnas.93.8.3602.

Sanchez, A. *et al.* (1998) “Biochemical Analysis of the Secreted and Virion Glycoproteins of Ebola Virus,” *Journal of Virology*, 72(8), pp. 6442–6447. Available at: https://doi.org/10.1128/jvi.72.8.6442-6447.1998.

Sander, L.E. *et al.* (2011) “Sensing prokaryotic mRNA signifies microbial viability and promotes immunity,” *Nature*, 474(7351), pp. 385–389. Available at: https://doi.org/10.1038/nature10072.

Scheibe, M. *et al.* (2013) “Quantitative interaction screen of telomeric repeat-containing RNA reveals novel TERRA regulators,” *Genome Research*, 23(12), pp. 2149–2157. Available at: https://doi.org/10.1101/gr.151878.112.

Scherer, M. *et al.* (2020) “Quantitative Proteomics to Identify Nuclear RNA-Binding Proteins of Malat1,” *International Journal of Molecular Sciences*, 21(3), p. 1166. Available at: https://doi.org/10.3390/ijms21031166.

Schibler, U. and Perry, R.P. (1977) “The 5’-termini of heterogeneous nuclear RNA: a comparison among molecules of different sizes and ages.,” *Nucleic Acids Research*, 4(12), pp. 4133–4149. Available at: https://doi.org/10.1093/nar/4.12.4133.

Schilling, E. *et al.* (2022) “CD14 Is Involved in the Interferon Response of Human Macrophages to Rubella Virus Infection,” *Biomedicines*, 10(2). Available at: https://doi.org/10.3390/biomedicines10020266.

Schmitt, F.C.F. *et al.* (2017) “Identification of an optimized 2’-O-methylated trinucleotide RNA motif inhibiting Toll-like receptors 7 and 8,” *RNA*, 23(9), pp. 1344–1351. Available at: https://doi.org/10.1261/rna.061952.117.

Schoggins, J.W. and Rice, C.M. (2011) “Interferon-stimulated genes and their antiviral effector functions,” *Current Opinion in Virology*, 1(6), pp. 519–525. Available at: https://doi.org/10.1016/j.coviro.2011.10.008.

Schudt, G. *et al.* (2015) “Transport of Ebolavirus Nucleocapsids Is Dependent on Actin Polymerization: Live-Cell Imaging Analysis of Ebolavirus-Infected Cells,” *The Journal of Infectious Diseases*, 212(suppl_2), pp. S160–S166. Available at: https://doi.org/10.1093/infdis/jiv083.

Schuh, A.J., Amman, B.R. and Towner, J.S. (2017) “Filoviruses and bats,” *Microbiology Australia*, 38(1), pp. 12–16. Available at: https://doi.org/10.1071/MA17005.

Schüssler, M. *et al.* (2023) “Gene editing of SAMHD1 in macrophage-like cells reveals complex relationships between SAMHD1 phospho-regulation, HIV-1 restriction, and cellular dNTP levels,” *mBio*, 14(5), pp. e02252-23. Available at: https://doi.org/10.1128/mbio.02252-23.

Schwarz, T.M. *et al.* (2017) “VP24-Karyopherin Alpha Binding Affinities Differ between Ebolavirus Species, Influencing Interferon Inhibition and VP24 Stability,” *Journal of Virology*, 91(4), p. 10.1128/jvi.01715-16. Available at: https://doi.org/10.1128/jvi.01715-16.

Scur, M. *et al.* (2023) “The diverse roles of C-type lectin-like receptors in immunity,” *Frontiers in Immunology*, 14, p. 1126043. Available at: https://doi.org/10.3389/fimmu.2023.1126043.

Sherwood, E.R. and Toliver-Kinsky, T. (2004) “Mechanisms of the inflammatory response,” *Best Practice & Research Clinical Anaesthesiology*, 18(3), pp. 385–405. Available at: https://doi.org/10.1016/j.bpa.2003.12.002.

Shevchenko, A. *et al.* (2006) “In-gel digestion for mass spectrometric characterization of proteins and proteomes,” *Nature Protocols*, 1(6), pp. 2856–2860. Available at: https://doi.org/10.1038/nprot.2006.468.

Shi, Y. *et al.* (2025) “Optimizing imputation strategies for mass spectrometry-based proteomics considering intensity and missing value rates,” *Computational and Structural Biotechnology Journal*, 27, pp. 1818–1826. Available at: https://doi.org/10.1016/j.csbj.2025.04.041.

Shin, J. *et al.* (2015) “Use of Composite Protein Database including Search Result Sequences for Mass Spectrometric Analysis of Cell Secretome,” *PLOS ONE*, 10(3), p. e0121692. Available at: https://doi.org/10.1371/journal.pone.0121692.

Shin, J. *et al.* (2019) “Comparative analysis of differentially secreted proteins in serum-free and serum-containing media by using BONCAT and pulsed SILAC,” *Scientific Reports*, 9(1), p. 3096. Available at: https://doi.org/10.1038/s41598-019-39650-z.

Shultz, J.M. *et al.* (2016) “Distinguishing epidemiological features of the 2013–2016 West Africa Ebola virus disease outbreak,” *Disaster Health*, 3(3), pp. 78–88. Available at: https://doi.org/10.1080/21665044.2016.1228326.

Sikora, M. *et al.* (2025) “The spatiotemporal distribution of human pathogens in ancient Eurasia,” *Nature*, 643(8073), pp. 1011–1019. Available at: https://doi.org/10.1038/s41586-025-09192-8.

Simón-Fuentes, M. *et al.* (2023) “TLR7 Activation in M-CSF-Dependent Monocyte-Derived Human Macrophages Potentiates Inflammatory Responses and Prompts Neutrophil Recruitment,” *Journal of Innate Immunity*, 15(1), pp. 517–530. Available at: https://doi.org/10.1159/000530249.

Sioud, M. (2006) “Innate sensing of self and non-self RNAs by Toll-like receptors,” *Trends in Molecular Medicine*, 12(4), pp. 167–176. Available at: https://doi.org/10.1016/j.molmed.2006.02.004.

Sleat, D.E. *et al.* (2013) “Extending the Mannose 6-Phosphate Glycoproteome by High Resolution/Accuracy Mass Spectrometry Analysis of Control and Acid Phosphatase 5-Deficient Mice*,” *Molecular & Cellular Proteomics*, 12(7), pp. 1806–1817. Available at: https://doi.org/10.1074/mcp.M112.026179.

Slenczka, W. (2017) “Filovirus Research: How it Began,” *Current Topics in Microbiology and Immunology*, 411, pp. 3–21. Available at: https://doi.org/10.1007/82_2017_8.

Sordyl, D. *et al.* (2026) “MODOMICS: a database of RNA modifications and related information. 2025 update and 20th anniversary,” *Nucleic Acids Research*, 54(D1), pp. D219–D225. Available at: https://doi.org/10.1093/nar/gkaf1284.

Spurgers, K.B. *et al.* (2010) “Identification of Essential Filovirion-associated Host Factors by Serial Proteomic Analysis and RNAi Screen,” *Molecular & Cellular Proteomics : MCP*, 9(12), pp. 2690–2703. Available at: https://doi.org/10.1074/mcp.M110.003418.

Ströher, U. *et al.* (2001) “Infection and Activation of Monocytes by Marburg and Ebola Viruses,” *Journal of Virology*, 75(22), pp. 11025–11033. Available at: https://doi.org/10.1128/JVI.75.22.11025-11033.2001.

Szaflarski, W. *et al.* (2021) “Early rRNA processing is a stress-dependent regulatory event whose inhibition maintains nucleolar integrity,” *Nucleic Acids Research*, 50(2), pp. 1033–1051. Available at: https://doi.org/10.1093/nar/gkab1231.

Szklarczyk, D. *et al.* (2023) “The STRING database in 2023: protein-protein association networks and functional enrichment analyses for any sequenced genome of interest,” *Nucleic Acids Research*, 51(D1), pp. D638–D646. Available at: https://doi.org/10.1093/nar/gkac1000.

Taliaferro, J.M. *et al.* (2016) “RNA Sequence Context Effects Measured In Vitro Predict In Vivo Protein Binding and Regulation,” *Molecular Cell*, 64(2), pp. 294–306. Available at: https://doi.org/10.1016/j.molcel.2016.08.035.

Tanji, H. *et al.* (2013) “Structural Reorganization of the Toll-Like Receptor 8 Dimer Induced by Agonistic Ligands,” *Science*, 339(6126), pp. 1426–1429. Available at: https://doi.org/10.1126/science.1229159.

Tanji, H. *et al.* (2015) “Toll-like receptor 8 senses degradation products of single-stranded RNA,” *Nature Structural & Molecular Biology*, 22(2), pp. 109–115. Available at: https://doi.org/10.1038/nsmb.2943.

van Tol, S. *et al.* (2022) “Ubiquitination of Ebola virus VP35 at lysine 309 regulates viral transcription and assembly,” *PLoS Pathogens*, 18(5), p. e1010532. Available at: https://doi.org/10.1371/journal.ppat.1010532.

Tong, A.-J. *et al.* (2023) “Nucleotide modifications enable rational design of TLR7-selective ligands by blocking RNase cleavage,” *The Journal of Experimental Medicine*, 221(2), p. e20230341. Available at: https://doi.org/10.1084/jem.20230341.

Tong, A.-J. *et al.* (2024) “Nucleotide modifications enable rational design of TLR7-selective ligands by blocking RNase cleavage,” *The Journal of Experimental Medicine*, 221(2), p. e20230341. Available at: https://doi.org/10.1084/jem.20230341.

Truman, L.A. *et al.* (2008) “CX3CL1/fractalkine is released from apoptotic lymphocytes to stimulate macrophage chemotaxis,” *Blood*, 112(13), pp. 5026–5036. Available at: https://doi.org/10.1182/blood-2008-06-162404.

Tsai, B.P. *et al.* (2011) “Quantitative Profiling of In Vivo-assembled RNA-Protein Complexes Using a Novel Integrated Proteomic Approach,” *Molecular & Cellular Proteomics : MCP*, 10(4), p. M110.007385. Available at: https://doi.org/10.1074/mcp.M110.007385.

Tschopp, J., Podack, E.R. and Müller-Eberhard, H.J. (1982) “Ultrastructure of the membrane attack complex of complement: detection of the tetramolecular C9-polymerizing complex C5b-8.,” *Proceedings of the National Academy of Sciences of the United States of America*, 79(23), pp. 7474–7478. Available at: https://doi.org/10.1073/pnas.79.23.7474.

Tseng, A.E. *et al.* (2023) “Hepatic proinflammatory myeloid phenotypes are a hallmark of Ebola virus Kikwit pathogenesis in rhesus monkeys,” *Veterinary Pathology*, 60(4), pp. 473–487. Available at: https://doi.org/10.1177/03009858231171906.

Tuladhar, R. *et al.* (2019) “CRISPR-Cas9-based mutagenesis frequently provokes on-target mRNA misregulation,” *Nature Communications*, 10, p. 4056. Available at: https://doi.org/10.1038/s41467-019-12028-5.

Uccellini, M.B. and García-Sastre, A. (2018) “ISRE-Reporter Mouse Reveals High Basal and Induced Type I IFN Responses in Inflammatory Monocytes,” *Cell Reports*, 25(10), pp. 2784-2796.e3. Available at: https://doi.org/10.1016/j.celrep.2018.11.030.

Villar, J. *et al.* (2023) “Monocytes differentiate along two alternative pathways during sterile inflammation,” *EMBO Reports*, 24(7), p. e56308. Available at: https://doi.org/10.15252/embr.202256308.

Villarreal, L. *et al.* (2013) “Unconventional Secretion is a Major Contributor of Cancer Cell Line Secretomes*,” *Molecular & Cellular Proteomics*, 12(5), pp. 1046–1060. Available at: https://doi.org/10.1074/mcp.M112.021618.

Volchkov, V.E. *et al.* (1998) “Processing of the Ebola virus glycoprotein by the proprotein convertase furin,” *Proceedings of the National Academy of Sciences of the United States of America*, 95(10), pp. 5762–5767. Available at: https://doi.org/10.1073/pnas.95.10.5762.

Volchkova, V.A. *et al.* (2015) “RNA Editing of the GP Gene of Ebola Virus is an Important Pathogenicity Factor,” *The Journal of Infectious Diseases*, 212(suppl_2), pp. S226–S233. Available at: https://doi.org/10.1093/infdis/jiv309.

Volkman, A. and Gowans, J.L. (1965) “The Origin of Macrophages from Bone Marrow in the Rat,” *British Journal of Experimental Pathology*, 46(1), pp. 62–70.

Volkmar, K. *et al.* (2024) “Investigating pyroptosis as a mechanism of L. major cell-to-cell spread in the human BLaER1 infection model,” *Molecular Microbiology*, 121(3), pp. 453–469. Available at: https://doi.org/10.1111/mmi.15142.

Vuletic, S. *et al.* (2011) “PLTP regulates STAT3 and NFκB in differentiated THP1 cells and human monocyte-derived macrophages,” *Biochimica et biophysica acta*, 1813(10), pp. 1917–1924. Available at: https://doi.org/10.1016/j.bbamcr.2011.06.013.

Walker, L.R., Hussein, H.A.M. and Akula, S.M. (2016) “Subcellular fractionation method to study endosomal trafficking of Kaposi’s sarcoma-associated herpesvirus,” *Cell & Bioscience*, 6(1), p. 1. Available at: https://doi.org/10.1186/s13578-015-0066-2.

Wan, L. *et al.* (2022) “GP73 is a glucogenic hormone contributing to SARS-CoV-2-induced hyperglycemia,” *Nature Metabolism*, 4(1), pp. 29–43. Available at: https://doi.org/10.1038/s42255-021-00508-2.

Wang, C. *et al.* (2013) “Characterization of murine macrophages from bone marrow, spleen and peritoneum,” *BMC Immunology*, 14(1), p. 6. Available at: https://doi.org/10.1186/1471-2172-14-6.

Wang, H. *et al.* (2016) “Ebola Viral Glycoprotein Bound to Its Endosomal Receptor Niemann-Pick C1,” *Cell*, 164(1), pp. 258–268. Available at: https://doi.org/10.1016/j.cell.2015.12.044.

Wang, R. *et al.* (2024) “The interaction of innate immune and adaptive immune system,” *MedComm*, 5(10), p. e714. Available at: https://doi.org/10.1002/mco2.714.

Wang, X. and Labzin, L.I. (2023) “Inflammatory cell death: how macrophages sense neighbouring cell infection and damage,” *Biochemical Society Transactions*, 51(1), pp. 303–313. Available at: https://doi.org/10.1042/BST20220807.

Wang, Y. *et al.* (2011) "M-CSF Induces Monocyte Survival by Activating NF-κB p65 Phosphorylation at Ser276 via Protein Kinase C," *PLOS ONE*, 6(12), p. e28081. Available at: https://doi.org/10.1371/journal.pone.0028081.

Watt, A. *et al.* (2014) "A Novel Life Cycle Modeling System for Ebola Virus Shows a Genome Length-Dependent Role of VP24 in Virus Infectivity," *Journal of Virology*, 88(18), pp. 10511–10524. Available at: https://doi.org/10.1128/JVI.01272-14.

Wauquier, N. *et al.* (2010) "Human Fatal Zaire Ebola Virus Infection Is Associated with an Aberrant Innate Immunity and with Massive Lymphocyte Apoptosis," *PLoS Neglected Tropical Diseases*, 4(10), p. e837. Available at: https://doi.org/10.1371/journal.pntd.0000837.

Wegner, J. *et al.* (2021) "An epigenetic GPI anchor defect impairs TLR4 signaling in the B cell transdifferentiation model for primary human monocytes BLaER1," *Scientific Reports*, 11, p. 14983. Available at: https://doi.org/10.1038/s41598-021-94386-z.

Wei, Y.-Y.C. *et al.* (2011) "Proteomics analysis of chinese hamster ovary cells undergoing apoptosis during prolonged cultivation," *Cytotechnology*, 63(6), pp. 663–677. Available at: https://doi.org/10.1007/s10616-011-9385-2.

Wichit, S. *et al.* (2019) "SAMHD1 Enhances Chikungunya and Zika Virus Replication in Human Skin Fibroblasts," *International Journal of Molecular Sciences*, 20(7). Available at: https://doi.org/10.3390/ijms20071695.

Willemsen, L. *et al.* (2022) "Monocyte and Macrophage Lipid Accumulation Results in Down-Regulated Type-I Interferon Responses," *Frontiers in Cardiovascular Medicine*, 9. Available at: https://doi.org/10.3389/fcvm.2022.829877.

Wu, R. *et al.* (2025) "Circulating FABP5 released by dying macrophages function as a DAMP to exacerbate septic inflammation," *Cell Reports*, 44(11), p. 116497. Available at: https://doi.org/10.1016/j.celrep.2025.116497.

Wu, W. and Krijgsveld, J. (2024) "Secretome Analysis: Reading Cellular Sign Language to Understand Intercellular Communication," *Molecular & Cellular Proteomics*, 23(1), p. 100692. Available at: https://doi.org/10.1016/j.mcpro.2023.100692.

Xie, H. *et al.* (2004) "Stepwise Reprogramming of B Cells into Macrophages," *Cell*, 117(5), pp. 663–676. Available at: https://doi.org/10.1016/S0092-8674(04)00419-2.

Xue, C. and Greene, E.C. (2021) "DNA repair pathway choices in CRISPR-Cas9 mediated genome editing," *Trends in genetics : TIG*, 37(7), pp. 639–656. Available at: https://doi.org/10.1016/j.tig.2021.02.008.

Yamaoka, S. and Ebihara, H. (2021) "Pathogenicity and Virulence of Ebolaviruses with Species- and Variant-specificity," *Virulence*, 12(1), pp. 885–901. Available at: https://doi.org/10.1080/21505594.2021.1898169.

Yang, S.-L. *et al.* (2018) "Hepatitis B virus upregulates GP73 expression by activating the HIF-2α signaling pathway," *Oncology Letters*, 15(4), pp. 5264–5270. Available at: https://doi.org/10.3892/ol.2018.7955.

Yang, Z. *et al.* (2000) "Identification of the Ebola virus glycoprotein as the main viral determinant of vascular cell cytotoxicity and injury," *Nature Medicine*, 6(8), pp. 886–889. Available at: https://doi.org/10.1038/78654.

Yao, J. *et al.* (2024) "The role of inflammasomes in human diseases and their potential as therapeutic targets," *Signal Transduction and Targeted Therapy*, 9(1), p. 10. Available at: https://doi.org/10.1038/s41392-023-01687-y.

Yue, Y. *et al.* (2015) "IL4I1 Is a Novel Regulator of M2 Macrophage Polarization That Can Inhibit T Cell Activation via L-Tryptophan and Arginine Depletion and IL-10 Production," *PLOS ONE*, 10(11), p. e0142979. Available at: https://doi.org/10.1371/journal.pone.0142979.

Zampieri, C.A., Sullivan, N.J. and Nabel, G.J. (2007) "Immunopathology of highly virulent pathogens: insights from Ebola virus," *Nature Immunology*, 8(11), pp. 1159–1164. Available at: https://doi.org/10.1038/ni1519.

Zarember, K.A. and Godowski, P.J. (2002) "Tissue Expression of Human Toll-Like Receptors and Differential Regulation of Toll-Like Receptor mRNAs in Leukocytes in Response to Microbes, Their Products, and Cytokines," *The Journal of Immunology*, 168(2), pp. 554–561. Available at: https://doi.org/10.4049/jimmunol.168.2.554.

Zhang, X. *et al.* (2017) “GP73 represses host innate immune response to promote virus replication by facilitating MAVS and TRAF6 degradation,” *PLoS Pathogens*, 13(4), p. e1006321. Available at: https://doi.org/10.1371/journal.ppat.1006321.

Zhou, K.I., Pecot, C.V. and Holley, C.L. (2024) “2′-O-methylation (Nm) in RNA: progress, challenges, and future directions,” *RNA*, 30(5), pp. 570–582. Available at: https://doi.org/10.1261/rna.079970.124.

Züst, R. *et al.* (2011) “Ribose 2′-O-methylation provides a molecular signature for the distinction of self and non-self mRNA dependent on the RNA sensor Mda5,” *Nature Immunology*, 12(2), pp. 137–143. Available at: https://doi.org/10.1038/ni.1979.

Curriculum Vitae

Acknowledgements